

# Concepts of electroweak symmetry breaking and Higgs physics

*M. Gomez-Bock*<sup>1</sup>, *M. Mondragón*<sup>2</sup>, *M. Mühlleitner*<sup>3,4</sup>, *M. Spira*<sup>5</sup>, *P.M. Zerwas*<sup>6,7,8</sup>

<sup>1</sup> Benemerita Univ. Auton. de Puebla, 72570 Puebla, Pue, Mexico

<sup>2</sup> Univ. Nac. Auton. de Mexico, 01000 Mexico D.F., Mexico

<sup>3</sup> Laboratoire d'Annecy-Le-Vieux de Physique Théorique, Annecy-Le-Vieux, France

<sup>4</sup> CERN, Geneva, Switzerland

<sup>5</sup> Paul Scherrer Institut, CH-5232 Villigen PSI, Switzerland

<sup>6</sup> Deutsches Elektronen-Synchrotron, D-22603 Hamburg, Germany

<sup>7</sup> RWTH Aachen, D-52074 Aachen, Germany

<sup>8</sup> U. Paris-Sud, F-91405 Orsay, France

## Abstract

We present an introduction to the basic concepts of electroweak symmetry breaking and Higgs physics within the Standard Model and its supersymmetric extensions. A brief overview will also be given on alternative mechanisms of electroweak symmetry breaking. In addition to the theoretical basis, the present experimental status of Higgs physics and prospects at the Tevatron, the LHC, and  $e^+e^-$  linear colliders are discussed.

## 1 Introduction

Revealing the physical mechanism which breaks the electroweak symmetries is one of the key problems in particle physics. If the fundamental particles of the Standard Model—leptons, quarks and gauge bosons—remain weakly interacting up to very high energies, potentially close to the Planck scale, the sector in which the electroweak symmetry is broken must contain one or more fundamental scalar Higgs bosons with light masses of the order of the symmetry-breaking scale  $v \simeq 246$  GeV. The masses of the fundamental particles are generated by the interaction with the scalar Higgs field, which is non-zero in the ground state [1]. Alternatively, the symmetry breaking could be generated dynamically by new strong forces characterized by an interaction scale  $\Lambda \sim 1$  TeV and beyond [2]. If global symmetries of the strong interactions are broken spontaneously, the associated Goldstone bosons can be absorbed by the gauge fields, generating the masses of the gauge particles. The masses of leptons and quarks can be generated by interactions with the fermion condensate of the new strong interaction theory. In other strong-interaction scenarios,  $\Lambda > \mathcal{O}(10 \text{ TeV})$ , the low-energy spectrum includes scalar Higgs fields [3] which acquire light masses as pseudo-Goldstone bosons only by collective symmetry breaking. Other breaking mechanisms of the electroweak symmetries are associated with the dynamics in extra space dimensions at low energies [4]. The Higgs field may be identified with the fifth component of a vector field in  $D = 5$  dimensions, or no light Higgs field is realized in four dimensions.

A simple mechanism for the breaking of the electroweak symmetry is incorporated in the Standard Model (SM) [5]. A complex isodoublet scalar field is introduced which acquires a non-vanishing vacuum expectation value by self-interactions, breaking spontaneously the electroweak symmetry  $SU(2)_I \times U(1)_Y$  down to the electromagnetic  $U(1)_{EM}$  symmetry. The interactions of the gauge bosons and fermions with the background field generate the masses of these particles. One scalar field component is not absorbed in this process, manifesting itself as the physical Higgs particle  $H$ .

The mass of the Higgs boson is the only unknown parameter in the symmetry-breaking sector of the Standard Model, while all couplings are fixed by the masses of the particles, a consequence of the Higgs mechanism *sui generis*. However, the mass of the Higgs boson is constrained in two ways. Since the quartic self-coupling of the Higgs field grows indefinitely with rising energy, an upper limit on the Higgs mass can be derived from demanding that the SM particles remain weakly interacting up to a scale  $\Lambda$  [6]. On the other hand, stringent lower bounds on the Higgs mass follow from requiring

the electroweak vacuum to be stable [7]. If the Standard Model is valid up to scales near the Planck scale, the SM Higgs mass is restricted to a narrow window between 130 and 190 GeV. For Higgs masses either above or below this window, new physical phenomena are expected to occur at a scale  $\Lambda$  between  $\sim 1$  TeV and the Planck scale. For Higgs masses of order 1 TeV, the scale of new strong interactions would be as low as  $\sim 1$  TeV [6, 8].

The electroweak observables are affected by the Higgs mass through radiative corrections [9]. Despite the weak logarithmic dependence to leading order, the high-precision electroweak data, cf. Fig. 1, indicate a preference for light Higgs masses close to  $\sim 100$  GeV [10]. At the 95% CL, they require a value of the Higgs mass less than  $\sim 144$  GeV. By searching directly for the SM Higgs particle, the LEP experiments have set a lower limit of  $M_H \gtrsim 114$  GeV on the Higgs mass [11]. Since the Higgs boson has not been found at LEP2, the search will continue at the Tevatron, which may reach masses up to  $\sim 140$  GeV [12]. The proton collider LHC can sweep the entire canonical Higgs mass range of the Standard Model [13, 14]. While first steps in analysing the properties of the Higgs particle can be taken at the LHC, a comprehensive and high-resolution picture of the Higgs mechanism can be established experimentally by performing very accurate analyses at  $e^+e^-$  linear colliders [15].

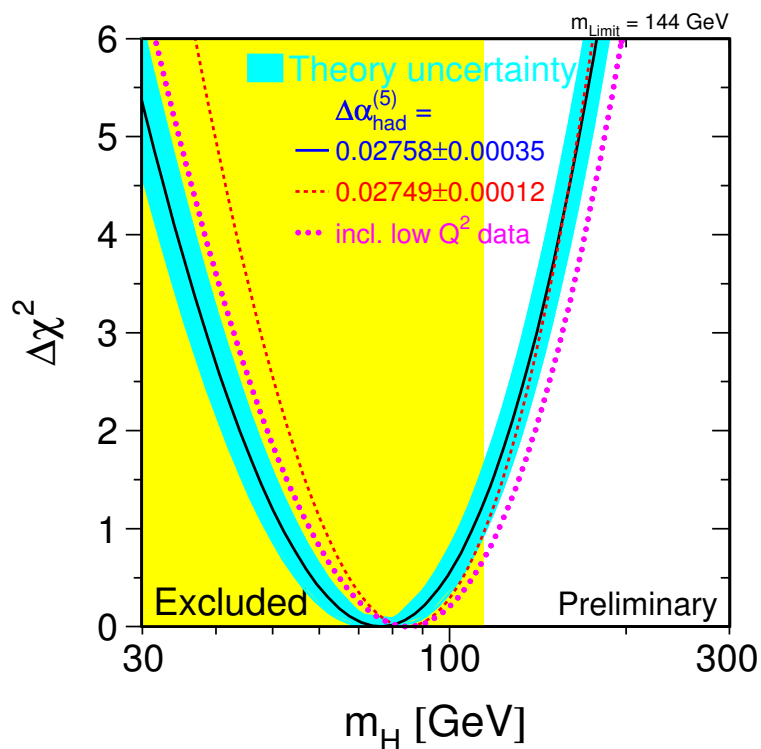


**Fig. 1:** The  $\Delta\chi^2$  curve derived from high- $Q^2$  precision electroweak measurements, performed at LEP, SLC and Tevatron, as a function of the Higgs boson mass in the Standard Model

If the Standard Model is embedded in a Grand Unified Theory (GUT) at high energies, the scale of electroweak symmetry breaking would naively be expected to be close to the unification scale  $M_{GUT}$ . Supersymmetry [16] provides a solution of this hierarchy problem. Once the fundamental parameters of the supersymmetric theory and its breaking mechanism are generated at the terascale, the quadratically divergent contributions to the radiative corrections of the scalar Higgs boson mass are cancelled by the destructive interference between bosonic and fermionic loops in supersymmetric theories [17]. The Minimal Supersymmetric extension of the Standard Model (MSSM) provides an illustrative example for deriving a terascale theory from a supersymmetric grand unified theory. A strong indication for the realization of the basic components of this physical picture in nature is the excellent agreement between the value of the electroweak mixing angle  $\sin^2\theta_W$  predicted by the unification of the gauge

couplings, and the experimentally measured value. If the gauge couplings are unified in the minimal supersymmetric theory at a scale  $M_{GUT} = \mathcal{O}(10^{16} \text{ GeV})$ , the electroweak mixing angle is predicted to be  $\sin^2 \theta_W = 0.2336 \pm 0.0017$  [18] for a mass spectrum of the supersymmetric particles of order  $M_Z$  to 1 TeV. This theoretical prediction is matched very well by the experimental result  $\sin^2 \theta_W^{exp} = 0.23153 \pm 0.00016$  [10]; the difference between the two numbers is less than 2 per-mille.

In the MSSM, the Higgs sector is built up by two Higgs doublets [19]. The doubling is necessary to generate masses for up- and down-type fermions in a supersymmetric theory and to render the theory anomaly-free. The Higgs particle spectrum consists of a quintet of states: two  $\mathcal{CP}$ -even scalar neutral ( $h, H$ ), one  $\mathcal{CP}$ -odd pseudoscalar neutral ( $A$ ), and a pair of charged ( $H^\pm$ ) Higgs bosons [20]. The masses of the heavy Higgs bosons,  $H, A, H^\pm$ , are expected to be of order  $v$ , but they may extend up to the TeV range. By contrast, since the quartic Higgs self-couplings are determined by the gauge couplings, the mass of the lightest Higgs boson  $h$  is constrained stringently. At tree level, the mass has been predicted to be smaller than the  $Z$  mass [20]. Radiative corrections, increasing as the fourth power of the top mass, shift the upper limit to a value between  $\sim 100 \text{ GeV}$  and  $\sim 140 \text{ GeV}$ , depending on the parameter  $\tan \beta$ , the ratio of the vacuum expectation values of the two neutral scalar Higgs fields.

Extensions beyond the minimal supersymmetric form of the theory may be motivated by slight fine-tuning problems in accommodating the experimentally observed  $Z$ -boson mass. The expansion of the Higgs sector introduces new couplings which grow with rising scale. In parallel with the Standard Model, the lightest Higgs boson mass is bounded [21] to less than about 200 GeV, however, if the fields remain weakly interacting up to scales close to the Planck scale.

A general lower bound of 91 GeV in  $\mathcal{CP}$ -invariant theories has been experimentally established for the Higgs particle  $h$  at LEP [11]. The search for  $h$  masses in excess of  $\sim 100 \text{ GeV}$  and the search for the heavy Higgs bosons continues at the Tevatron, the LHC and  $e^+e^-$  linear colliders.

A light Higgs boson may also be generated as a (pseudo-)Goldstone boson by spontaneous breaking of global symmetries of new interactions at multi-TeV scales, the mass kept small by collective symmetry-breaking mechanisms. Alternatively to supersymmetry, the quadratic divergencies of the Standard Model are cancelled by new partners of the Standard Model particles that do not differ in the fermionic/bosonic character. Symmetry schemes constrain the couplings in such a way that the cancellations are achieved in a natural way. Such scenarios are realized in Little Higgs models [3] which predict a large ensemble of new SM-type particles in the mass range of a few TeV.

Elastic-scattering amplitudes of massive vector bosons grow indefinitely with energy if they are calculated in a perturbative expansion in the weak coupling of a non-Abelian gauge theory. As a result, they violate unitarity beyond a critical energy scale of  $\sim 1.2 \text{ TeV}$ . Apart from introducing a light Higgs boson, this problem can also be solved by assuming that the  $W$  bosons become strongly interacting at TeV energies, thus damping the rise of the elastic-scattering amplitudes. Naturally, the strong forces between the  $W$  bosons may be traced back to new fundamental interactions characterized by a scale of order 1 TeV [2]. If the underlying theory is globally chiral-invariant, this symmetry may be broken spontaneously. The Goldstone bosons associated with the spontaneous breaking of the symmetry can be absorbed by gauge bosons to generate their masses and to build up the longitudinal components of their wave functions.

Since the longitudinally polarized  $W$  bosons are associated with the Goldstone modes of chiral symmetry breaking, the scattering amplitudes of the  $W_L$  bosons can be predicted for high energies by a systematic expansion in the energy. The leading term is parameter-free, a consequence of the chiral symmetry-breaking mechanism *per se*, which is independent of the particular structure of the dynamical theory. The higher-order terms in the chiral expansion, however, are defined by the detailed structure of the underlying theory. With rising energy the chiral expansion is expected to diverge and new resonances may be generated in  $WW$  scattering at mass scales between 1 and 3 TeV. This picture is analogous to pion dynamics in QCD, where the threshold amplitudes can be predicted in a chiral expansion, while at higher energies vector and scalar resonances are formed in  $\pi\pi$  scattering.

Such a scenario can be studied in  $WW$  scattering experiments where the  $W$  bosons are radiated, as quasi-real particles [22], off high-energy quarks in the proton beams of the LHC [13], [23–25], or off electrons and positrons in TeV linear colliders [15, 26, 27].

In theories formulated in extra space dimensions, suitably chosen boundary conditions for fields in the compactified space can be exploited to break symmetries [4]. In one class of models, the Higgs fields are identified with the zero-mass fifth components of vector boson fields, associated with broken gauge symmetries beyond the Standard Model, while other massive fifth components are transformed to the longitudinal degrees of freedom for the vector bosons of the Standard Model. Alternatively, the electroweak symmetries can be broken by transforming all fifth components to longitudinal components of the vector fields, ground-state vectors as well as Kaluza–Klein state vectors, so that higgsless theories emerge in such a scenario. In any such theory of extra space dimensions, Kaluza–Klein towers are generated above the Standard Model states. The additional exchange of the Kaluza–Klein towers in  $WW$  scattering damps the scattering amplitude of the Standard Model and allows one in principle to extend the theory to energies beyond the 1.2 TeV unitarity bound of naive higgsless scenarios.

This report is divided into three parts. A basic introduction and a summary of the main theoretical and experimental results will be presented in the next section on the Higgs sector of the Standard Model. Also the search for the Higgs particle at hadron and future  $e^+e^-$  colliders will be described. In the same way, the Higgs spectrum of supersymmetric theories will be discussed in the subsequent section. The main features of strong  $W$  interactions and their analysis in  $WW$  scattering experiments will be presented in the last section.

Only basic elements of electroweak symmetry breaking and Higgs mechanism can be reviewed in this report which is an updated version of the reports Ref. [28] and Refs. [29]. Other aspects may be traced back from Refs. [30], the canon Ref. [31] and the recent reports Refs. [32].

## 2 The Higgs sector of the Standard Model

### 2.1 Physical basis

At high energies, the amplitude for the elastic scattering of massive  $W$  bosons,  $WW \rightarrow WW$ , grows indefinitely with energy for longitudinally polarized particles, Fig. 2(a). This is a consequence of the linear rise of the longitudinal  $W_L$  wave function  $\epsilon_L = (p, 0, 0, E)/M_W$  with the energy of the particle. Even though the term of the scattering amplitude rising as the fourth power in the energy is cancelled by virtue of the non-Abelian gauge symmetry, the amplitude remains quadratically divergent in the energy. On the other hand, unitarity requires elastic-scattering amplitudes of partial waves  $J$  to be bounded by  $\Re e A_J \leq 1/2$ . Applied to the asymptotic  $S$ -wave amplitude  $A_0 = G_F s / 8\pi\sqrt{2}$  of the isospin-zero channel  $2W_L^+ W_L^- + Z_L Z_L$ , the bound [33]

$$s \leq 4\pi\sqrt{2}/G_F \sim (1.2 \text{ TeV})^2 \quad (1)$$

on the c.m. energy  $\sqrt{s}$  can be derived for the validity of a theory of weakly coupled massive gauge bosons.

However, the quadratic rise in the energy can be damped by exchanging a new scalar particle, Fig. 2(b). To achieve the cancellation, the size of the coupling must be given by the product of the gauge coupling with the gauge boson mass. For high energies, the amplitude  $A'_0 = -G_F s / 8\pi\sqrt{2}$  cancels exactly the quadratic divergence of the pure gauge-boson amplitude  $A_0$ . Thus, unitarity can be restored by introducing a fundamental, weakly coupled Higgs particle.

In the same way, the linear divergence of the amplitude  $A(f\bar{f} \rightarrow W_L W_L) \sim gm_f\sqrt{s}$  for the annihilation of a fermion–antifermion pair to a pair of longitudinally polarized gauge bosons can be damped by adding the Higgs exchange to the gauge-boson exchange. In this case the Higgs particle must couple proportionally to the mass  $m_f$  of the fermion  $f$ .

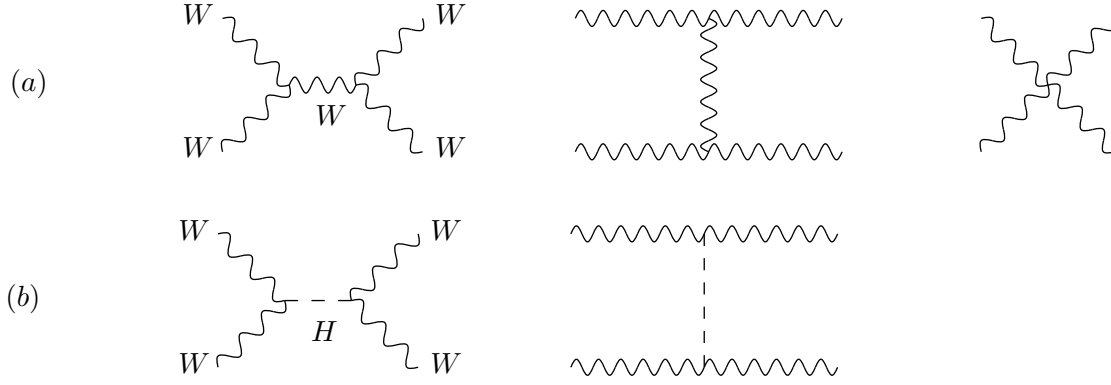


**Fig. 2:** Generic diagrams of elastic  $WW$  scattering: (a) pure gauge-boson dynamics; (b) Higgs-boson exchange

These observations can be summarized in a rule: *A theory of massive gauge bosons and fermions which are weakly coupled up to asymptotic energies, requires, by unitarity, the existence of a Higgs particle; the Higgs particle is a scalar  $0^+$  particle that couples to other particles proportionally to the masses of the particles.*

The assumption that the couplings of the fundamental particles are weak up to asymptotic energies is qualitatively supported by the perturbative renormalization of the electroweak mixing angle  $\sin^2 \theta_W$  from the symmetry value  $3/8$  at the GUT scale down to  $\sim 0.2$  at the electroweak scale, which is close to the experimentally observed value.

These ideas can be cast into an elegant mathematical form by interpreting the electroweak interactions as a gauge theory with spontaneous symmetry breaking in the scalar sector<sup>1</sup>. Such a theory consists of fermion fields, gauge fields, and a scalar field coupled by the standard gauge interactions and Yukawa interactions to the other fields. Moreover, a self-interaction

$$V = \frac{\lambda}{2} \left[ |\phi|^2 - \frac{v^2}{2} \right]^2 \quad (2)$$

is introduced in the scalar sector, which leads to a non-zero ground-state value  $v/\sqrt{2}$  of the scalar field. By fixing the phase of the vacuum amplitude at an arbitrarily chosen value, say zero, the gauge symmetry is broken spontaneously in the scalar sector. Interactions of the gauge fields with the scalar background field, Fig. 3(a), and Yukawa interactions of the fermion fields with the background field, Fig. 3(b), shift the masses of these fields from zero to non-zero values:

$$\begin{aligned} (a) \quad \frac{1}{q^2} &\rightarrow \frac{1}{q^2} + \sum_j \frac{1}{q^2} \left[ \left( \frac{gv}{2} \right)^2 \frac{1}{q^2} \right]^j = \frac{1}{q^2 - M^2} \quad : \quad M^2 = g^2 \frac{v^2}{4} \\ (b) \quad \frac{1}{\not{q}} &\rightarrow \frac{1}{\not{q}} + \sum_j \frac{1}{\not{q}} \left[ \frac{g_f v}{\sqrt{2}} \frac{1}{\not{q}} \right]^j = \frac{1}{\not{q} - m_f} \quad : \quad m_f = g_f \frac{v}{\sqrt{2}}. \end{aligned} \quad (3)$$

Thus, in theories with gauge and Yukawa interactions, in which the scalar field acquires a non-zero ground-state value, the couplings are naturally proportional to the masses. This ensures the unitarity of the theory as discussed before. These theories are renormalizable (as a result of the gauge invariance, which is only disguised in the unitary formulation adopted here), and thus they describe a well-defined physical system.

<sup>1</sup>The mechanisms of spontaneous symmetry breaking, including the Goldstone theorem as well as the Higgs mechanism, are exemplified for the illustrative  $O(3)$   $\sigma$  model in Appendix A.

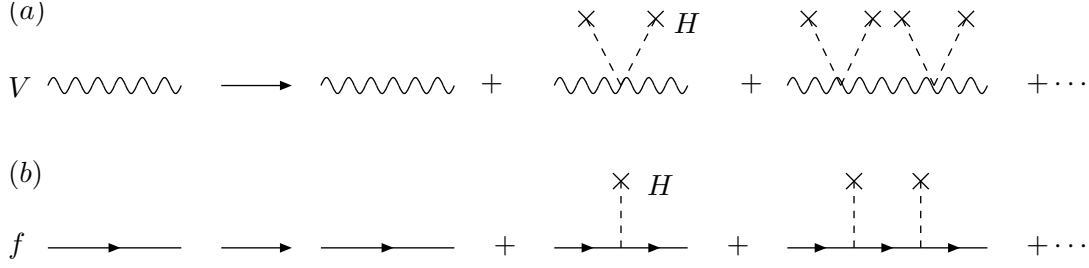


**Fig. 3:** Generating (a) gauge boson and (b) fermion masses through interactions with the scalar background field

## 2.2 The Higgs mechanism in the Standard Model

Besides the Yang–Mills and the fermion parts, the electroweak  $SU_2 \times U_1$  Lagrangian includes a scalar isodoublet field  $\phi$ , coupled to itself in the potential  $V$ , cf. Eq. (2), to the gauge fields through the covariant derivative  $iD = i\partial - g\vec{I}\vec{W} - g'YB$ , and to the up and down fermion fields  $u, d$  by Yukawa interactions:

$$\mathcal{L}_0 = |D\phi|^2 - \frac{\lambda}{2} \left[ |\phi|^2 - \frac{v^2}{2} \right]^2 - g_d \bar{d}_L \phi d_R - g_u \bar{u}_L \phi_c u_R + \text{hc} . \quad (4)$$

In the unitary gauge, the isodoublet  $\phi$  is effectively replaced by the physical Higgs field  $H$ ,  $\phi \rightarrow [0, (v + H)/\sqrt{2}]$ , which describes the fluctuation of the  $I_3 = -1/2$  component about the ground-state value  $v/\sqrt{2}$ . The scale  $v$  of the electroweak symmetry breaking is fixed by the weak gauge coupling and the  $W$  mass, which in turn can be re-expressed by the Fermi coupling:

$$v = 1/\sqrt{\sqrt{2}G_F} \approx 246 \text{ GeV} . \quad (5)$$

While the  $W$  mass is related to  $v$  by the gauge coupling, the Yukawa couplings  $g_f$  and the quartic coupling  $\lambda$  can likewise be re-expressed in terms of the Higgs mass  $M_H$  and the fermion masses  $m_f$ :

$$\begin{aligned} M_W^2 &= g^2 v^2 / 4 , \\ m_f &= g_f v / \sqrt{2} , \\ M_H^2 &= \lambda v^2 , \end{aligned} \quad (6)$$

respectively.

Since the couplings of the Higgs particle to gauge particles, to fermions, and to itself are given by the gauge couplings and the masses of the particles, the only unknown parameter in the Higgs sector (apart from the CKM mixing matrix) is the Higgs mass. When this mass is fixed, all properties of the Higgs particle can be predicted, i.e., the lifetime and decay branching ratios, as well as the production mechanisms and the corresponding cross-sections.

### 2.2.1 The Standard Model Higgs mass

Even though the mass of the Higgs boson cannot be predicted in the Standard Model, stringent upper and lower bounds can nevertheless be derived from internal consistency conditions and extrapolations of the model to high energies.

The Higgs boson has been introduced as a fundamental particle to render 2–2 scattering amplitudes involving longitudinally polarized  $W$  bosons compatible with unitarity. Based on the general principle of time–energy uncertainty, particles must decouple from a physical system if their mass grows indefinitely. The mass of the Higgs particle must therefore be bounded to restore unitarity in the perturbative regime. From the asymptotic expansion of the elastic  $W_L W_L$   $S$ -wave scattering amplitude including  $W$  and

Higgs exchanges,  $A(W_L W_L \rightarrow W_L W_L) \rightarrow -G_F M_H^2 / 4\sqrt{2}\pi$ , it follows [33] that

$$M_H^2 \leq 2\sqrt{2}\pi/G_F \sim (850 \text{ GeV})^2. \quad (7)$$

Within the canonical formulation of the Standard Model, consistency conditions therefore require a Higgs mass below 1 TeV.

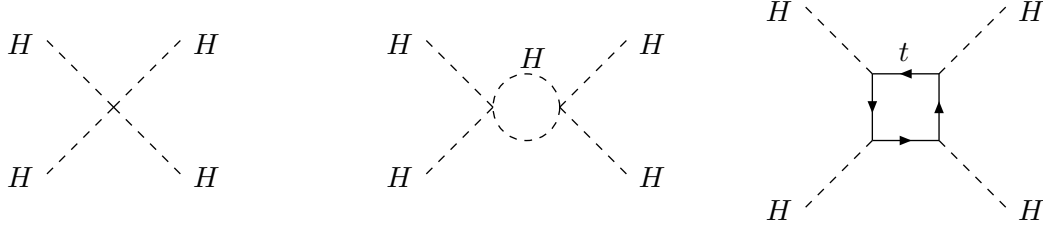


**Fig. 4:** Diagrams generating the evolution of the Higgs self-interaction  $\lambda$

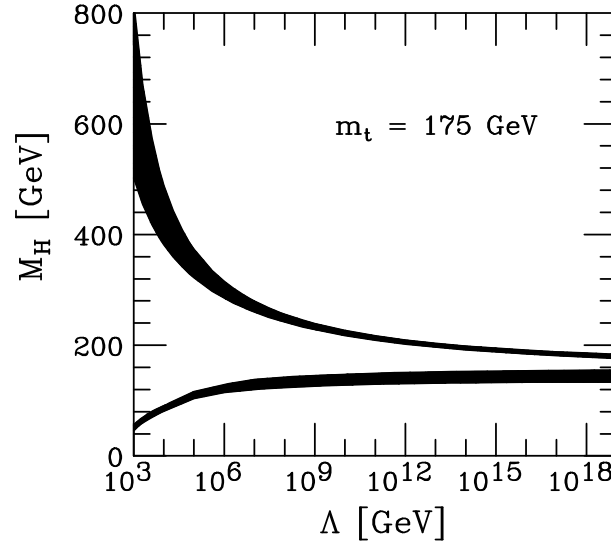


**Fig. 5:** Bounds on the mass of the Higgs boson in the Standard Model.  $\Lambda$  denotes the energy scale at which the SM Higgs boson with mass  $M_H$  would become strongly interacting (upper bound); the lower bound follows from the requirement of vacuum stability. Refs. [6, 7].

Quite restrictive bounds on the value of the SM Higgs mass follow from limits on the energy scale  $\Lambda$  up to which the Standard Model can be extended before new strong interaction phenomena emerge. The key to these bounds is the evolution of the quartic coupling  $\lambda$  with the energy due to quantum fluctuations [6]. The basic contributions are depicted in Fig. 4. The Higgs loop itself gives rise to an indefinite increase of the coupling while the fermionic top-quark loop, with increasing top mass, drives the coupling to smaller values, finally even to values below zero. The variation of the quartic Higgs coupling  $\lambda$  and the top-Higgs Yukawa coupling  $g_t$  with energy, parametrized by  $t = \log \mu^2/v^2$ , may be written as [6]

$$\begin{aligned} \frac{d\lambda}{dt} &= \frac{3}{8\pi^2} [\lambda^2 + \lambda g_t^2 - g_t^4] \quad : \quad \lambda(v^2) = M_H^2/v^2 \\ \frac{dg_t}{dt} &= \frac{1}{32\pi^2} \left[ \frac{9}{2} g_t^3 - 8g_t g_s^2 \right] \quad : \quad g_t(v^2) = \sqrt{2} m_f/v. \end{aligned} \quad (8)$$

Only the leading loop contributions from Higgs, top, and QCD [coupling  $g_s$ ] are taken into account.

For moderate top masses, the quartic coupling  $\lambda$  rises indefinitely,  $d\lambda/dt \sim +\lambda^2$ , and the coupling becomes strong shortly before reaching the Landau pole:

$$\lambda(\mu^2) = \frac{\lambda(v^2)}{1 - \frac{3\lambda(v^2)}{8\pi^2} \log \frac{\mu^2}{v^2}}. \quad (9)$$

Re-expressing the initial value of  $\lambda(v^2)$  by the Higgs mass, the condition  $\lambda(\Lambda^2) < \infty$ , can be translated to an upper bound on the Higgs mass:

$$M_H^2 \leq \frac{8\pi^2 v^2}{3 \log \Lambda^2/v^2}. \quad (10)$$

This mass bound is related logarithmically to the energy  $\Lambda$  up to which the Standard Model is assumed to be valid. The maximal value of  $M_H$  for the minimal cut-off  $\Lambda \sim 1$  TeV is given by  $\sim 750$  GeV. This bound is close to the estimate of  $\sim 700$  GeV in lattice calculations for  $\Lambda \sim 1$  TeV, which allow proper control of non-perturbative effects near the boundary [8].

**Table 1:** Higgs mass bounds for two values of the cut-off  $\Lambda$

$\Lambda$	$M_H$
1 TeV	60 GeV $\lesssim M_H \lesssim$ 700 GeV
$10^{19}$ GeV	130 GeV $\lesssim M_H \lesssim$ 190 GeV

A lower bound on the Higgs mass can be derived from the requirement of vacuum stability [6, 7]. Since top-loop corrections reduce  $\lambda$ , driven finally to negative values, the self-energy potential becomes unbounded negative and the ground state is no longer stable. To avoid the instability for cut-off values less than  $\Lambda$ , the Higgs mass must exceed a minimal value depending on the cut-off  $\Lambda$ .

The scales  $\Lambda$  up to which the Standard Model can be extended before new interactions must become effective are displayed in Fig. 5 as a function of the Higgs mass. The allowed Higgs mass values are collected in Table 1 for two specific cut-off values of  $\Lambda$ . If the Standard Model is assumed to be valid up to the Planck scale, the Higgs mass is restricted to a narrow window between 130 and 190 GeV. The window is widened to 200 GeV for the cut-off near the grand unification scale. The observation of a Higgs mass above or below this window would demand a new physics scale below the Planck/GUT scales.

Indirect evidence for a light Higgs boson can be derived from the high-precision measurements of electroweak observables at LEP and elsewhere. Indeed, the fact that the Standard Model is renormalizable only after including the top and Higgs particles in the loop corrections indicates that the electroweak observables are sensitive to the masses of these particles.

The Fermi coupling can be rewritten in terms of the weak coupling and the  $W$  mass; to lowest order,  $G_F/\sqrt{2} = g^2/8M_W^2$ . After substituting the electromagnetic coupling  $\alpha$ , the electroweak mixing angle and the  $Z$  mass for the weak coupling and the  $W$  mass, this relation can be rewritten as

$$\frac{G_F}{\sqrt{2}} = \frac{2\pi\alpha}{\sin^2 2\theta_W M_Z^2} [1 + \Delta r_\alpha + \Delta r_t + \Delta r_H]. \quad (11)$$

The terms  $\Delta$  take account of the radiative corrections, cf. Fig. 6:  $\Delta r_\alpha$  describes the shift in the electromagnetic coupling  $\alpha$  if evaluated at the scale  $M_Z^2$  instead of zero-momentum;  $\Delta r_t$  denotes the top/bottom

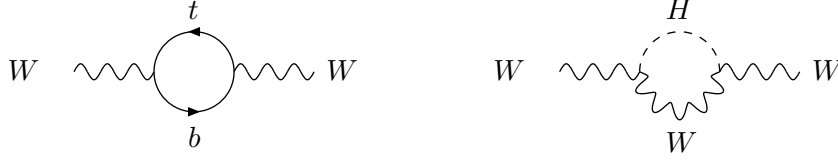


**Fig. 6:** Virtual t,b and W,Higgs radiative corrections to the propagators of the electroweak gauge boson

quark contributions to the  $W$  and  $Z$  masses, which are quadratic in the top mass. Finally,  $\Delta r_H$  accounts for the virtual Higgs contribution to the masses; this term depends only logarithmically [9] on the Higgs mass at leading order:

$$\Delta r_H = \frac{G_F M_Z^2 (1 + 9 \sin^2 \theta_W)}{24\sqrt{2}\pi^2} \log \frac{M_H^2}{M_W^2} + \dots \quad (M_H^2 \gg M_W^2). \quad (12)$$

The screening effect reflects the role of the Higgs field as a regulator that renders the electroweak theory renormalizable.

Although the sensitivity on the Higgs mass is only logarithmic, the increasing precision in the measurement of the electroweak observables allows us to derive interesting estimates and constraints on the Higgs mass [10], cf. Fig. 1:

$$\begin{aligned} M_H &= 76_{-24}^{+33} \text{ GeV} \\ &\lesssim 144 \text{ GeV} \quad (95\% \text{ CL}). \end{aligned} \quad (13)$$

With a value of 15.1%, the probability for the fit is not overwhelmingly large but not forbiddingly small either. The 95% confidence level is still significantly above the direct search limit,

$$M_H \geq 114.1 \text{ GeV} \quad (14)$$

derived from LEP2 analyses, Ref. [11], of the dominant Higgs-strahlung channel  $e^+e^- \rightarrow ZH$ .

It may be concluded from these numbers that the canonical formulation of the Standard Model including the existence of a light Higgs boson is compatible with the electroweak data. However, alternative mechanisms cannot be ruled out if the system is opened up to contributions from physics areas beyond the Standard Model.

### 2.2.2 Decays of the Higgs particle

The profile of the Higgs particle is uniquely determined if the Higgs mass is fixed. The strength of the coupling of the Higgs boson to the electroweak gauge bosons  $V = W, Z$  is fixed by their masses  $M_V$ , and the strength of the Yukawa couplings of the Higgs boson to fermions is set by the fermion masses  $m_f$ ; the couplings may be defined uniformly as

$$\begin{aligned} g_{HVV} &= \left[ 2\sqrt{2}G_F \right]^{1/2} M_V \\ g_{Hff} &= \left[ 2\sqrt{2}G_F \right]^{1/2} m_f. \end{aligned} \quad (15)$$

The total decay width and lifetime, as well as the branching ratios for specific decay channels, are determined by these parameters. The measurement of the decay characteristics can therefore be exploited to establish, experimentally, that Higgs couplings grow with the masses of the particles, a direct consequence of the Higgs mechanism.

For Higgs particles in the intermediate mass range  $\mathcal{O}(M_Z) \leq M_H \leq 2M_Z$ , the main decay modes are decays into  $b\bar{b}$  pairs and  $WW, ZZ$  pairs, one of the gauge bosons being virtual below the

respective thresholds. Above the  $WW, ZZ$  pair thresholds, the Higgs particles decay almost exclusively into these two channels, with a small admixture of top decays near the  $t\bar{t}$  threshold. Below 140 GeV, the decays  $H \rightarrow \tau^+\tau^-, c\bar{c}$  and  $gg$  are also important besides the dominating  $b\bar{b}$  channel;  $\gamma\gamma$  decays, though suppressed in rate, nevertheless provide a clear 2-body signature for the formation of Higgs particles in this mass range.

### 2.2.2.1 Higgs decays to fermions

The partial width of Higgs decays to lepton and quark pairs is given by [34]

$$\Gamma(H \rightarrow f\bar{f}) = \mathcal{N}_c \frac{G_F}{4\sqrt{2}\pi} m_f^2(M_H^2) M_H, \quad (16)$$

$\mathcal{N}_c = 1$  or  $3$  being the colour factor. (Near the threshold the partial width is suppressed by the additional  $P$ -wave factor  $\beta_f^3$ , where  $\beta_f$  is the fermion velocity.) Asymptotically, the fermionic width grows only linearly with the Higgs mass. The bulk of QCD radiative corrections can be mapped into the scale dependence of the quark mass, evaluated at the Higgs mass. For  $M_H \sim 100$  GeV the relevant parameters are  $m_b(M_H^2) \simeq 3$  GeV and  $m_c(M_H^2) \simeq 0.6$  GeV. The reduction of the effective  $c$ -quark mass overcompensates the colour factor in the ratio between charm and  $\tau$  decays of Higgs bosons. The residual QCD corrections,  $\sim 5.7 \times (\alpha_s/\pi)$ , modify the widths only slightly.

### 2.2.2.2 Higgs decays to $WW$ and $ZZ$ boson pairs

Above the  $WW$  and  $ZZ$  decay thresholds, the partial widths for these channels may be written as [35]

$$\Gamma(H \rightarrow VV) = \delta_V \frac{G_F}{16\sqrt{2}\pi} M_H^3 (1 - 4x + 12x^2) \beta_V, \quad (17)$$

where  $x = M_V^2/M_H^2$  and  $\delta_V = 2$  and  $1$  for  $V = W$  and  $Z$ , respectively. For large Higgs masses, the vector bosons are longitudinally polarized. Since the wave functions of these states are linear in the energy, the widths grow as the third power of the Higgs mass. Below the threshold for two real bosons, the Higgs particle can decay into  $VV^*$  pairs, one of the vector bosons being virtual. The partial width is given in this case [36] by

$$\Gamma(H \rightarrow VV^*) = \frac{3G_F^2 M_V^4}{16\pi^3} M_H R(x) \delta'_V, \quad (18)$$

where  $\delta'_W = 1$ ,  $\delta'_Z = 7/12 - 10 \sin^2 \theta_W/9 + 40 \sin^4 \theta_W/27$  and

$$R(x) = \frac{3(1 - 8x + 20x^2)}{(4x - 1)^{1/2}} \arccos\left(\frac{3x - 1}{2x^{3/2}}\right) - \frac{1 - x}{2x} (2 - 13x + 47x^2) - \frac{3}{2} (1 - 6x + 4x^2) \log x.$$

The  $ZZ^*$  channel becomes relevant for Higgs masses beyond  $\sim 140$  GeV. Above the threshold, the 4-lepton channel  $H \rightarrow ZZ \rightarrow 4\ell^\pm$  provides a very clear signal for Higgs bosons. Despite of escaping neutrinos in leptonic  $W$  decays, also the  $WW$  decay channel proves useful if the on-shell  $ZZ$  channel is still closed kinematically.

### 2.2.2.3 Higgs decays to $gg$ and $\gamma\gamma$ pairs

In the Standard Model, gluonic Higgs decays are mediated by top- and bottom-quark loops, photonic decays in addition by  $W$  loops. Since these decay modes are significant only far below the top and  $W$  thresholds, they are described by the approximate expressions [37, 38]

$$\Gamma(H \rightarrow gg) = \frac{G_F \alpha_s^2 (M_H^2)}{36\sqrt{2}\pi^3} M_H^3 \left[ 1 + \left( \frac{95}{4} - \frac{7N_F}{6} \right) \frac{\alpha_s}{\pi} \right] \quad (19)$$

$$\Gamma(H \rightarrow \gamma\gamma) = \frac{G_F \alpha^2}{128 \sqrt{2} \pi^3} M_H^3 \left[ \frac{4}{3} \mathcal{N}_C e_t^2 - 7 \right]^2, \quad (20)$$

which are valid in the limit  $M_H^2 \ll 4M_W^2, 4M_t^2$ . The QCD radiative corrections, which include the  $ggg$  and  $gq\bar{q}$  final states in (19), are very important; they increase the partial width by about 65%. Even though photonic Higgs decays are very rare, they nevertheless open an attractive resonance-type channel for the search of Higgs particles.

#### 2.2.2.4 Summary

By adding up all possible decay channels, we obtain the total width shown in Fig. 7(a). Up to masses of 140 GeV, the Higgs particle is very narrow,  $\Gamma(H) \leq 10$  MeV. After the real and virtual gauge-boson channels open up, the state rapidly becomes wider, reaching a width of  $\sim 1$  GeV at the  $ZZ$  threshold. The width cannot be measured directly in the intermediate mass region at the LHC or  $e^+e^-$  colliders. However, it can be determined indirectly; measuring, for example, the partial width  $\Gamma(H \rightarrow WW)$  in the fusion process  $WW \rightarrow H$ , and the branching fraction  $BR(H \rightarrow WW)$  in the decay process  $H \rightarrow WW$ , the total width follows from the ratio of the two observables. Above a mass of  $\sim 250$  GeV, the state would become wide enough to be resolved experimentally.

The branching ratios of the main decay modes are displayed in Fig. 7(b). A large variety of channels will be accessible for Higgs masses below 140 GeV. The dominant mode is  $b\bar{b}$  decays, yet  $c\bar{c}, \tau^+\tau^-$  and  $gg$  decays still occur at a level of several per cent. At  $M_H = 120$  GeV for instance, the branching ratios are 68% for  $b\bar{b}$ , 3.1% for  $c\bar{c}$ , 6.9% for  $\tau^+\tau^-$  and 7% for  $gg$ .  $\gamma\gamma$  decays occur at a level of 1 per-mille. Above this mass value, the Higgs boson decay into  $W$ 's becomes dominant, overwhelming all other channels if the decay mode into two real  $W$ 's is kinematically possible. For Higgs masses far above the thresholds,  $ZZ$  and  $WW$  decays occur at a ratio of 1:2, slightly modified only just above the  $t\bar{t}$  threshold. Since the decay widths to vector-boson pairs grow as the third power of the mass, the Higgs particle becomes very wide asymptotically,  $\Gamma(H) \sim \frac{1}{2} M_H^3$  [TeV]. In fact, for  $M_H \sim 1$  TeV, the width reaches  $\sim \frac{1}{2}$  TeV.

### 2.3 Higgs production at hadron colliders

Several processes can be exploited to produce Higgs particles in hadron colliders [29, 40]:

gluon fusion	: $gg \rightarrow H$
$WW, ZZ$ fusion	: $W^+W^-, ZZ \rightarrow H$
Higgs-strahlung off $W, Z$	: $q\bar{q} \rightarrow W, Z \rightarrow W, Z + H$
Higgs bremsstrahlung off top	: $q\bar{q}, gg \rightarrow t\bar{t} + H$ .

Gluon fusion plays the dominant role throughout the entire Higgs mass range of the Standard Model. While the  $WW/ZZ$  fusion process becomes increasingly important with rising Higgs mass, it also plays an important role in the search for the Higgs boson and the study of its properties in the intermediate mass range. The last two radiation processes are of interest only for light Higgs masses.

The production cross-sections at hadron colliders, at the LHC in particular, are quite sizeable so that a large sample of SM Higgs particles can be produced in this machine. Experimental difficulties arise from the huge number of background events that come along with the Higgs signal events. This problem will be tackled by either triggering on leptonic decays of  $W, Z$  and  $t$  in the radiation processes or by exploiting the resonance character of the Higgs decays  $H \rightarrow \gamma\gamma$  and  $H \rightarrow ZZ \rightarrow 4\ell^\pm$ . In this way, the Tevatron is expected to search for Higgs particles in the mass range above LEP2 up to about 110

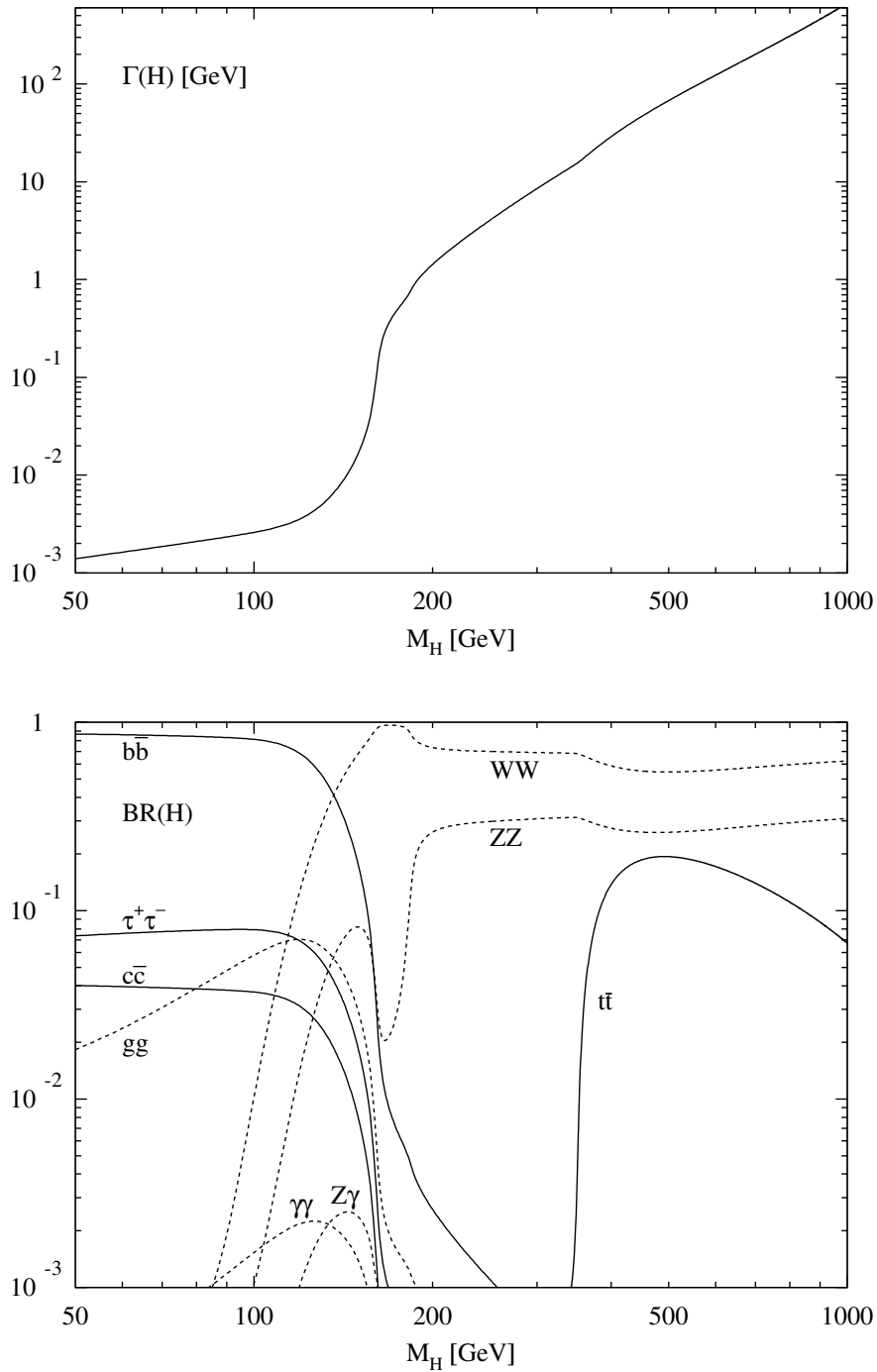


**Fig. 7:** (a) Total decay width (in GeV) of the SM Higgs boson as a function of its mass. (b) Branching ratios of the dominant decay modes of the SM Higgs particle. All relevant higher-order corrections are taken into account. Code: HDECAY, Ref. [39].

to 130 GeV [12]. The LHC is expected to cover the entire canonical Higgs mass range  $M_H \lesssim 700$  GeV of the Standard Model [13].

### 2.3.1 Gluon fusion

The gluon-fusion mechanism [37, 40–42]

$$pp \rightarrow gg \rightarrow H$$

provides the dominant production mechanism of Higgs bosons at the LHC in the entire relevant Higgs mass range up to about 1 TeV. The gluon coupling to the Higgs boson in the SM is mediated by triangular loops of top and bottom quarks, cf. Fig. 8. Since the Yukawa coupling of the Higgs particle to heavy quarks grows with the quark mass, thus balancing the decrease of the triangle amplitude, the form factor approaches a non-zero value for large loop-quark masses. (If the masses of heavy quarks beyond the third generation were generated solely by the Higgs mechanism, these particles would add the same amount to the form factor as the top quark in the asymptotic heavy-quark limit.)

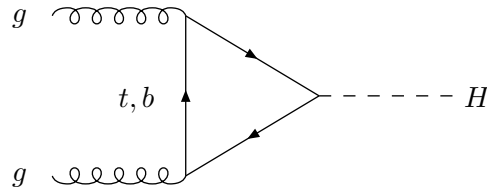


**Fig. 8:** Diagram contributing to the formation of Higgs bosons in gluon–gluon collisions at lowest order

The partonic cross-section, Fig. 8, can be expressed by the gluonic width of the Higgs boson at lowest order [40]:

$$\hat{\sigma}_{LO}(gg \rightarrow H) = \sigma_0 M_H^2 \times BW(\hat{s}) \quad (21)$$

$$\sigma_0 = \frac{\pi^2}{8M_H^2} \Gamma_{LO}(H \rightarrow gg) = \frac{G_F \alpha_s^2}{288\sqrt{2}\pi} \left| \sum_Q A_Q^H(\tau_Q) \right|^2,$$

where the scaling variable is defined as  $\tau_Q = 4M_Q^2/M_H^2$  and  $\hat{s}$  denotes the partonic c.m. energy squared. The form factor can easily be evaluated:

$$A_Q^H(\tau_Q) = \frac{3}{2} \tau_Q [1 + (1 - \tau_Q) f(\tau_Q)] \quad (22)$$

$$f(\tau_Q) = \begin{cases} \arcsin^2 \frac{1}{\sqrt{\tau_Q}} & \tau_Q \geq 1 \\ -\frac{1}{4} \left[ \log \frac{1 + \sqrt{1 - \tau_Q}}{1 - \sqrt{1 - \tau_Q}} - i\pi \right]^2 & \tau_Q < 1. \end{cases}$$

For small loop masses the form factor vanishes,  $A_Q^H(\tau_Q) \sim -3/8\tau_Q [\log(\tau_Q/4) + i\pi]^2$ , while for large loop masses it approaches a non-zero value,  $A_Q^H(\tau_Q) \rightarrow 1$ . The final term  $BW$  is the normalized Breit–Wigner function

$$BW(\hat{s}) = \frac{M_H \Gamma_H / \pi}{[\hat{s} - M_H^2]^2 + M_H^2 \Gamma_H^2} \quad (23)$$

approaching in the narrow-width approximation a  $\delta$ -function at  $\hat{s} = M_H^2$ .

In the narrow-width approximation, the hadronic cross-section can be cast into the form

$$\sigma_{LO}(pp \rightarrow H) = \sigma_0 \tau_H \frac{d\mathcal{L}^{gg}}{d\tau_H}, \quad (24)$$

with  $d\mathcal{L}^{gg}/d\tau_H$  denoting the  $gg$  luminosity of the  $pp$  collider,

$$d\mathcal{L}^{gg}/d\tau_H = \int_{\tau_H}^1 \frac{d\xi}{\xi} g(\xi; \tau_H s) g(\tau_H/\xi; \tau_H s), \quad (25)$$

built up by the gluon densities  $g$  and evaluated for the Drell–Yan variable  $\tau_H = M_H^2/s$ , where  $s$  is the total hadronic energy squared.

The QCD corrections to the gluon fusion process [37, 40, 42] are very important. They stabilize the theoretical predictions for the cross-section when the renormalization and factorization scales are varied. Moreover, they are large and positive, thus increasing the production cross-section for Higgs bosons. The QCD corrections consist of virtual corrections to the basic process  $gg \rightarrow H$ , and of real corrections due to the associated production of the Higgs boson with massless partons,  $gg \rightarrow Hg$  and  $gq \rightarrow Hq$ ,  $q\bar{q} \rightarrow Hg$ . These subprocesses contribute to Higgs production at  $\mathcal{O}(\alpha_s^3)$ . The virtual corrections rescale the lowest-order fusion cross-section with a coefficient that depends only on the ratios of the Higgs and quark masses. Gluon radiation leads to two-parton final states with invariant energy  $\hat{s} \geq M_H^2$  in the  $gg$ ,  $gq$  and  $q\bar{q}$  channels.

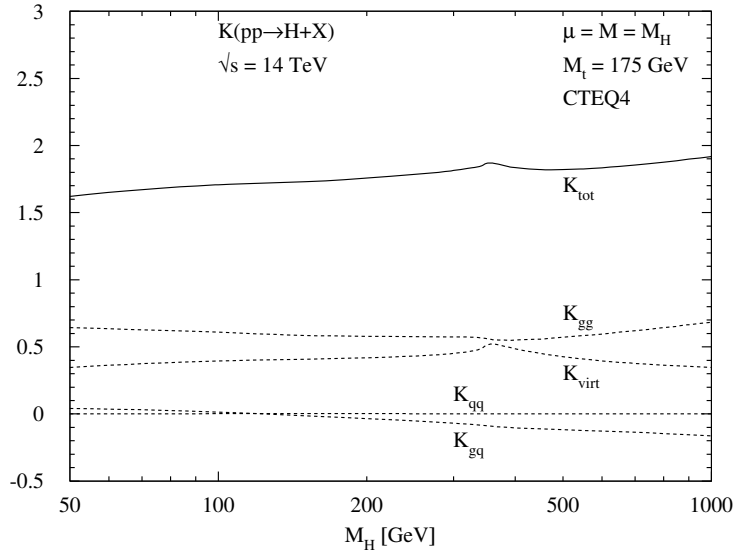


**Fig. 9:**  $K$  factors of the QCD-corrected gluon-fusion cross-section  $\sigma(pp \rightarrow H + X)$  at the LHC with c.m. energy  $\sqrt{s} = 14$  TeV. The dashed lines show the individual contributions of the QCD corrections. The renormalization and factorization scales have been identified with the Higgs mass, and CTEQ4 parton densities have been adopted.

The size of the radiative corrections can be parametrized by defining the  $K$  factor as  $K = \sigma_{NLO}/\sigma_{LO}$ , in which all quantities are evaluated in the numerator and denominator in next-to-leading and leading order, respectively. The results of this calculation are shown in Fig. 9. The virtual corrections  $K_{virt}$  and the real corrections  $K_{gg}$  for the  $gg$  collisions are apparently of the same size, and both are large and positive; the corrections for  $q\bar{q}$  collisions and the  $gq$  inelastic Compton contributions are less important. Depending only mildly on the Higgs bosons mass, the overall  $K$  factor,  $K_{tot}$ , turns out to be close to 2 [37, 40, 42, 43]. The main contributions are generated by the virtual corrections and the 3-parton final states initiated by  $gg$  initial states. Large NLO corrections are expected for these gluon

processes as a result of the large colour charges. However, by studying the next order of corrections in the large top-mass limit, the N<sup>2</sup>LO corrections generate only a modest additional increase of the  $K$  factor,  $\delta_2 K_{tot} \lesssim 0.2$  [44], and even less at N<sup>3</sup>LO [45]. This proves the expansion to be convergent with the most important correction to be attributed to the next-to leading order contribution [43], cf. Fig. 10. In addition, when the higher-order QCD corrections are included, the dependence of the cross-section on the renormalization and factorization scales is significantly reduced, Fig. 11.

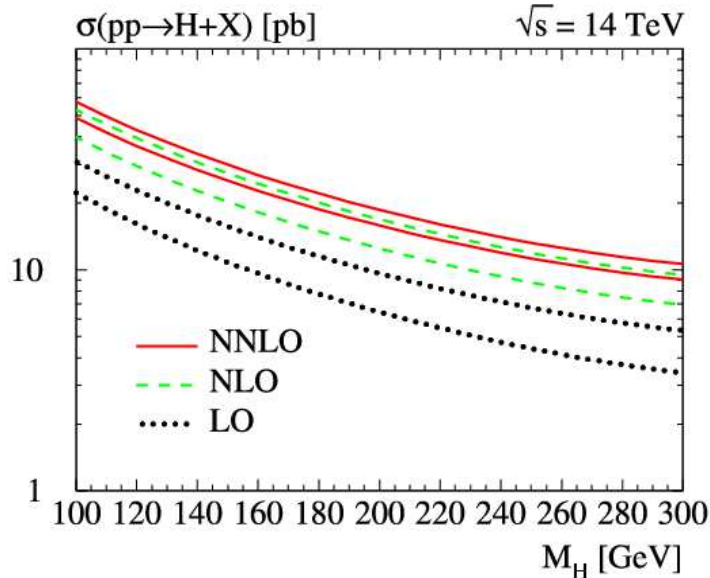


**Fig. 10:** Gluon-fusion cross-section  $\sigma(pp \rightarrow H + X)$  at the LHC with c.m. energy  $\sqrt{s} = 14$  TeV at LO, NLO and NNLO. The size of the error bands is determined by the variation of the renormalization and factorization scales between  $M_H/2$  and  $2M_H$ . First reference in Ref. [44].

The theoretical prediction for the production cross-section of Higgs particles is presented in Fig. 12 for the LHC as a function of the Higgs mass. The cross-section decreases with increasing Higgs mass. This is, to a large extent, a consequence of the sharply falling  $gg$  luminosity for large invariant masses. The bump in the cross-section is induced by the  $t\bar{t}$  threshold in the top triangle. The overall theoretical accuracy of this calculation is expected to be at a level of 10 to 20%.

### 2.3.2 Vector-boson fusion

The second important channel for Higgs production at the LHC is vector-boson fusion,  $W^+W^- \rightarrow H$  [23]. For large Higgs masses this mechanism becomes competitive to gluon fusion; for intermediate masses the cross-section is smaller but very important nevertheless for searching for light Higgs bosons with a reduced background-to-signal ratio and for exploring its properties [46].

For large Higgs masses, the two electroweak bosons  $W, Z$  that form the Higgs boson are predominantly longitudinally polarized. At high energies, the equivalent particle spectra of the longitudinal  $W, Z$  bosons in quark beams are given by

$$f_L^W(x) = \frac{G_F M_W^2}{2\sqrt{2}\pi^2} \frac{1-x}{x} \quad (26)$$

$$f_L^Z(x) = \frac{G_F M_Z^2}{2\sqrt{2}\pi^2} [(I_3^q - 2e_q \sin^2 \theta_W)^2 + (I_3^q)^2] \frac{1-x}{x},$$

where  $x$  is the fraction of energy transferred from the quark to the  $W, Z$  boson in the splitting process

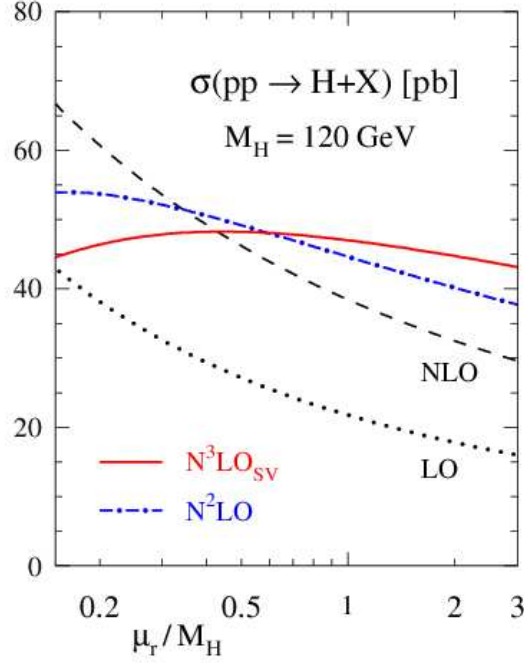


**Fig. 11:** Renormalization-scale dependence of the gluon-fusion cross-section  $\sigma(pp \rightarrow H + X)$  at the LHC with c.m. energy  $\sqrt{s} = 14$  TeV at LO, NLO, NNLO and the soft/virtual approximation at  $N^3\text{LO}$ ; from Ref. [45]

$q \rightarrow q + W/Z$ . From these particle spectra, the  $WW$  and  $ZZ$  luminosities can easily be derived:

$$\begin{aligned} \frac{d\mathcal{L}^{WW}}{d\tau_W} &= \frac{G_F^2 M_W^4}{8\pi^4} \left[ 2 - \frac{2}{\tau_W} - \frac{1 + \tau_W}{\tau_W} \log \tau_W \right] \\ \frac{d\mathcal{L}^{ZZ}}{d\tau_Z} &= \frac{G_F^2 M_Z^4}{8\pi^4} \left[ (I_3^q - 2e_q \sin^2 \theta_W)^2 + (I_3^q)^2 \right] \left[ (I_3^{q'} - 2e_{q'} \sin^2 \theta_W)^2 + (I_3^{q'})^2 \right] \\ &\quad \times \left[ 2 - \frac{2}{\tau_Z} - \frac{1 + \tau_Z}{\tau_Z} \log \tau_Z \right] \end{aligned} \quad (27)$$

with the Drell–Yan variable defined as  $\tau_V = M_{VV}^2/s$ . The cross-section for Higgs production in quark–quark collisions is given by the convolution of the parton cross-sections  $WW, ZZ \rightarrow H$  with the luminosities:

$$\hat{\sigma}(qq \rightarrow qqH) = \frac{d\mathcal{L}^{VV}}{d\tau_V} \sqrt{2\pi} G_F. \quad (28)$$

The hadronic cross-section is finally obtained by summing the parton cross-section (28) over the flux of all possible pairs of quark–quark and antiquark combinations.

Since to lowest order the proton remnants are colour singlets in the  $WW, ZZ$  fusion processes, no colour will be exchanged between the two quark lines from which the two vector bosons are radiated. As a result, the leading QCD corrections to these processes are already accounted for by the corrections to the quark parton densities.

The  $WW/ZZ$  fusion cross-section for Higgs bosons at the LHC is shown in Fig. 12. The process is apparently very important for the search for the Higgs boson in the upper mass range, where the cross-section approaches values close to gluon fusion. For intermediate masses, it comes close within an order of magnitude to the leading gluon-fusion cross-section.

### 2.3.3 Higgs-strahlung off vector bosons

Higgs-strahlung  $q\bar{q} \rightarrow V^* \rightarrow VH$  ( $V = W, Z$ ) is a very important mechanism (Fig. 12) for the search for light Higgs bosons at the hadron colliders Tevatron and LHC. Though the cross-section is smaller than for gluon fusion, leptonic decays of the electroweak vector bosons are useful to filter Higgs signal events out of the huge background. Since the dynamical mechanism is the same as for  $e^+e^-$  colliders (see later), except for the folding with the quark–antiquark densities, intermediate steps of the calculation will not be noted here, and merely the final values of the cross-sections for the Tevatron and the LHC are recorded in Fig. 12.

### 2.3.4 Higgs bremsstrahlung off top quarks

Also the process  $gg, q\bar{q} \rightarrow t\bar{t}H$  is relevant only for small Higgs masses, Fig. 12. The analytical expression for the parton cross-section, even at lowest order, is quite involved, so that just the final results for the LHC cross-section are shown in Fig. 12. Higher order corrections have been presented in Ref. [47]. Separating the signal from the background is experimentally very difficult for this channel.

Nevertheless, Higgs bremsstrahlung off top quarks may be an interesting process for measurements of the fundamental  $Htt$  Yukawa coupling in coherent LHC/LC analyses. The cross-section  $\sigma(pp \rightarrow t\bar{t}H)$  is directly proportional to the square of this fundamental coupling.

### 2.3.5 Summary

A comprehensive overview of the production cross-sections for Higgs particles at the LHC is presented in Fig. 12. Three classes of channels can be distinguished. The gluon fusion of Higgs particles is a universal process, dominant over the entire SM Higgs mass range. Higgs-strahlung off electroweak  $W, Z$  bosons or top quarks is prominent for light Higgs bosons. The  $WW/ZZ$  fusion channel, by contrast, becomes increasingly important in the upper part of the SM Higgs mass range, though it proves very useful also in the intermediate mass range.

The signatures for the search for Higgs particles are dictated by the decay branching ratios. In the lower part of the intermediate mass range, resonance reconstruction in  $\gamma\gamma$  final states and  $b\bar{b}$  jets can be exploited. In the upper part of the intermediate mass range, decays to  $ZZ^*$  and  $WW^*$  are important, with the two electroweak bosons decaying leptonically. In the mass range above the on-shell  $ZZ$  decay threshold, the charged-lepton decays  $H \rightarrow ZZ \rightarrow 4\ell^\pm$  provide a gold-plated signature. At the upper end of the classical SM Higgs mass range, decays to neutrinos and jets, generated in  $W$  and  $Z$  decays, complete the search techniques.

Experimental expectations at the LHC for the search of the Higgs particle in the Standard Model are summarized in Fig. 13. The significance of the Higgs signal is shown as a function of the Higgs mass for the integrated luminosity of  $30 \text{ fb}^{-1}$ . The entire mass range can be covered for searching the SM Higgs boson at the LHC.

Expectations for the search for the SM Higgs boson at the Tevatron are summarized in Fig. 14. The SM Higgs boson may be excluded at the  $2\sigma$  level across the entire intermediate mass range. Discovering the particle, even in restricted mass intervals, is a demanding task which requires the collection of a large integrated luminosity.

## 2.4 Higgs production channels at $e^+e^-$ colliders

The first process that was used to search directly for Higgs bosons over a large mass range, was the Bjorken process,  $Z \rightarrow Z^*H, Z^* \rightarrow f\bar{f}$  [48]. By exploring this production channel, Higgs bosons with masses less than 65.4 GeV were excluded by the LEP1 experiments. The search continued by reversing the role of the real and virtual  $Z$  bosons in the  $e^+e^-$  continuum at LEP2.

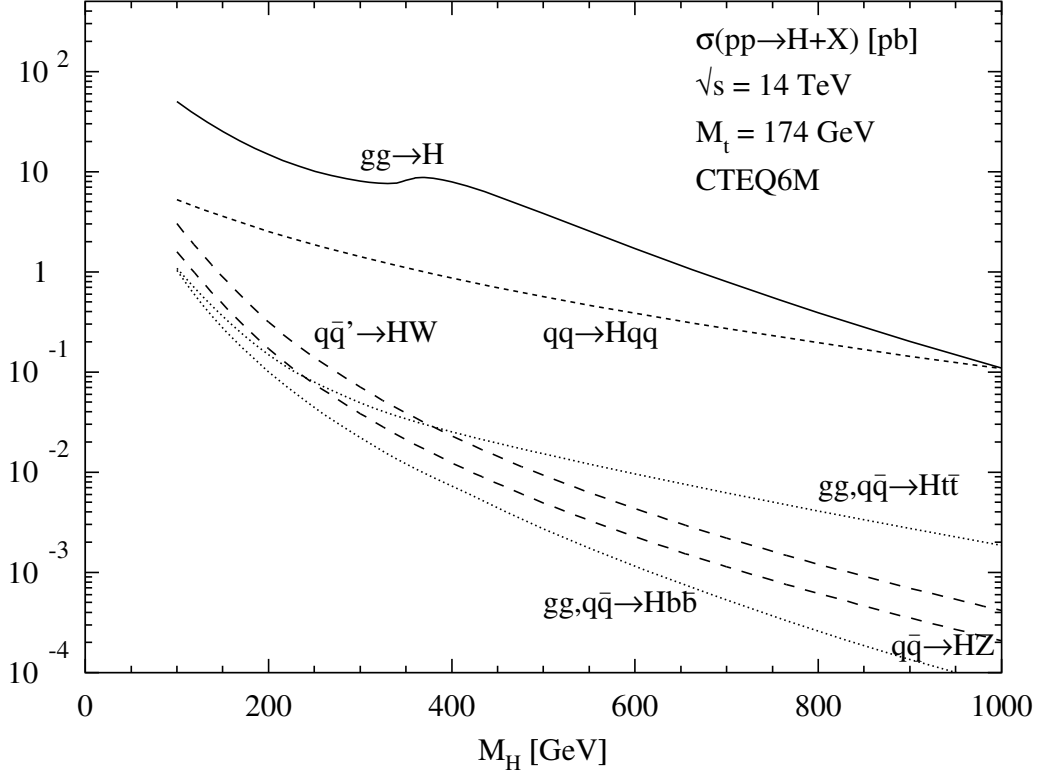


**Fig. 12:** Higgs production cross-sections at the LHC for the various production mechanisms as a function of the Higgs mass. The full QCD-corrected results for the gluon fusion  $gg \rightarrow H$ , vector-boson fusion  $qq \rightarrow VVqq \rightarrow Hqq$ , vector-boson bremsstrahlung  $q\bar{q} \rightarrow V^* \rightarrow HV$  and associated production  $gg, q\bar{q} \rightarrow Ht\bar{t}, Hb\bar{b}$  are shown.

The main production mechanisms for Higgs bosons in  $e^+e^-$  collisions are

$$\text{Higgs-strahlung} : e^+e^- \rightarrow Z^* \rightarrow ZH \quad (29)$$

$$WW \text{ fusion} : e^+e^- \rightarrow \bar{\nu}_e\nu_e(WW) \rightarrow \bar{\nu}_e\nu_e H . \quad (30)$$

In Higgs-strahlung [38,48,49] the Higgs boson is emitted from the  $Z$ -boson line, while  $WW$  fusion is a formation process of Higgs bosons in the collision of two quasi-real  $W$  bosons radiated off the electron and positron beams [50].

As evident from the subsequent analyses, LEP2 could cover the SM Higgs mass range up to about 114 GeV [11]. The high-energy  $e^+e^-$  linear colliders can cover the entire Higgs mass range, the intermediate mass range is covered at a 500 GeV collider [15], the upper mass range is covered in the second phase of the machines expected to reach a total energy of 3 TeV [51].

#### 2.4.1 Higgs-strahlung

The cross-section for Higgs-strahlung can be written in a compact form as

$$\sigma(e^+e^- \rightarrow ZH) = \frac{G_F^2 M_Z^4}{96\pi s} [v_e^2 + a_e^2] \lambda^{1/2} \frac{\lambda + 12M_Z^2/s}{[1 - M_Z^2/s]^2}, \quad (31)$$

where  $v_e = -1 + 4\sin^2\theta_W$  and  $a_e = -1$  are the vector and axial-vector  $Z$  charges of the electron and  $\lambda = [1 - (M_H + M_Z)^2/s][1 - (M_H - M_Z)^2/s]$  is the usual two-particle phase-space function. The cross-section is of the size  $\sigma \sim \alpha_W^2/s$ , i.e., of second order in the weak coupling, and it scales in the squared energy. Higher order contributions to the cross-sections are under theoretical control [52,53].

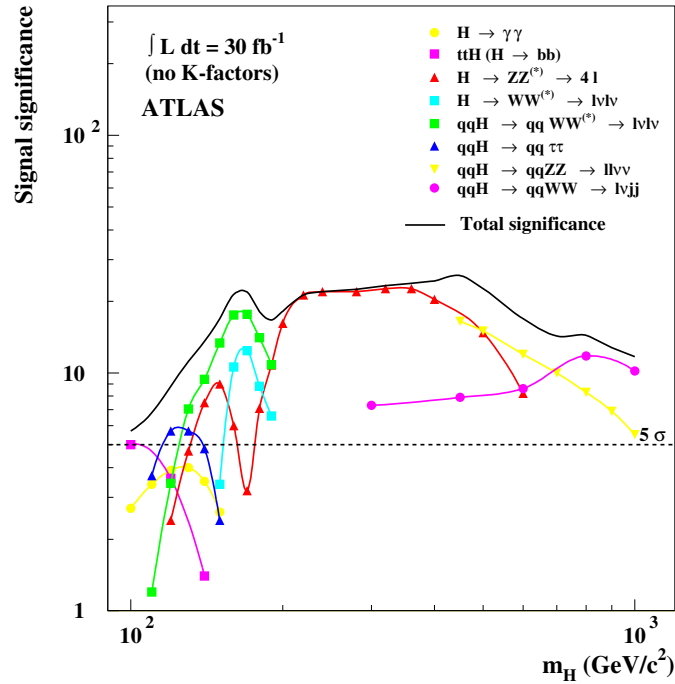


**Fig. 13:** Significances of various channels in the search for the SM Higgs boson at the LHC as a function of the mass for an integrated luminosity of  $30 \text{ fb}^{-1}$ ; Refs. [13, 14]

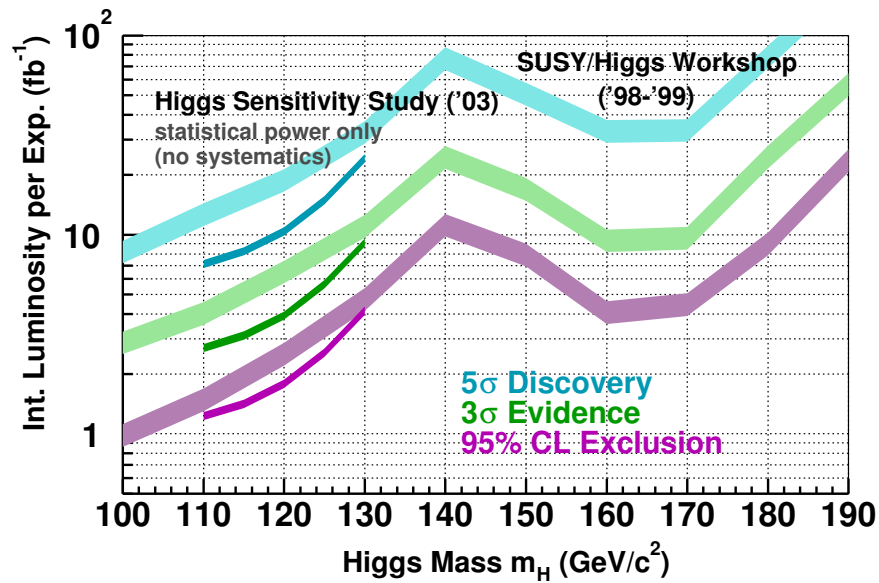


**Fig. 14:** Integrated luminosities needed to exclude or to discover the SM Higgs boson at the Tevatron; Ref. [12]

Since the cross-section vanishes for asymptotic energies, the Higgs-strahlung process is most useful for studying Higgs bosons in the range where the collider energy is of the same order as the Higgs mass,  $\sqrt{s} \gtrsim \mathcal{O}(M_H)$ . The size of the cross-section is illustrated in Fig. 15 for the energy  $\sqrt{s} = 500 \text{ GeV}$  of  $e^+e^-$  linear colliders as a function of the Higgs mass. Since the recoiling  $Z$  mass in the two-body reaction  $e^+e^- \rightarrow ZH$  is mono-energetic, the mass of the Higgs boson can be reconstructed from the energy of the  $Z$  boson,  $M_H^2 = s - 2\sqrt{s}E_Z + M_Z^2$ , without any need to analyse the decay products of the Higgs boson. For leptonic  $Z$  decays, missing-mass techniques provide a very clear signal, as demonstrated in Fig. 16.

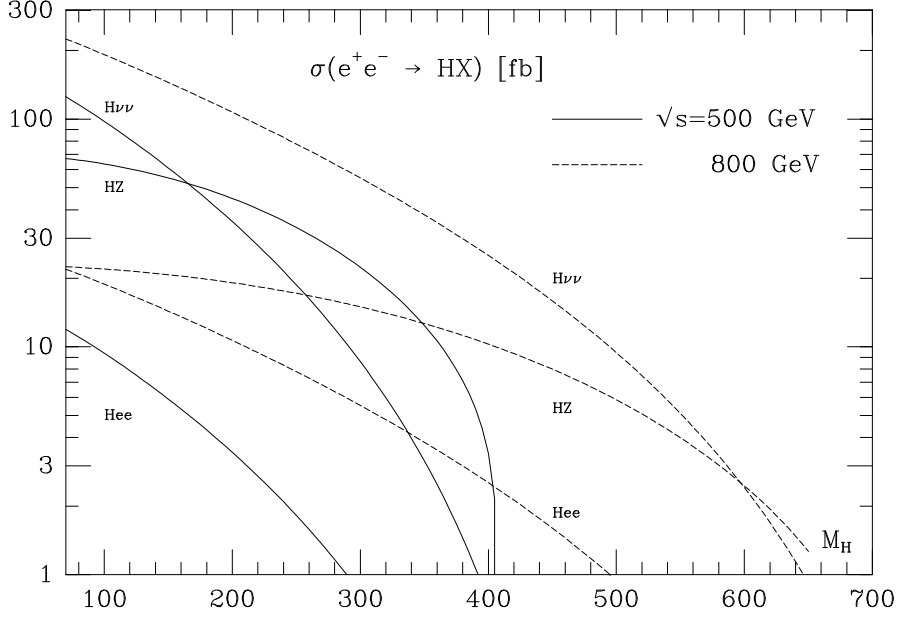


**Fig. 15:** The cross-section for the production of SM Higgs bosons in Higgs-strahlung  $e^+e^- \rightarrow ZH$  and  $WW/ZZ$  fusion  $e^+e^- \rightarrow \bar{\nu}_e\nu_e/e^+e^-H$ ; solid curves:  $\sqrt{s} = 500$  GeV, dashed curves:  $\sqrt{s} = 800$  GeV

### 2.4.2 $WW$ fusion

Also the cross-section for the fusion process (30) can be cast implicitly into a compact form:

$$\sigma(e^+e^- \rightarrow \bar{\nu}_e\nu_e H) = \frac{G_F^3 M_W^4}{4\sqrt{2}\pi^3} \int_{\kappa_H}^1 \int_x^1 \frac{dx dy}{[1 + (y-x)/\kappa_W]^2} f(x, y) \quad (32)$$

$$f(x, y) = \left( \frac{2x}{y^3} - \frac{1+3x}{y^2} + \frac{2+x}{y} - 1 \right) \left[ \frac{z}{1+z} - \log(1+z) \right] + \frac{x}{y^3} \frac{z^2(1-y)}{1+z}$$

with  $\kappa_H = M_H^2/s$ ,  $\kappa_W = M_W^2/s$  and  $z = y(x - \kappa_H)/(\kappa_W x)$ .

Since the fusion process is a  $t$ -channel exchange process, the size is set by the  $W$  Compton wavelength, suppressed, however, with respect to Higgs-strahlung by the third power of the electroweak coupling,  $\sigma \sim \alpha_W^3/M_W^2$ . As a result,  $W$  fusion becomes the leading production process for Higgs particles at high energies. At asymptotic energies the cross-section simplifies to

$$\sigma(e^+e^- \rightarrow \bar{\nu}_e\nu_e H) \rightarrow \frac{G_F^3 M_W^4}{4\sqrt{2}\pi^3} \left[ \log \frac{s}{M_H^2} - 2 \right]. \quad (33)$$

In this limit,  $W$  fusion to Higgs bosons can be interpreted as a two-step process: the  $W$  bosons are radiated as quasi-real particles from electrons and positrons,  $e \rightarrow \nu W$ , with a lifetime of the split state of order  $E_W/M_W^2$ ; the Higgs bosons are formed subsequently in the colliding  $W$  beams. The electroweak higher order corrections are under control [53].

The size of the fusion cross-section is compared with Higgs-strahlung in Fig. 15. At  $\sqrt{s} = 500$  GeV the two cross-sections are of the same order, yet the fusion process becomes increasingly important with rising energy.

## 2.5 The profile of the Standard Model Higgs particle

To establish the Higgs mechanism experimentally, the nature of this particle must be explored by measuring all its characteristics, the mass and lifetime, the external quantum numbers spin-parity, the couplings

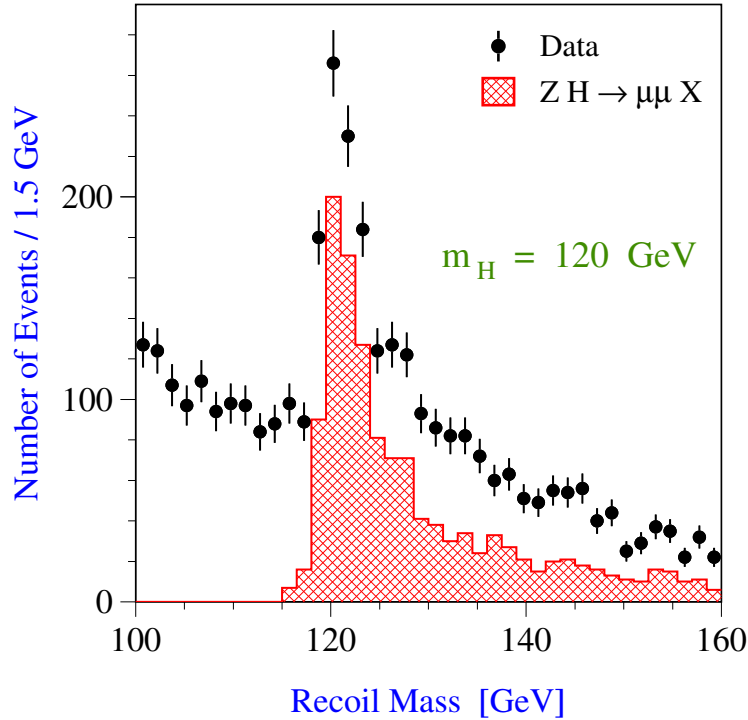


**Fig. 16:** The  $\mu^+\mu^-$  recoil mass distribution in the process  $e^+e^- \rightarrow H^0 Z \rightarrow X\mu^+\mu^-$  for  $M_H = 120$  GeV and  $\int \mathcal{L} = 500 fb^{-1}$  at  $\sqrt{s} = 350$  GeV. The dots with error bars are Monte Carlo simulations of the Higgs signal and the background. The shaded histogram represents the signal only. Ref. [15].

to gauge bosons and fermions, and last but not least, the Higgs self-couplings. While part of this programme can be realized at the LHC [13, 54], the complete profile of the particle can be reconstructed across the entire mass range in  $e^+e^-$  colliders [15].

### 2.5.1 Mass

The mass of the Higgs particle can be measured by collecting the decay products of the particle at hadron and  $e^+e^-$  colliders. Values at the level of 2 per-mille may be reached by this method at the LHC [13, 14]. Moreover, in  $e^+e^-$  collisions Higgs-strahlung can be exploited to reconstruct the mass very precisely from the  $Z$  recoil energy in the two-body process  $e^+e^- \rightarrow ZH$ . An overall accuracy of about  $\delta M_H \sim 100$  MeV can be expected [15].

### 2.5.2 Width/lifetime

The width of the state, i.e., the lifetime of the particle, can be measured directly above the  $ZZ$  decay threshold where the width grows rapidly. In the lower part of the intermediate mass range the width can be measured indirectly [13–15], by combining the branching ratio for  $H \rightarrow WW$  with the measurement of the partial  $WW$  width, accessible through the cross-section for  $W$  boson fusion:  $\Gamma_{tot} = \Gamma_{WW}/BR_{WW}$ . Thus, the total width of the Higgs particle can be determined throughout the entire mass range when the experimental results from the LHC and  $e^+e^-$  colliders can be combined.

### 2.5.3 Spin-parity

The zero-spin of the Higgs particle can be determined from the isotropic distribution of the decay products [55, 56]. Moreover, the parity can be measured by observing the spin correlations of the

decay products. According to the equivalence theorem, the azimuthal angles of the decay planes in  $H \rightarrow ZZ \rightarrow (\mu^+\mu^-)(\mu^+\mu^-)$  are asymptotically uncorrelated,  $d\Gamma^+/d\phi_* \rightarrow 0$ , for a  $0^+$  particle; this is to be contrasted with  $d\Gamma^-/d\phi_* \rightarrow 1 - \frac{1}{4} \cos 2\phi_*$  for the distribution of the azimuthal angle between the planes for the decay of a  $0^-$  particle. The difference between the angular distributions is a consequence of the different polarization states of the vector bosons in the two cases. While they approach states of longitudinal polarization for scalar Higgs decays, they are transversely polarized for pseudoscalar particle decays.

In the low mass range in which Higgs decays to  $Z$ -boson pairs are suppressed, the azimuthal angular distribution between the accompanying quark jets in  $WW$  fusion can be exploited to measure the parity [57]. While the jets are nearly uncorrelated for Higgs boson production in the Standard Model, the correlation is of markedly different oscillatory character for the production of a pseudoscalar particle [i.e.  $\mathcal{CP}$ -odd], the jets pointing preferentially into directions perpendicular to each other.

The angular distribution of the  $Z/H$  bosons in the Higgs-strahlung process is sensitive to the spin and parity of the Higgs particle [58]. Since the production amplitude is given by  $\mathcal{A}(0^+) \sim \vec{\epsilon}_{Z^*} \cdot \vec{\epsilon}_Z$ , the  $Z$  boson is produced in a state of longitudinal polarization at high energies—in accordance with the equivalence theorem. As a result, the angular distribution

$$\frac{d\sigma}{d\cos\theta} \sim \sin^2\theta + \frac{8M_Z^2}{\lambda s} \quad (34)$$

approaches the spin-zero  $\sin^2\theta$  law asymptotically. This may be contrasted with the distribution  $\sim 1 + \cos^2\theta$  for negative parity states, which follows from the transverse polarization amplitude  $\mathcal{A}(0^-) \sim \vec{\epsilon}_{Z^*} \times \vec{\epsilon}_Z \cdot \vec{k}_Z$ . It is also characteristically different from the distribution of the background process  $e^+e^- \rightarrow ZZ$ , which, as a result of  $t/u$ -channel  $e$  exchange, is strongly peaked in the forward/backward direction, Fig. 17 left.

A different method to determine the spin of the Higgs boson is provided by scanning the onset of the excitation curve in Higgs-strahlung [59]  $e^+e^- \rightarrow ZH$ . For Higgs spin  $S_H = 0$  the excitation curve rises steeply at the threshold  $\sim \sqrt{s - (M_H + M_Z)^2}$ . This behaviour is distinctly different from higher spin excitations which rise with a power  $> 1$  of the threshold factor. An ambiguity for states with spin/parity  $1^+$  and  $2^+$  can be resolved by evaluating also the angular distribution of the Higgs and  $Z$  boson in the Higgs-strahlung process. The experimental precision will be sufficient to discriminate the spin-0 assignment to the Higgs boson from other assignments as shown in Fig. 17 right.

#### 2.5.4 Higgs couplings

Since fundamental particles acquire mass by interaction with the Higgs field, the strength of the Higgs couplings to fermions and gauge bosons is set by the masses of the particles. It will therefore be a crucial experimental task to measure these couplings, which are uniquely predicted by the very nature of the Higgs mechanism.

At the LHC only ratios of Higgs couplings can be determined in the intermediate mass range in a model-independent way. Since only the product  $\sigma_i \cdot BR_f \sim \Gamma_i \Gamma_f / \Gamma_{tot}$  can be measured, the partial widths  $\Gamma_{i,f}$  may be rescaled and the shifts balanced in  $\Gamma_{tot}$  by unidentified decay channels. The expected accuracy for the ratios of various decay channels is displayed in Fig. 18 [61]. Apparently first insight can be obtained at the LHC into the fundamental rule

$$g_i/g_j = m_i/m_j \quad (35)$$

for various particles  $i, j = W, Z, \tau$ , etc.

At  $e^+e^-$  colliders the absolute values of the Higgs couplings can be measured in a model-independent way and with high precision.

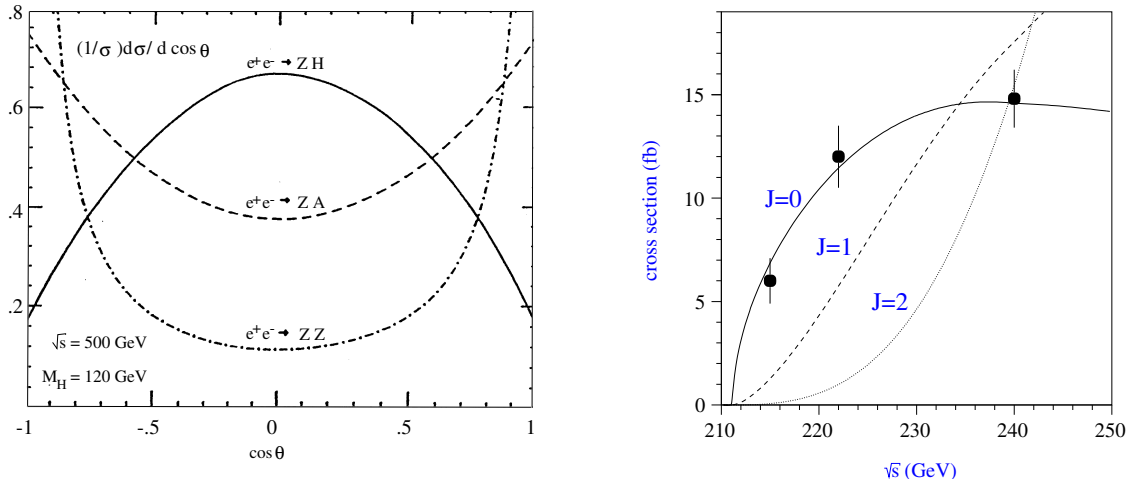


**Fig. 17:** Left: Angular distribution of  $Z/H$  bosons in Higgs-strahlung, compared with the production of pseudoscalar particles and the  $ZZ$  background final states. Ref. [58]. Right: Threshold excitation of Higgs-strahlung which discriminates spin=0 from other assignments, Refs. [59, 60].

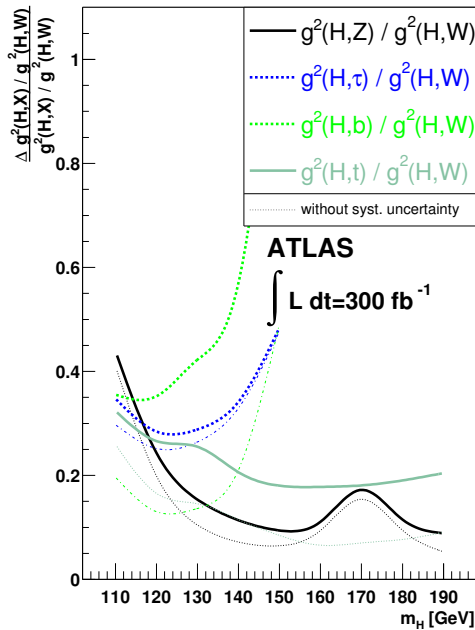


**Fig. 18:** Expected accuracies in measurements of ratios of Higgs couplings at the LHC. Ref. [61]

The Higgs couplings to massive gauge bosons can be determined from the production cross-sections in Higgs-strahlung and  $WW, ZZ$  fusion, with an accuracy expected at the per-cent level. For heavy enough Higgs bosons the decay width can be exploited to determine the couplings to the electroweak gauge bosons. For Higgs couplings to fermions the branching ratios  $H \rightarrow b\bar{b}, c\bar{c}, \tau^+\tau^-$  can be used in the lower part of the intermediate mass range, cf. Fig. 19; these observables allow the direct measurement of the Higgs Yukawa couplings.

A particularly interesting coupling is the Higgs coupling to top quarks. Since the top quark is by far the heaviest fermion in the Standard Model, irregularities in the standard picture of electroweak symmetry breaking by a fundamental Higgs field may become apparent first in this coupling. Thus the

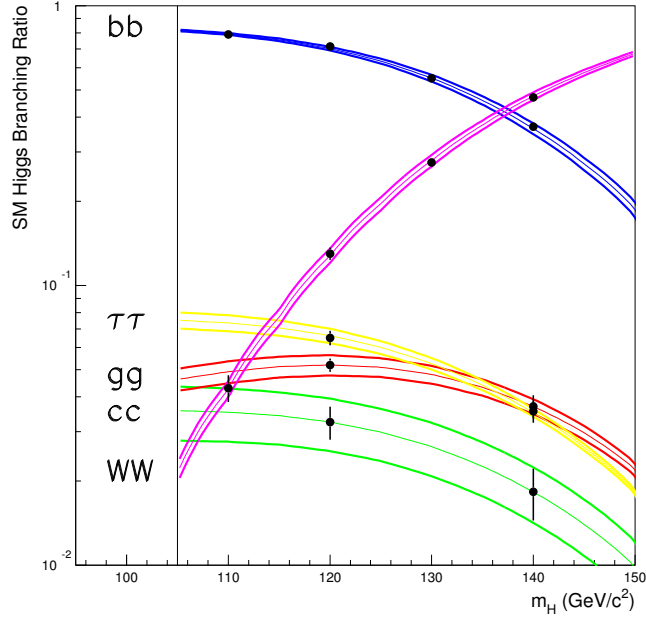


**Fig. 19:** The predicted SM Higgs boson branching ratios. Points with error bars show the expected experimental accuracy, while the lines show the estimated uncertainties on the SM predictions. Ref. [15].

$Htt$  Yukawa coupling may eventually provide essential clues to the nature of the mechanism breaking the electroweak symmetries.

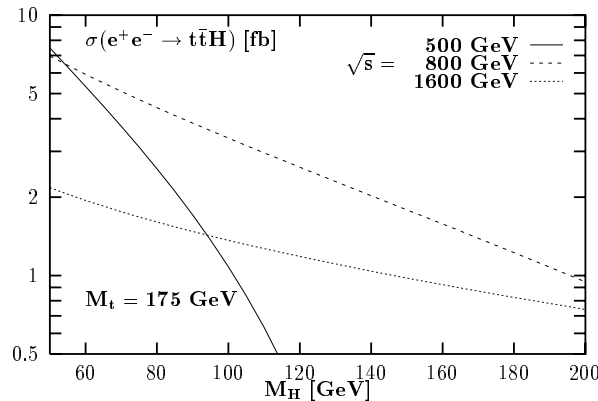


**Fig. 20:** The cross-section for bremsstrahlung of SM Higgs bosons off top quarks in the Yukawa process  $e^+e^- \rightarrow t\bar{t}H$ . (The amplitude for radiation off the intermediate  $Z$ -boson line is small.) Ref. [62].

Top loops mediating the production processes  $gg \rightarrow H$  and  $\gamma\gamma \rightarrow H$  (and the corresponding decay channels) give rise to cross-sections and partial widths, which are proportional to the square of the Higgs–top Yukawa coupling. This Yukawa coupling can be measured directly, for the lower part of the intermediate mass range, in the bremsstrahlung processes  $pp \rightarrow t\bar{t}H$  and  $e^+e^- \rightarrow t\bar{t}H$  [62]. The Higgs boson is radiated, in the first process exclusively, in the second process predominantly, from the heavy top quarks. Even though these experiments are difficult because of the small cross-sections (cf. Fig. 20 for  $e^+e^-$  collisions) and of the complex topology of the  $b\bar{b}b\bar{b}W^+W^-$  final state, this process is an important tool for exploring the mechanism of electroweak symmetry breaking. For large Higgs masses above the  $t\bar{t}$  threshold, the decay channel  $H \rightarrow t\bar{t}$  can be studied; in  $e^+e^-$  collisions the cross-section of  $e^+e^- \rightarrow t\bar{t}Z$  increases through the reaction  $e^+e^- \rightarrow ZH(\rightarrow t\bar{t})$  [63]. Higgs exchange between  $t\bar{t}$  quarks also affects the excitation curve near the threshold at a level of a few per cent.

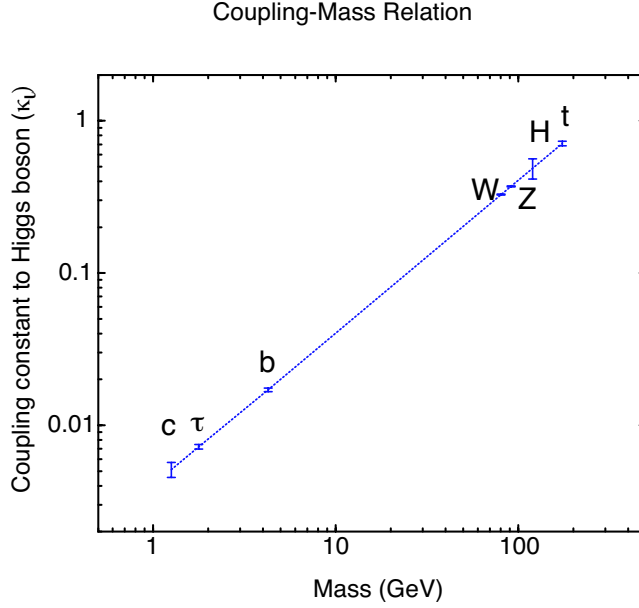


**Fig. 21:** The predicted normalized coupling constants of the SM Higgs boson to the heavy SM fermions and vector bosons as well as the Higgs boson itself as a function of the corresponding SM particle mass. Points with error bars show the expected experimental accuracy, while the lines show the linear rise of the couplings with the corresponding masses. Ref. [64].

The expected accuracies for some of the couplings are collected in Table 2. The linear rise of the Higgs couplings with the masses of the particles is clearly visible in Fig. 21 in which the slope is uniquely predicted within the Standard Model. Mixing between the Higgs boson and other scalar particles, like radions, may change these couplings in a universal way. It is necessary therefore to scrutinize not only the mass dependence but also the absolute values of the Higgs couplings.

**Table 2:** Relative accuracy on the Higgs couplings assuming  $\int \mathcal{L} = 500 \text{ fb}^{-1}$ ,  $\sqrt{s} = 500 \text{ GeV}$  ( $\int \mathcal{L} = 1 \text{ ab}^{-1}$ ,  $\sqrt{s} = 800 \text{ GeV}$  for  $g_{Htt}$ )

Coupling	$M_H = 120 \text{ GeV}$	$M_H = 140 \text{ GeV}$
$g_{HWW}$	$\pm 0.012$	$\pm 0.020$
$g_{HZZ}$	$\pm 0.012$	$\pm 0.013$
$g_{Htt}$	$\pm 0.030$	$\pm 0.061$
$g_{Hbb}$	$\pm 0.022$	$\pm 0.022$
$g_{Hcc}$	$\pm 0.037$	$\pm 0.102$
$g_{H\tau\tau}$	$\pm 0.033$	$\pm 0.048$

### 2.5.5 Higgs self-couplings

The Higgs mechanism, based on a non-zero value of the Higgs field in the vacuum, must finally be made manifest experimentally by reconstructing the interaction potential that generates the non-zero field in the vacuum. This programme can be carried out by measuring the strength of the trilinear and quartic self-couplings of the Higgs particles:

$$g_{H^3} = 3\sqrt{\sqrt{2}G_F}M_H^2, \quad (36)$$

$$g_{H^4} = 3\sqrt{2}G_F M_H^2. \quad (37)$$

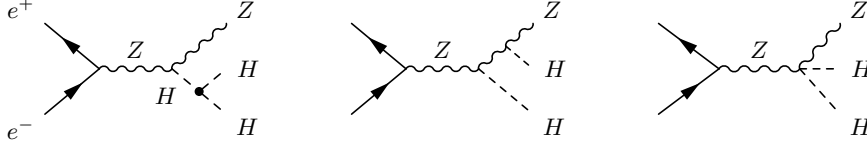


**Fig. 22:** Generic diagrams contributing to the double Higgs-strahlung process  $e^+e^- \rightarrow ZHH$

This is a difficult task since the processes to be exploited are suppressed by small couplings and phase space. At the LHC it does not seem possible to determine the self-couplings, leaving some hope though for the high-luminosity version VLHC. However, this problem can be solved for the trilinear coupling  $g_{H^3}$  in the high-energy phase of an  $e^+e^-$  linear collider for sufficiently high luminosities [65]. A well-suited reaction at  $e^+e^-$  colliders for the measurement of the trilinear coupling for Higgs masses in the theoretically preferred mass range of  $\mathcal{O}(100 \text{ GeV})$  is the double Higgs-strahlung process

$$e^+e^- \rightarrow ZH^* \rightarrow ZHH \quad (38)$$

in which, among other mechanisms, the two-Higgs final state is generated by the exchange of a virtual Higgs particle so that this process is sensitive to the trilinear  $HHH$  coupling in the Higgs potential, Fig. 22. Since the cross-section is only a fraction of 1 fb, an integrated luminosity of  $\sim 1 \text{ ab}^{-1}$  is needed to isolate the events at linear colliders. If combined with measurements of the double-Higgs fusion process

$$e^+e^- \rightarrow \bar{\nu}\nu H^* \rightarrow \bar{\nu}\nu HH. \quad (39)$$

experimental accuracies close to 12% can be expected [66]. The quartic coupling  $H^4$  seems to be accessible only through loop effects in the foreseeable future.

To sum up: *The essential elements of the Higgs mechanism can be established experimentally at the LHC and TeV  $e^+e^-$  linear colliders.*

### 3 Higgs bosons in supersymmetric theories

Arguments deeply rooted in the Higgs sector play an eminent role in introducing supersymmetry as a fundamental symmetry of nature [16]. This is the only symmetry which correlates bosonic with fermionic degrees of freedom, cf. Ref. [67].

The cancellation between bosonic and fermionic contributions to the radiative corrections of the light Higgs masses in supersymmetric theories provides part of the solution to the hierarchy problem in the Standard Model. If the Standard Model is embedded in a grand-unified theory, the large gap between the high grand-unification scale and the low scale of electroweak symmetry breaking can be stabilized in a natural way in boson–fermion symmetric theories [17, 68]. Denoting the bare Higgs mass by  $M_{H,0}^2$ , the radiative corrections due to vector-boson loops in the Standard Model by  $\delta M_{H,V}^2$ , and the contributions of supersymmetric fermionic gaugino partners by  $\delta M_{\tilde{H},\tilde{V}}^2$ , the physical Higgs mass is given by the sum  $M_H^2 = M_{H,0}^2 + \delta M_{H,V}^2 + \delta M_{\tilde{H},\tilde{V}}^2$ . The vector-boson correction is quadratically divergent,  $\delta M_{H,V}^2 \sim \alpha[\Lambda^2 - M^2]$ , so that, if present alone, for a cut-off scale  $\Lambda \sim \Lambda_{GUT}$  extreme fine-tuning between the intrinsic bare mass and the radiative quantum fluctuations would be needed to generate a Higgs mass of order  $M_W$ . However, owing to Pauli’s principle, the additional fermionic gaugino contributions in supersymmetric theories are just opposite in sign,  $\delta M_{\tilde{H},\tilde{V}}^2 \sim -\alpha[\Lambda^2 - \tilde{M}^2]$ , so that the divergent terms cancel<sup>2</sup>. Since  $\delta M_H^2 \sim \alpha[\tilde{M}^2 - M^2]$ , any fine-tuning is avoided for supersymmetric

<sup>2</sup>Different statistics for bosons and fermions are sufficient for the cancellation of the divergencies. However, they are not necessary; symmetry relations among couplings, as realized in Little Higgs models, may also lead to cancellations individually between boson–boson or fermion–fermion amplitudes.

particle masses  $\tilde{M} \lesssim \mathcal{O}(1 \text{ TeV})$ . Thus within this symmetry scheme the Higgs sector is stable in the low-energy range  $M_H \sim M_W$  even in the context of high-energy GUT scales. This mechanism leads in a natural way to low-energy supersymmetry.

The concept of supersymmetry is strongly supported by the successful prediction of the electroweak mixing angle in the minimal version of this theory [18]. The extended particle spectrum of the theory drives the evolution of the electroweak mixing angle from the GUT value  $3/8$  down to  $\sin^2 \theta_W = 0.2336 \pm 0.0017$ , the error including unknown threshold contributions at the low and the high supersymmetric mass scales. The prediction coincides with the experimentally measured value  $\sin^2 \theta_W^{exp} = 0.23153 \pm 0.00016$  within the theoretical uncertainty of less than 2 per-mille.

Conceptually very interesting is the interpretation of the Higgs mechanism in supersymmetric theories as a quantum effect [69]. The breaking of the electroweak symmetry  $SU(2)_L \times U(1)_Y$  can be induced radiatively while leaving the electromagnetic gauge symmetry  $U(1)_{EM}$  and the colour gauge symmetry  $SU(3)_C$  unbroken for top-quark masses between 150 and 200 GeV. Starting with a set of universal scalar masses at the high GUT scale, one of the squared mass parameters in the Higgs sector evolves to negative values at the low electroweak scale, while the squared squark and slepton masses remain positive.

The Higgs sector of supersymmetric theories differs in several aspects from the Standard Model [19]. To preserve supersymmetry and gauge invariance, at least two iso-doublet fields must be introduced, leaving us with a spectrum of five or more physical Higgs particles. In the minimal supersymmetric extension of the Standard Model the Higgs self-interactions are generated by the scalar-gauge field action, so that the quartic couplings are related to the gauge couplings in this scenario. After including radiative corrections this leads to strong bounds [20] of less than about 140 GeV for the mass of the lightest Higgs boson. If the system is assumed to remain weakly interacting up to scales of the order of the GUT or Planck scale, the mass remains small, for reasons quite analogous to those described in the Standard Model, even in more complex supersymmetric theories involving additional Higgs fields and Yukawa interactions. The masses of the heavy Higgs bosons are expected to be of the scale of electroweak symmetry breaking up to order 1 TeV.

### 3.1 The Higgs sector of the MSSM

The particle spectrum of the MSSM [16] consists of leptons, quarks and their scalar supersymmetric partners, and gauge particles, Higgs particles and their spin-1/2 partners. The matter and force fields are coupled in supersymmetric and gauge-invariant actions:

$$\begin{aligned}
 S = S_V + S_\phi + S_W : \quad S_V &= \frac{1}{4} \int d^6 z \hat{W}_\alpha \hat{W}_\alpha && \text{gauge action,} \\
 S_\phi &= \int d^8 z \hat{\phi}^* e^{gV} \hat{\phi} && \text{matter action,} \\
 S_W &= \int d^6 z W[\hat{\phi}] && \text{superpotential.}
 \end{aligned} \tag{40}$$

Decomposing the superfields into fermionic and bosonic components, and carrying out the integration over the Grassmann variables in  $z \rightarrow x$ , the following Lagrangians are derived, which describe the interactions of the gauge, matter and Higgs fields:

$$\begin{aligned}
 \mathcal{L}_V &= -\frac{1}{4} F_{\mu\nu} F_{\mu\nu} + \dots + \frac{1}{2} D^2, \\
 \mathcal{L}_\phi &= D_\mu \phi^* D_\mu \phi + \dots + \frac{g}{2} D|\phi|^2, \\
 \mathcal{L}_W &= -\left| \frac{\partial W}{\partial \phi} \right|^2.
 \end{aligned}$$

The  $D$  field is an auxiliary field that does not propagate in space–time and it can be eliminated by applying the equations of motion:  $D = -\frac{g}{2}|\phi|^2$ . Reinserted into the Lagrangian, the quartic self-coupling of the scalar Higgs fields is generated,

$$\mathcal{L}[\phi^4] = -\frac{g^2}{8}|\phi^2|^2, \quad (41)$$

in theories like MSSM in which the superpotential does not generate a quartic term. Thus the quartic coupling of the Higgs fields is given, in the minimal supersymmetric theory, by the square of the gauge coupling. Unlike the Standard Model case, the quartic coupling is not a free parameter. Moreover, this coupling is weak.

Two independent Higgs doublet fields  $H_1$  and  $H_2$  must be introduced into the superpotential:

$$W = -\mu\epsilon_{ij}\hat{H}_1^i\hat{H}_2^j + \epsilon_{ij}[f_1\hat{H}_1^i\hat{L}^j\hat{R} + f_2\hat{H}_1^i\hat{Q}^j\hat{D} - f'_2\hat{H}_2^i\hat{Q}^j\hat{U}] \quad (42)$$

to provide the down-type particles ( $H_1$ ) and the up-type particles ( $H_2$ ) with mass. Unlike the Standard Model, the second Higgs field cannot be identified with the charge conjugate of the first Higgs field since  $W$  must be analytic to preserve supersymmetry. In addition, the Higgsino fields associated with a single Higgs field would generate triangle anomalies; they cancel if the two conjugate doublets are added up, and the gauge invariance of the classical interactions is not destroyed at the quantum level. Integrating the superpotential over the Grassmann coordinates generates the supersymmetric Higgs self-energy  $V_0 = |\mu|^2(|H_1|^2 + |H_2|^2)$ . The breaking of supersymmetry can be incorporated in the Higgs sector by introducing bilinear mass terms  $\mu_{ij}H_iH_j$ . Added to the supersymmetric self-energy part  $H^2$  and the quartic part  $H^4$  generated by the gauge action, they lead to the following Higgs potential

$$\begin{aligned} V = & m_1^2 H_1^{*i} H_1^i + m_2^2 H_2^{*i} H_2^i - m_{12}^2 (\epsilon_{ij} H_1^i H_2^j + hc) \\ & + \frac{1}{8}(g^2 + g'^2)[H_1^{*i} H_1^i - H_2^{*i} H_2^i]^2 + \frac{1}{2}g^2 |H_1^{*i} H_2^i|^2. \end{aligned} \quad (43)$$

The Higgs potential includes three bilinear mass terms, while the strength of the quartic couplings is set by the  $SU(2)_L$  and  $U(1)_Y$  gauge couplings squared. The three mass terms are free parameters.

The potential develops a stable minimum for  $H_1 \rightarrow [v_1, 0]$  and  $H_2 \rightarrow [0, v_2]$  if the following conditions are met:  $m_1^2 + m_2^2 > 2|m_{12}^2|$  and  $m_1^2 m_2^2 < |m_{12}^2|^2$ .

Expanding the fields about the ground-state values  $v_1$  and  $v_2$ ,

$$\begin{aligned} H_1^1 &= v_1 + [H^0 \cos \alpha - h^0 \sin \alpha + iA^0 \sin \beta - iG^0 \cos \beta]/\sqrt{2} \\ H_1^2 &= H^- \sin \beta - G^- \cos \beta \end{aligned} \quad (44)$$

and

$$\begin{aligned} H_2^1 &= H^+ \cos \beta + G^+ \sin \beta \\ H_2^2 &= v_2 + [H^0 \sin \alpha + h^0 \cos \alpha + iA^0 \cos \beta + iG^0 \sin \beta]/\sqrt{2}, \end{aligned} \quad (45)$$

the mass eigenstates are given by the neutral states  $h^0$ ,  $H^0$  and  $A^0$ , which are even and odd under  $\mathcal{CP}$  transformations, and by the charged states  $H^\pm$ ; the  $G$  states correspond to the Goldstone modes, which are absorbed by the gauge fields to build up the longitudinal components. After introducing the three parameters

$$M_Z^2 = \frac{1}{2}(g^2 + g'^2)(v_1^2 + v_2^2)$$

$$\begin{aligned}
 M_A^2 &= m_{12}^2 \frac{v_1^2 + v_2^2}{v_1 v_2} \\
 \operatorname{tg} \beta &= \frac{v_2}{v_1},
 \end{aligned} \tag{46}$$

the mass matrix can be decomposed into three  $2 \times 2$  blocks, which are easy to diagonalize:

**pseudoscalar mass:**  $M_A^2$

**charged mass:**  $M_{\pm}^2 = M_A^2 + M_W^2$

**scalar mass:**  $M_{h,H}^2 = \frac{1}{2} \left[ M_A^2 + M_Z^2 \mp \sqrt{(M_A^2 + M_Z^2)^2 - 4M_A^2 M_Z^2 \cos^2 2\beta} \right]$

$$\operatorname{tg} 2\alpha = \operatorname{tg} 2\beta \frac{M_A^2 + M_Z^2}{M_A^2 - M_Z^2} \quad \text{with} \quad -\frac{\pi}{2} < \alpha < 0.$$

From the mass formulae, two important inequalities can readily be derived,

$$M_h \leq M_Z, M_A \leq M_H \tag{47}$$

$$M_W \leq M_{H\pm}, \tag{48}$$

which, by construction, are valid in the tree approximation. As a result, the lightest of the scalar Higgs masses is predicted to be bounded by the  $Z$  mass, *modulo* radiative corrections. These bounds follow from the fact that the quartic coupling of the Higgs fields is determined in the MSSM by the size of the gauge couplings squared.

*SUSY radiative corrections:* The tree-level relations between the Higgs masses are strongly modified by radiative corrections that involve the supersymmetric particle spectrum of the top sector [70]; cf. Refs. [32, 71] for recent summaries. These effects are proportional to the fourth power of the top mass and to the logarithm of the stop mass. Their origin are incomplete cancellations between virtual top and stop loops, reflecting the breaking of supersymmetry. Moreover, the mass relations are affected by the potentially large mixing between  $\tilde{t}_L$  and  $\tilde{t}_R$  due to the top Yukawa coupling.

To leading order in  $M_t^4$  the radiative corrections can be summarized in the parameter

$$\epsilon = \frac{3G_F}{\sqrt{2}\pi^2} \frac{M_t^4}{\sin^2 \beta} \log \frac{\langle M_{\tilde{t}}^2 \rangle}{M_{\tilde{t}}^2} \tag{49}$$

with  $\langle M_{\tilde{t}}^2 \rangle = M_{\tilde{t}_1} M_{\tilde{t}_2}$ . In this approximation the light Higgs mass  $M_h$  can be expressed by  $M_A$  and  $\operatorname{tg} \beta$  in the following compact form:

$$\begin{aligned}
 M_h^2 &= \frac{1}{2} \left[ M_A^2 + M_Z^2 + \epsilon \right. \\
 &\quad \left. - \sqrt{(M_A^2 + M_Z^2 + \epsilon)^2 - 4M_A^2 M_Z^2 \cos^2 2\beta - 4\epsilon(M_A^2 \sin^2 \beta + M_Z^2 \cos^2 \beta)} \right].
 \end{aligned}$$

The heavy Higgs masses  $M_H$  and  $M_{H\pm}$  follow from the sum rules

$$\begin{aligned}
 M_H^2 &= M_A^2 + M_Z^2 - M_h^2 + \epsilon \\
 M_{H\pm}^2 &= M_A^2 + M_W^2.
 \end{aligned}$$

Finally, the mixing parameter  $\alpha$ , which diagonalizes the  $\mathcal{CP}$ -even mass matrix, is given by the radiatively improved relation:

$$\operatorname{tg} 2\alpha = \operatorname{tg} 2\beta \frac{M_A^2 + M_Z^2}{M_A^2 - M_Z^2 + \epsilon / \cos 2\beta}. \quad (50)$$

For large  $A$  mass, the masses of the heavy Higgs particles coincide approximately,  $M_A \simeq M_H \simeq M_{H^\pm}$ , while the light Higgs mass approaches a small asymptotic value. The spectrum for large values of  $\operatorname{tg} \beta$  is quite regular: for small  $M_A$  one finds  $\{M_h \simeq M_A; M_H \simeq \text{const}\}$  [72]; for large  $M_A$  the opposite relationship  $\{M_h \simeq \text{const}, M_H \simeq M_{H^\pm} \simeq M_A\}$ , cf. Fig. 23 which includes the radiative corrections.

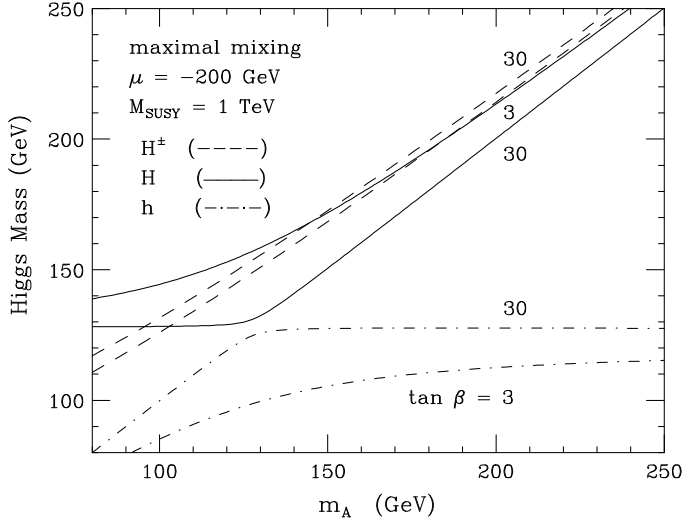


**Fig. 23:** The  $\mathcal{CP}$ -even and charged MSSM Higgs boson masses as a function of  $m_A$  for  $\tan \beta = 3$  and 30, including radiative corrections. Ref. [73].

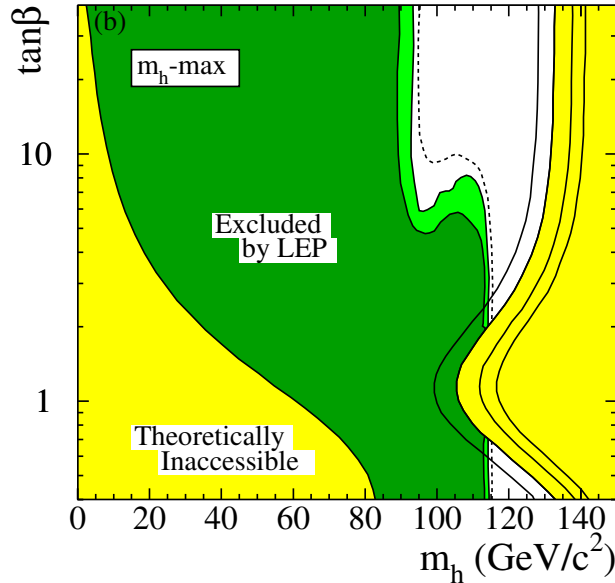


**Fig. 24:** Upper bounds on the light Higgs boson mass as a function of  $\operatorname{tg} \beta$  for varying top mass, and the region excluded by the negative searches at the LEP experiments. Ref. [74].

While the non-leading effects of mixing on the Higgs mass relations are quite involved, the impact on the upper bound of the light Higgs mass  $M_h$  can be summarized in a simple form:

$$M_h^2 \leq M_Z^2 + \delta M_t^2 + \delta M_X^2. \quad (51)$$

The leading top contribution is related to the parameter  $\epsilon$  while the second contribution depends on the mixing parameter in the scalar top sector,

$$M_t X_t = M_t [A_t - \mu \operatorname{ctg} \beta], \quad (52)$$

which couples left- and right-chirality states in the stop mass matrix:

$$M_h^2 \leq M_Z^2 + \frac{3G_F M_t^4}{2\sqrt{2}\pi^2} \left[ \log \frac{\langle M_t^2 \rangle}{M_t^2} + \frac{X_t^2}{\langle M_t^2 \rangle} \left( 1 - \frac{X_t^2}{\langle 12M_t^2 \rangle} \right) \right]. \quad (53)$$

Subdominant contributions can essentially be reduced to higher-order QCD effects. They can effectively be incorporated by interpreting the top mass parameter  $M_t \rightarrow M_t(\mu_t)$  as the  $\overline{\text{MS}}$  top mass evaluated at the geometric mean between top and stop masses,  $\mu_t^2 = M_t M_{\bar{t}}$ .

Upper bounds on the light Higgs mass are shown in Fig. 24 as a function of  $\operatorname{tg} \beta$ . The curves are the results of calculations taking into account the mixing effects. It turns out that the general upper bound for maximal mixing is given by  $M_h \lesssim 140$  GeV, including large values of  $\operatorname{tg} \beta$ . Thus, the light Higgs sector could not entirely be covered by the LEP2 experiments due to the increase of the mass limit with the top mass.

### 3.2 SUSY Higgs couplings to Standard Model particles

The size of MSSM Higgs couplings to quarks, leptons and gauge bosons is similar to the Standard Model, yet modified by the mixing angles  $\alpha$  and  $\beta$ . Normalized to the SM values, they are listed in Table 3. The pseudoscalar Higgs boson  $A$  does not couple to gauge bosons at the tree level, but the coupling, compatible with  $\mathcal{CP}$  symmetry, can be generated by higher-order loops. The charged Higgs bosons couple to up and down fermions with the left- and right-chiral amplitudes  $g_{\pm} = -[g_t(1 \mp \gamma_5) + g_b(1 \pm \gamma_5)]/\sqrt{2}$  where  $g_{t,b} = (\sqrt{2}G_F)^{1/2}m_{t,b}$ .

**Table 3:** Higgs couplings in the MSSM to fermions and gauge bosons [ $V = W, Z$ ] relative to SM couplings

$\Phi$	$g_u^{\Phi}$	$g_d^{\Phi}$	$g_V^{\Phi}$
SM $H$	1	1	1
MSSM $h$	$\cos \alpha / \sin \beta$	$-\sin \alpha / \cos \beta$	$\sin(\beta - \alpha)$
$H$	$\sin \alpha / \sin \beta$	$\cos \alpha / \cos \beta$	$\cos(\beta - \alpha)$
$A$	$1 / \operatorname{tg} \beta$	$\operatorname{tg} \beta$	0

The modified couplings incorporate the renormalization due to SUSY radiative corrections, to leading order in  $M_t$ , if the mixing angle  $\alpha$  is related to  $\beta$  and  $M_A$  as given in the corrected formula Eq. (50). For large  $M_A$ , in practice  $M_A \gtrsim 200$  GeV, the couplings of the light Higgs boson  $h$  to the fermions and gauge bosons approach the SM values asymptotically. This is the essence of the decoupling theorem in the Higgs sector [75]: Particles with large masses must decouple from the light-particle system as a consequence of the quantum-mechanical uncertainty principle. In the same limit, the heavy Higgs boson  $H$  decouples from vector bosons, and the coupling to up-type fermions is suppressed by  $1/\tan \beta$  while the coupling to down-type fermions is enhanced by  $\tan \beta$ . Thus the couplings of the two degenerate heavy Higgs bosons  $A, H$  are isomorphic in the decoupling limit.

### 3.3 Decays of Higgs particles

The lightest *neutral Higgs boson*  $h$  will decay mainly into fermion pairs since the mass is smaller than  $\sim 140$  GeV, Fig. 25 (cf. Ref. [76] for a comprehensive summary). This is, in general, also the dominant decay mode of the pseudoscalar boson  $A$ . For values of  $\tan\beta$  larger than unity and for masses less than  $\sim 140$  GeV, the main decay modes of the neutral Higgs bosons are decays into  $b\bar{b}$  and  $\tau^+\tau^-$  pairs; the branching ratios are of order  $\sim 90\%$  and  $8\%$ , respectively. The decays into  $c\bar{c}$  pairs and gluons are suppressed, especially for large  $\tan\beta$ . For large masses, the top decay channels  $H, A \rightarrow t\bar{t}$  open up; yet for large  $\tan\beta$  this mode remains suppressed and the neutral Higgs bosons decay almost exclusively into  $b\bar{b}$  and  $\tau^+\tau^-$  pairs. In contrast to the pseudoscalar Higgs boson  $A$ , the heavy  $\mathcal{CP}$ -even Higgs boson  $H$  can in principle decay into weak gauge bosons,  $H \rightarrow WW, ZZ$ , if the mass is large enough. However, since the partial widths are proportional to  $\cos^2(\beta - \alpha)$ , they are strongly suppressed in general, and the gold-plated  $ZZ$  signal of the heavy Higgs boson in the Standard Model is lost in the supersymmetric extension. As a result, the total widths of the Higgs bosons are much smaller in supersymmetric theories than in the Standard Model.

The heavy neutral Higgs boson  $H$  can also decay into two lighter Higgs bosons. Other possible channels are Higgs cascade decays and decays into supersymmetric particles [77–79], Fig. 26. In addition to light sfermions, Higgs boson decays into charginos and neutralinos could eventually be important. These new channels are kinematically accessible, at least for the heavy Higgs bosons  $H, A$  and  $H^\pm$ ; in fact, the branching fractions can be very large and they can even become dominant in some regions of the MSSM parameter space. Decays of  $h$  into the lightest neutralinos (LSP) are also important, exceeding 50% in some parts of the parameter space. These decays strongly affect experimental search techniques.

The *charged Higgs particles* decay into fermions, but also, if allowed kinematically, into the lightest neutral Higgs and a  $W$  boson. Below the  $tb$  and  $Wh$  thresholds, the charged Higgs particles will decay mostly into  $\tau\nu_\tau$  and  $cs$  pairs, the former being dominant for  $\tan\beta > 1$ . For large  $M_{H^\pm}$  values, the top–bottom decay mode  $H^\pm \rightarrow t\bar{b}$  becomes dominant. In some parts of the SUSY parameter space, decays into supersymmetric particles may exceed 50%.

Adding up the various decay modes, the width of all five Higgs bosons remains very narrow, being of order 10 GeV even for large masses.

### 3.4 The Production of SUSY Higgs particles in hadron collisions

The basic production processes of SUSY Higgs particles at hadron colliders [29, 40, 80] are essentially the same as in the Standard Model. Important differences are nevertheless generated by the modified couplings, the extended particle spectrum, and the negative parity of the  $A$  boson. For large  $\tan\beta$  the coupling  $hb\bar{b}$  is enhanced so that the bottom-quark loop becomes competitive to the top-quark loop in the effective  $hgg$  coupling. Moreover squark loops will contribute to this coupling [81].

The partonic cross-section  $\sigma(gg \rightarrow \Phi)$  for the gluon fusion of Higgs particles can be expressed by couplings  $g$ , in units of the corresponding SM couplings, and form factors  $A$ ; to lowest order [40, 82]:

$$\begin{aligned} \hat{\sigma}_{LO}^\Phi(gg \rightarrow \Phi) &= \sigma_0^\Phi M_\Phi^2 \times BW(\hat{s}) & (54) \\ \sigma_0^{h/H} &= \frac{G_F \alpha_s^2(\mu)}{128\sqrt{2}\pi} \left| \sum_Q g_Q^{h/H} A_Q^{h/H}(\tau_Q) + \sum_{\tilde{Q}} g_{\tilde{Q}}^{h/H} A_{\tilde{Q}}^{h/H}(\tau_{\tilde{Q}}) \right|^2 \\ \sigma_0^A &= \frac{G_F \alpha_s^2(\mu)}{128\sqrt{2}\pi} \left| \sum_Q g_Q^A A_Q^A(\tau_Q) \right|^2. \end{aligned}$$

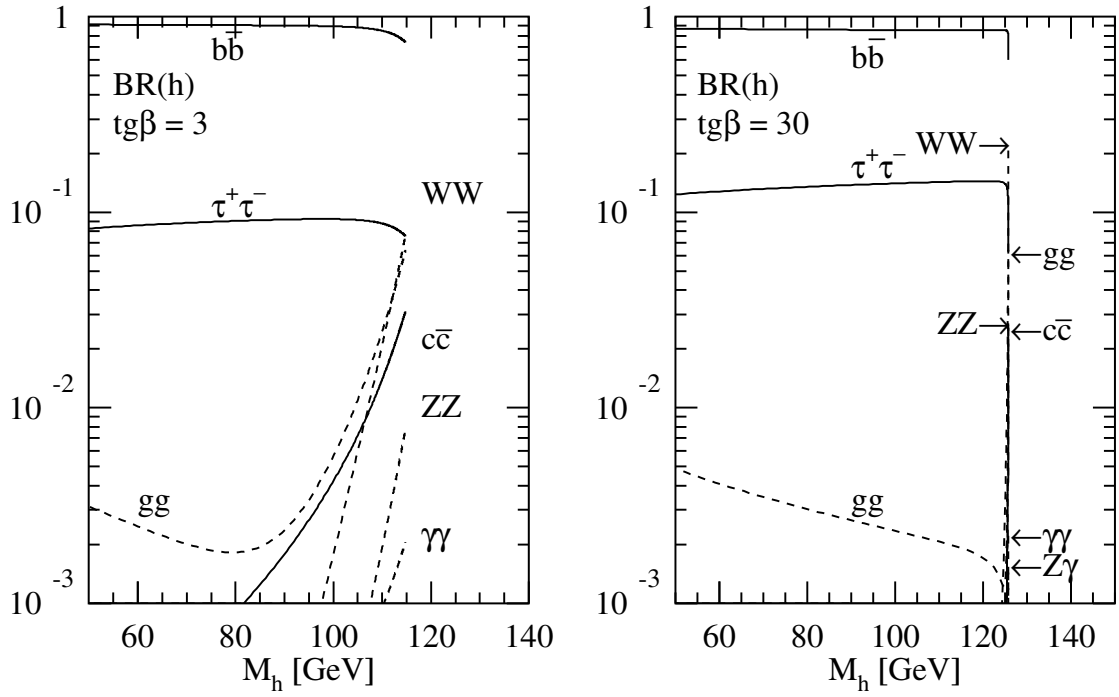


Fig. 25a

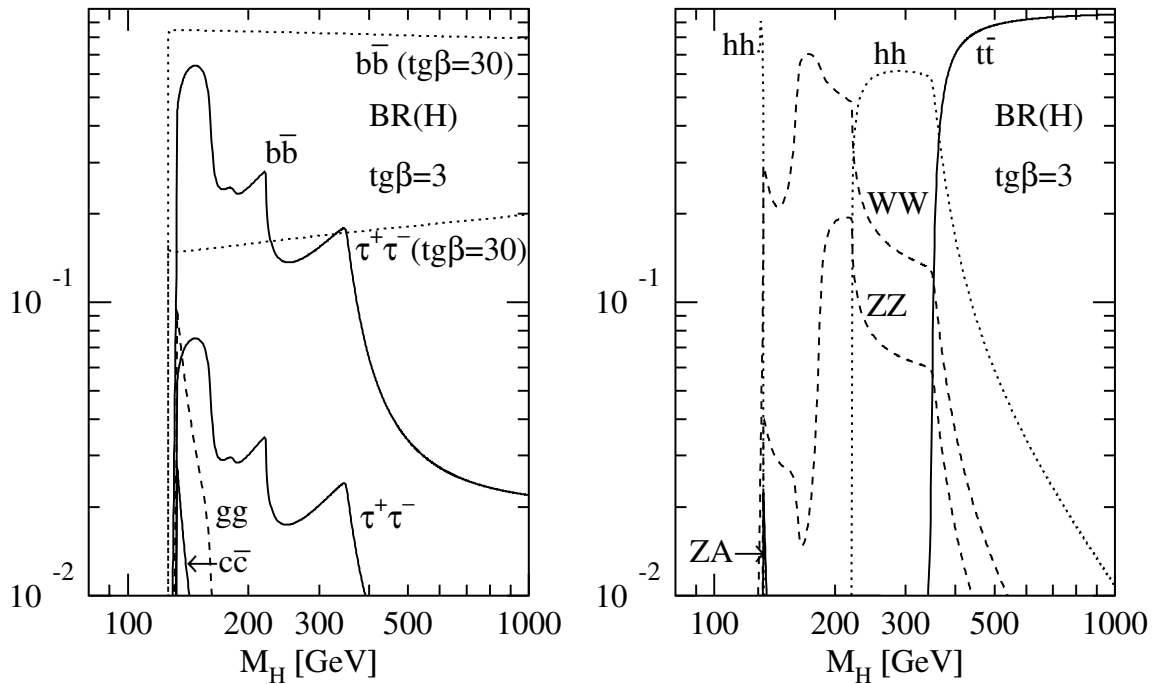


Fig. 25b

**Fig. 25:** Branching ratios of the MSSM Higgs bosons  $h, H, A, H^\pm$  for non-SUSY decay modes as a function of the masses for two values of  $\tan\beta = 3, 30$  and vanishing mixing. The common squark mass has been chosen as  $M_S = 1$  TeV.

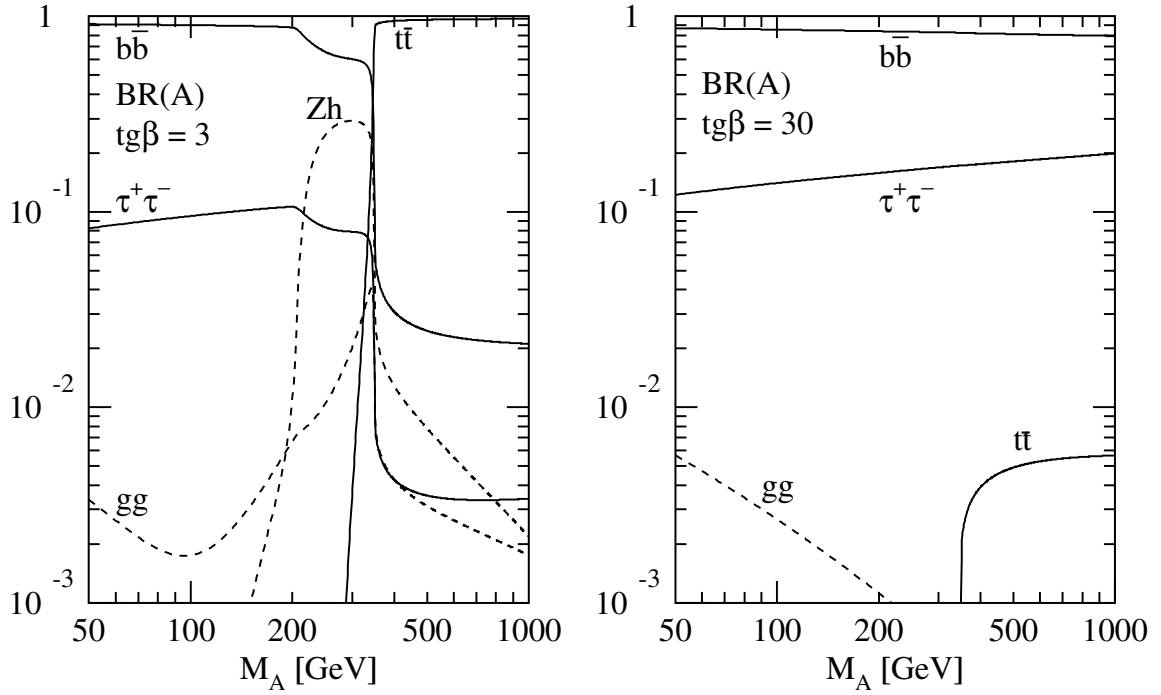


Fig. 25c

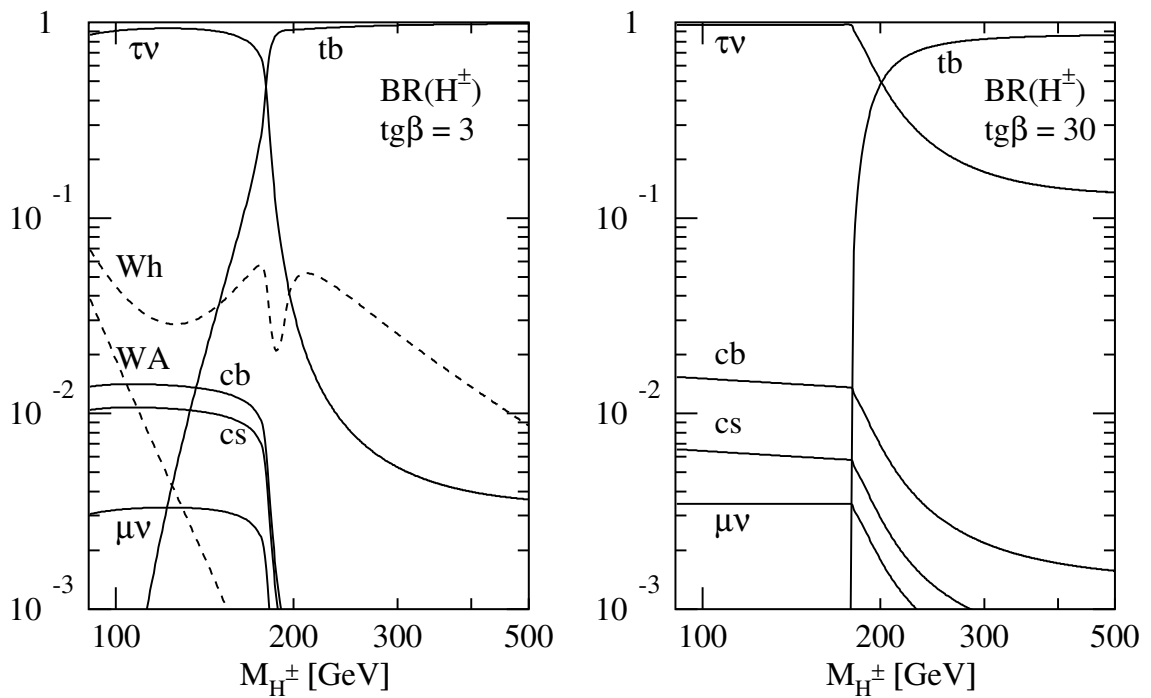
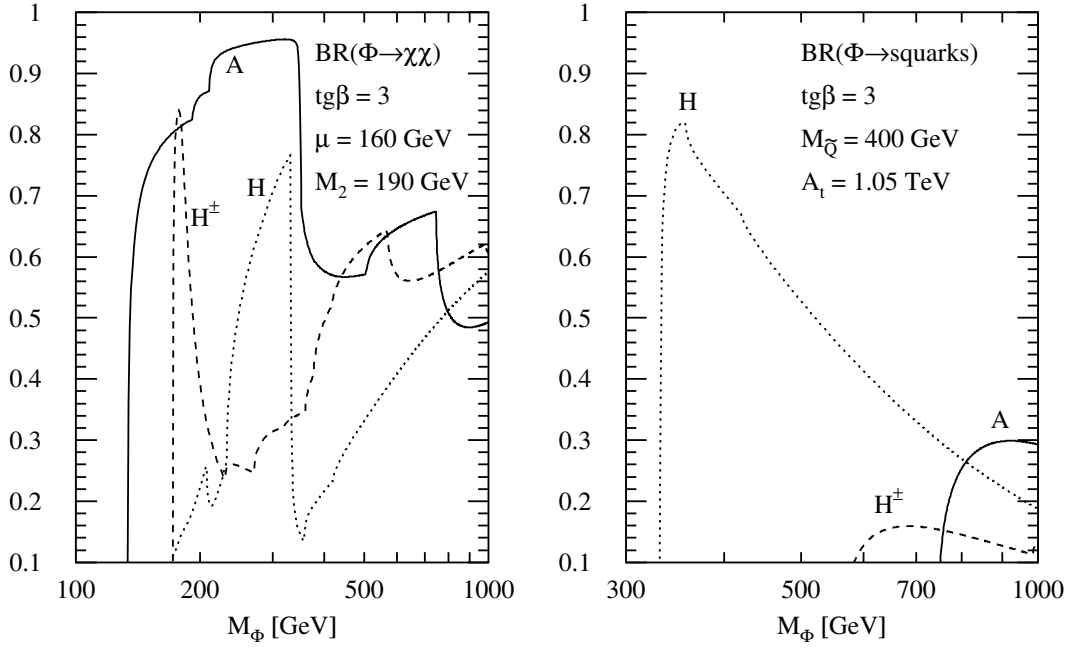


Fig. 25d

Fig. 25: Continued



**Fig. 26:** Branching ratios of the MSSM Higgs boson  $H$ ,  $A$ ,  $H^\pm$  decays into charginos/neutralinos and squarks as a function of their masses for  $\tan\beta = 3$ . The mixing parameters have been chosen as  $\mu = 160$  GeV,  $A_t = 1.05$  TeV,  $A_b = 0$  and the squark masses of the first two generations as  $M_{\tilde{Q}} = 400$  GeV. The gaugino mass parameter has been set to  $M_2 = 190$  GeV.

While the quark couplings have been defined in Table 3, the couplings of the Higgs particles to squarks are given by

$$\begin{aligned}
 g_{\tilde{Q}_{L,R}}^h &= \frac{M_{\tilde{Q}}^2}{M_{\tilde{Q}}^2} g_{\tilde{Q}}^h \mp \frac{M_Z^2}{M_{\tilde{Q}}^2} (I_3^Q - e_Q \sin^2 \theta_W) \sin(\alpha + \beta) \\
 g_{\tilde{Q}_{L,R}}^H &= \frac{M_{\tilde{Q}}^2}{M_{\tilde{Q}}^2} g_{\tilde{Q}}^H \pm \frac{M_Z^2}{M_{\tilde{Q}}^2} (I_3^Q - e_Q \sin^2 \theta_W) \cos(\alpha + \beta).
 \end{aligned} \tag{55}$$

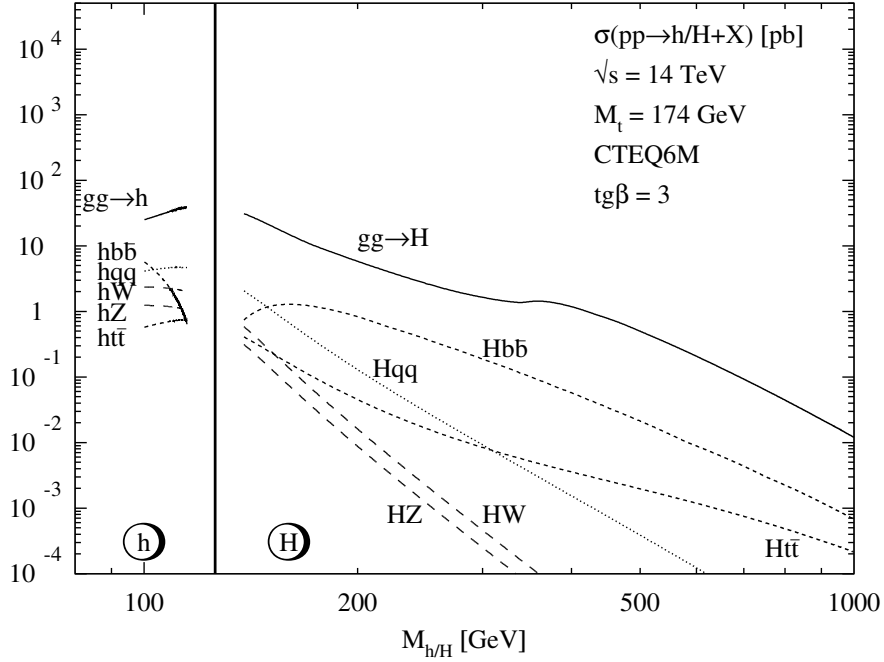
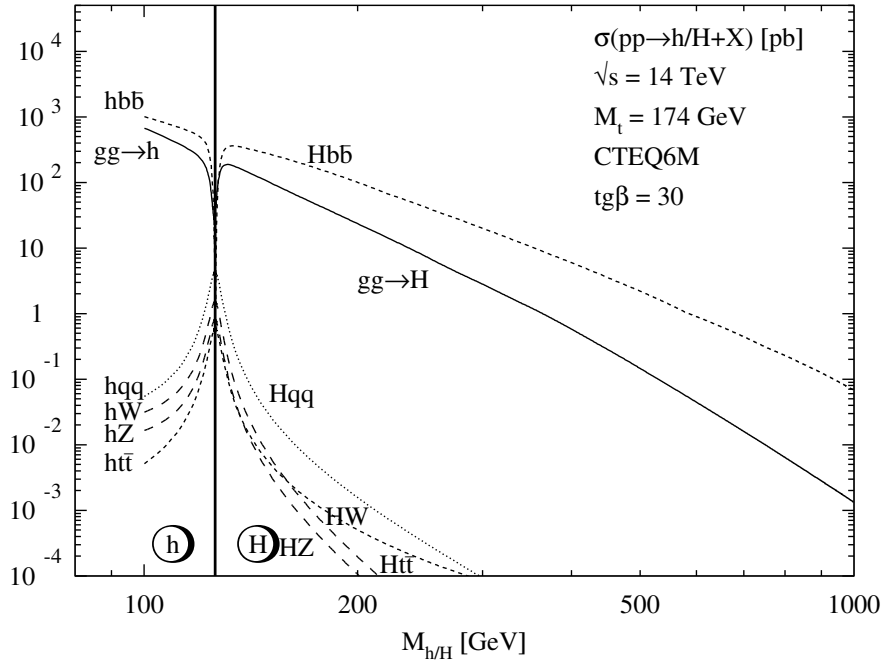
Only  $\mathcal{CP}$  non-invariance allows for non-zero squark contributions to pseudoscalar  $A$  boson production. The form factors can be expressed in terms of the scaling function  $f(\tau_i = 4M_i^2/M_\Phi^2)$ , cf. Eq. (22):

$$\begin{aligned}
 A_{\tilde{Q}}^{h/H}(\tau) &= \tau[1 + (1 - \tau)f(\tau)] \\
 A_{\tilde{Q}}^A(\tau) &= \tau f(\tau) \\
 A_{\tilde{Q}}^{h/H}(\tau) &= -\frac{1}{2}\tau[1 - \tau f(\tau)].
 \end{aligned} \tag{56}$$

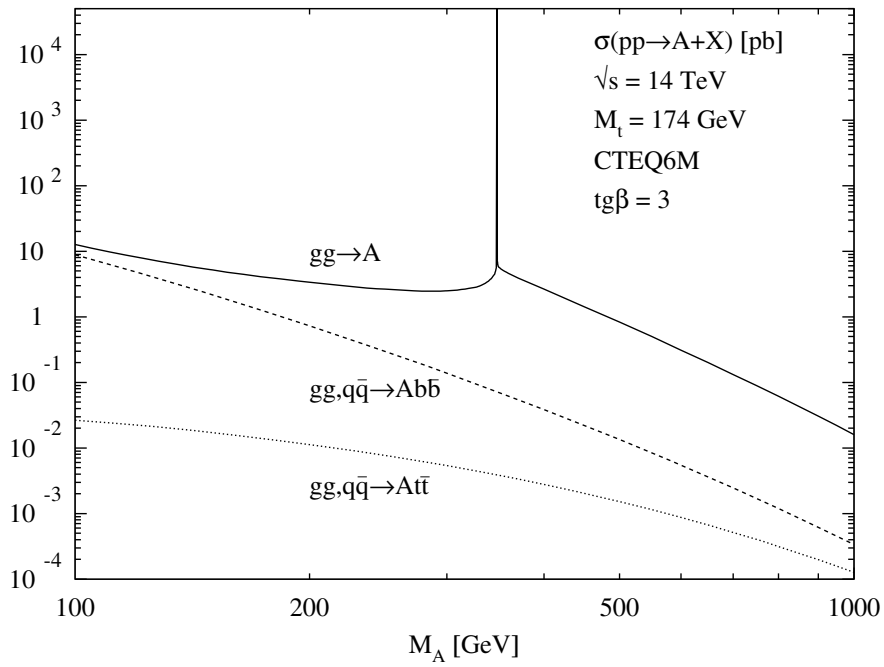
For small  $\tan\beta$  the contribution of the top loop is dominant, while for large  $\tan\beta$  the bottom loop is strongly enhanced. The squark loops can be significant for squark masses below  $\sim 400$  GeV [82, 83].

Other production mechanisms for SUSY Higgs bosons, vector boson fusion, Higgs-strahlung off  $W$ ,  $Z$  bosons and Higgs-bremsstrahlung off top quarks and bottom-quark fusion, can be treated in analogy to the corresponding SM processes.

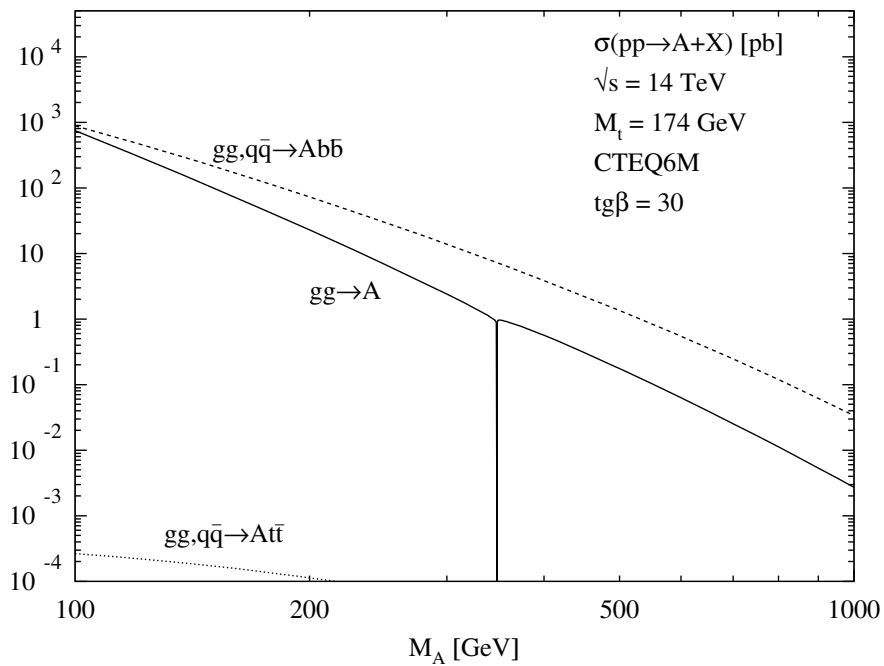
Particularly important is the process of  $b$ -quark fusion for large values of  $\tan\beta$  when the Higgs couplings to  $b$  quarks are enhanced [84]. Since  $b$  quarks are moderately light, gluon splitting  $g \rightarrow \bar{b}b$  gives rise to high-energy  $b$ -quark/anti-quark beams in fast moving protons/antiprotons. The fusion of  $\bar{b} + b \rightarrow h, H, A$  is therefore a rich source of Higgs bosons at the Tevatron and the LHC for large  $\tan\beta$ .


**Fig. 27a**

**Fig. 27b**

**Fig. 27:** Neutral MSSM Higgs production cross-sections at the LHC for gluon fusion  $gg \rightarrow \Phi$ , vector-boson fusion  $qq \rightarrow qqV \rightarrow qqh/qqH$ , Higgs-strahlung  $q\bar{q} \rightarrow V^* \rightarrow hV/HV$  and the associated production  $gg, q\bar{q} \rightarrow b\bar{b}\Phi/t\bar{t}\Phi$ , including all known QCD corrections. (a)  $h, H$  production for  $\tan\beta = 3$ , (b)  $h, H$  production for  $\tan\beta = 30$ , (c)  $A$  production for  $\tan\beta = 3$ , (d)  $A$  production for  $\tan\beta = 30$ .



**Fig. 27c**



**Fig. 27d**

**Fig. 27: Continued**

Data from the Tevatron in the channel  $p\bar{p} \rightarrow b\bar{b}\tau^+\tau^-$  have been exploited to exclude part of the supersymmetric Higgs parameter space in the  $[M_A, \text{tg}\beta]$  plane. In the interesting range of  $\text{tg}\beta$  between 30 and 50, pseudoscalar masses  $M_A$  of up to 150 to 190 GeV appear to be excluded.

The cross-sections of the various MSSM Higgs production mechanisms at the LHC are shown in Figs. 27(a)–(d) for two representative values of  $\text{tg}\beta = 3$  and 30, as a function of the corresponding Higgs mass. The CTEQ6M parton densities have been adopted with  $\alpha_s(M_Z) = 0.118$ ; the top and bottom masses have been set to  $M_t = 174$  GeV and  $M_b = 4.62$  GeV. For the pseudoscalar Higgs bremsstrahlung off  $t, b$  quarks,  $pp \rightarrow Q\bar{Q}A + X$ , the leading-order CTEQ6L1 parton densities have been used. For small and moderate values of  $\text{tg}\beta \lesssim 10$  the gluon-fusion cross-section provides the dominant production cross-section for the entire Higgs mass region up to  $M_\Phi \sim 1$  TeV. However, for large  $\text{tg}\beta$ , Higgs bremsstrahlung off bottom quarks,  $pp \rightarrow b\bar{b}\Phi + X$ , dominates over the gluon-fusion mechanism since the bottom Yukawa couplings are strongly enhanced in this case.

The MSSM Higgs search at the LHC will be more involved than the SM Higgs search. The final summary is presented in Fig. 28. It exhibits a difficult region for the MSSM Higgs search at the LHC. For  $\text{tg}\beta \sim 5$  and  $M_A \sim 150$  GeV, the full luminosity and the full data sample of both the ATLAS and CMS experiments at the LHC are needed to cover the problematic parameter region [85]. On the other hand, if no excess of Higgs events above the SM background processes beyond 2 standard deviations is found, the MSSM Higgs bosons can be excluded at 95% C.L.

Even though the entire supersymmetric Higgs parameter space of the MSSM is expected to be finally covered by the LHC experiments, the entire ensemble of individual Higgs bosons is accessible only in part of the parameter space. Particularly in the blind wedge opening in the parameter space at about  $M_A \sim 200$  GeV and centred around  $\tan\beta \sim 7$ , only the lightest Higgs boson  $h$  can be discovered, while the heavy Higgs bosons  $A, H, H^\pm$  cannot be found in non-supersymmetric decay channels. Moreover, the search for heavy  $H, A$  Higgs particles is very difficult, because of the  $t\bar{t}$  continuum background for masses  $\gtrsim 500$  GeV.

### 3.5 The production of SUSY Higgs particles in $e^+e^-$ collisions

The search for the neutral SUSY Higgs bosons at  $e^+e^-$  linear colliders will be a straightforward extension of the search performed at LEP2, which covered the mass range up to  $\sim 100$  GeV for neutral Higgs bosons. Higher energies,  $\sqrt{s}$  in excess of 250 GeV, are required to sweep the entire parameter space of the MSSM for moderate to large values of  $\text{tg}\beta$ .

The main production mechanisms of *neutral Higgs bosons* at  $e^+e^-$  colliders [20, 78, 86] are the Higgs-strahlung process and associated pair production, as well as the fusion processes:

$$\begin{aligned}
(a) \text{ Higgs-strahlung:} & \quad e^+e^- \xrightarrow{Z} Z + h/H \\
(b) \text{ Pair production:} & \quad e^+e^- \xrightarrow{Z} A + h/H \\
(c) \text{ Fusion processes:} & \quad e^+e^- \xrightarrow{WW} \bar{\nu}_e \nu_e + h/H \\
& \quad e^+e^- \xrightarrow{ZZ} e^+e^- + h/H .
\end{aligned}$$

The  $\mathcal{CP}$ -odd Higgs boson  $A$  cannot be produced in fusion processes to leading order. The cross-sections for the four Higgs-strahlung and pair production processes can be expressed as

$$\begin{aligned}
\sigma(e^+e^- \rightarrow Z + h/H) &= \sin^2 / \cos^2(\beta - \alpha) \sigma_{SM} \\
\sigma(e^+e^- \rightarrow A + h/H) &= \cos^2 / \sin^2(\beta - \alpha) \bar{\lambda} \sigma_{SM} ,
\end{aligned} \tag{57}$$

where  $\sigma_{SM}$  is the SM cross-section for Higgs-strahlung and the coefficient  $\bar{\lambda} \sim \lambda_{Aj}^{3/2} / \lambda_{Zj}^{1/2}$  accounts for the suppression of the  $P$ -wave  $Ah/H$  cross-sections near the threshold.

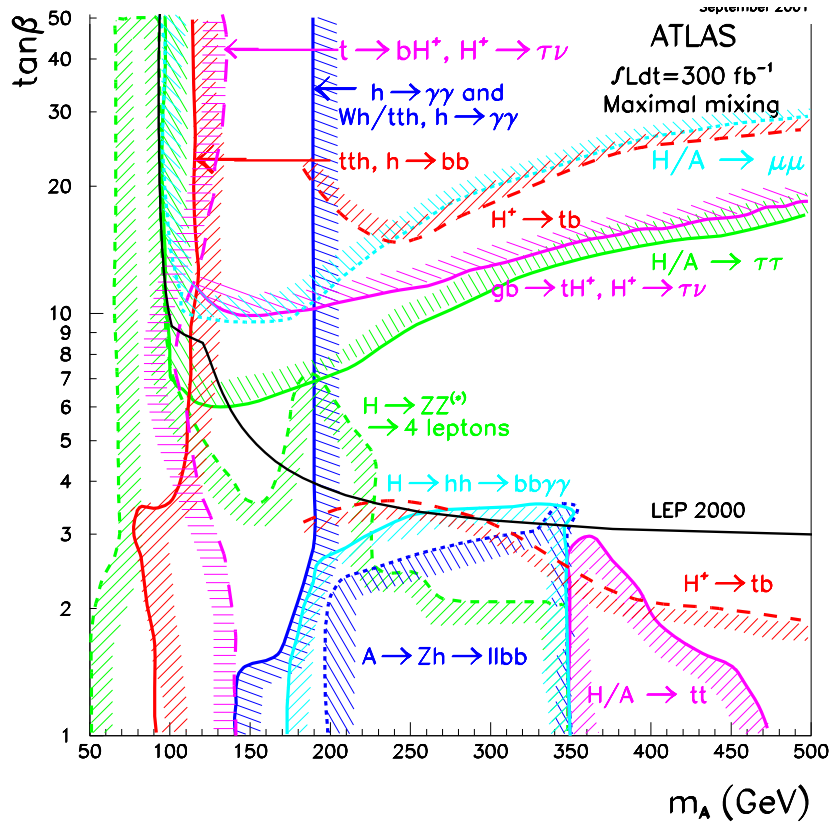


**Fig. 28:** The ATLAS sensitivity for the discovery of the MSSM Higgs bosons in the case of maximal mixing. The  $5\sigma$  discovery curves are shown in the  $(\tan\beta, m_A)$  plane for the individual channels and for an integrated luminosity of  $300\text{ fb}^{-1}$ . The corresponding LEP limit is also shown. Ref. [85].

The cross-sections for Higgs-strahlung and for pair production, much as those for the production of the light and the heavy neutral Higgs bosons  $h$  and  $H$ , are complementary, coming either with coefficients  $\sin^2(\beta - \alpha)$  or  $\cos^2(\beta - \alpha)$ . As a result, since  $\sigma_{SM}$  is large, at least the lightest  $\mathcal{CP}$ -even Higgs boson must be detected in  $e^+e^-$  experiments.

Representative examples of cross-sections for the production mechanisms of the neutral Higgs bosons are exemplified in Fig. 29, as a function of the Higgs masses, for  $\tan\beta = 3$  and  $30$ . The cross-section for  $hZ$  is large for  $M_h$  near the maximum value allowed for  $\tan\beta$ ; it is of order  $50\text{ fb}$ , corresponding to  $\sim 2500$  events for an integrated luminosity of  $50\text{ fb}^{-1}$ . By contrast, the cross-section for  $HZ$  is large if  $M_h$  is sufficiently below the maximum value (implying small  $M_H$ ). For  $h$  and for a low-mass  $H$ , the signals consist of a  $Z$  boson accompanied by a  $b\bar{b}$  or  $\tau^+\tau^-$  pair. These signals are easy to separate from the background, which comes mainly from  $ZZ$  production if the Higgs mass is close to  $M_Z$ . For the associated channels  $e^+e^- \rightarrow Ah$  and  $AH$ , the situation is opposite to the previous case: the cross-section for  $Ah$  is large for light  $h$ , whereas  $AH$  pair production is the dominant mechanism in the complementary region for heavy  $H$  and  $A$  bosons. The sum of the two cross-sections decreases from  $\sim 50$  to  $10\text{ fb}$  if  $M_A$  increases from  $\sim 50$  to  $200\text{ GeV}$  at  $\sqrt{s} = 500\text{ GeV}$ . In major parts of the parameter space, the signals consist of four  $b$  quarks in the final state, requiring provisions for efficient  $b$ -quark tagging. Mass constraints will help to eliminate the backgrounds from QCD jets and  $ZZ$  final states. For the  $WW$  fusion mechanism, the cross-sections are larger than for Higgs-strahlung, if the Higgs mass is moderately small—less than  $160\text{ GeV}$  at  $\sqrt{s} = 500\text{ GeV}$ . However, since the final state cannot be fully reconstructed, the signal is more difficult to extract. As in the case of the Higgs-strahlung processes, the production of light  $h$  and heavy  $H$  Higgs bosons complement each other in  $WW$  fusion, too.

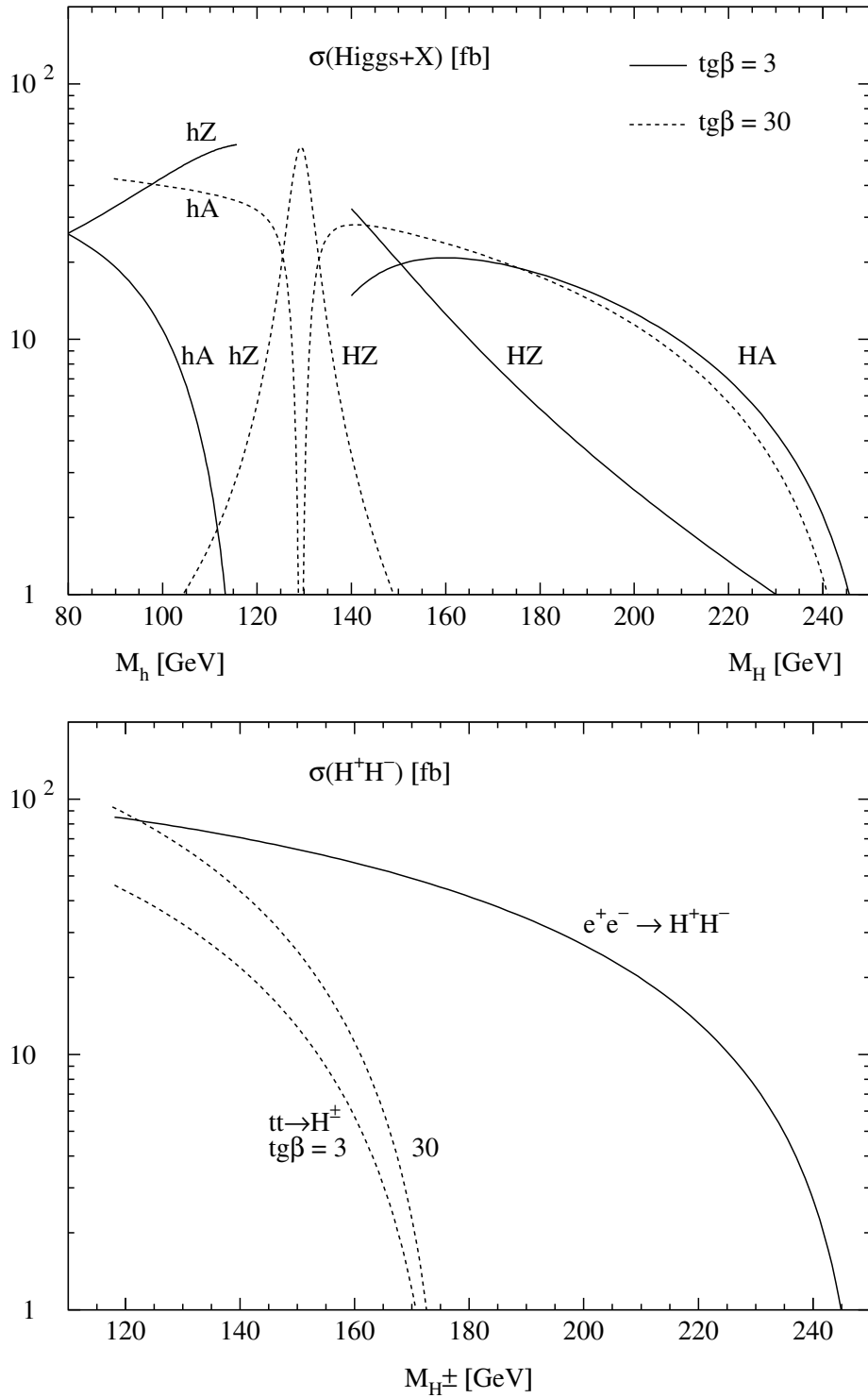


**Fig. 29:** Production cross-sections of MSSM Higgs bosons at  $\sqrt{s} = 500$  GeV: Higgs-strahlung and pair production; upper part: neutral Higgs bosons, lower part: charged Higgs bosons. Ref. [76].

The *charged Higgs bosons*, if lighter than the top quark, can be produced in top decays,  $t \rightarrow b + H^+$ , with a branching ratio varying between 2% and 20% in the kinematically allowed region. Since the cross-section for top-pair production is of order 0.5 pb at  $\sqrt{s} = 500$  GeV, this corresponds to 1000 to 10 000 charged Higgs bosons at a luminosity of  $50 \text{ fb}^{-1}$ . Since, for  $\text{tg } \beta$  larger than unity, the charged Higgs bosons will decay mainly into  $\tau\nu_\tau$ , there is a surplus of  $\tau$  final states over  $e, \mu$  final states in  $t$  decays, an apparent breaking of lepton universality. For large Higgs masses the dominant decay mode is the top decay  $H^+ \rightarrow t\bar{b}$ . In this case the charged Higgs particles must be pair-produced in  $e^+e^-$  colliders:

$$e^+e^- \rightarrow H^+H^- .$$

The cross-section depends only on the charged Higgs mass. It is of order 100 fb for small Higgs masses at  $\sqrt{s} = 500$  GeV, but it drops very quickly owing to the  $P$ -wave suppression  $\sim \beta^3$  near the threshold. For  $M_{H^\pm} = 230$  GeV, the cross-section falls to a level of  $\simeq 5$  fb. The cross-section is considerably larger for  $\gamma\gamma$  collisions.

### 3.5.1 Experimental search strategies

Search strategies have been described for neutral and charged Higgs bosons in Ref. [15]. The overall experimental situation can be summarized in the following two points:

(i) The lightest  $\mathcal{CP}$ -even Higgs particle  $h$  can be detected in the entire range of the MSSM parameter space, either via Higgs-strahlung  $e^+e^- \rightarrow hZ$  or via pair production  $e^+e^- \rightarrow hA$ . This conclusion holds true even at a c.m. energy of 250 GeV, independently of the squark mass values; it is also valid if decays to invisible neutralinos and other SUSY particles are realized in the Higgs sector.

(ii) The area in the parameter space where *all SUSY Higgs bosons* can be discovered at  $e^+e^-$  colliders is characterized by  $M_H, M_A \lesssim \frac{1}{2}\sqrt{s}$ , independently of  $\text{tg } \beta$ . The  $h, H$  Higgs bosons can be produced either via Higgs-strahlung or in  $Ah, AH$  associated production; charged Higgs bosons will be produced in  $H^+H^-$  pairs. Thus the blind LHC wedge can be covered up to  $A, H, H^\pm$  Higgs masses of 500 GeV at the 1 TeV collider ILC, and up to 1.5 TeV at the 3 TeV collider CLIC. If the  $ee$  collider is turned into a high-energy photon collider by Compton back-scattering of laser light [87–89], the Higgs mass range in single formation experiments  $\gamma\gamma \rightarrow A, H$  can be extended to 80% of the total  $e^+e^-$  energy, i.e., 800 GeV and 2.4 TeV at ILC and CLIC, respectively, cf. Refs. [90, 91].

The search for the lightest neutral SUSY Higgs boson  $h$  had been one of the most important experimental tasks at LEP2. Mass values of the pseudoscalar boson  $A$  of less than about 90 GeV have been excluded, independently of  $\text{tg } \beta$ , cf. Fig. 24.

## 3.6 Measuring the parity of Higgs bosons

Once the Higgs bosons are discovered, the properties of the particles must be established. Besides the reconstruction of the supersymmetric Higgs potential [65, 92], which will be a very demanding task, the external quantum numbers must be established, in particular the parity of the heavy scalar and pseudoscalar Higgs particles  $H$  and  $A$  [93].

For large  $H, A$  masses the decays  $H, A \rightarrow t\bar{t}$  to top final states can be used to discriminate between the different parity assignments [93]. For example, the  $W^+$  and  $W^-$  bosons in the  $t$  and  $\bar{t}$  decays tend to be emitted antiparallel and parallel in the plane perpendicular to the  $t\bar{t}$  axis:

$$\frac{d\Gamma^\pm}{d\phi_*} \propto 1 \mp \left(\frac{\pi}{4}\right)^2 \cos \phi_* \quad (58)$$

for  $H$  and  $A$  decays, respectively.

Alternatively, the  $\mathcal{CP}$  parity of Higgs bosons can be measured by analysing the magnitude of the total cross-section and the top-quark polarization in associated top-Higgs production in  $e^+e^-$  collisions [94].

For light  $H, A$  masses,  $\gamma\gamma$  collisions appear to provide a viable solution [93]. The fusion of Higgs particles in linearly polarized photon beams depends on the angle between the polarization vectors. For scalar  $0^+$  particles the production amplitude is non-zero for parallel polarization vectors, while pseudoscalar  $0^-$  particles require perpendicular polarization vectors:

$$\mathcal{M}(H)^+ \sim \vec{\epsilon}_1 \cdot \vec{\epsilon}_2 \quad \text{and} \quad \mathcal{M}(A)^- \sim \vec{\epsilon}_1 \times \vec{\epsilon}_2 . \quad (59)$$

The experimental set-up for Compton back-scattering of laser light can be tuned in such a way that the linear polarization of the hard-photon beams approaches values close to 100%. Depending on the  $\pm$  parity of the resonance produced, the measured asymmetry for photons of parallel and perpendicular polarization,

$$\mathcal{A} = \frac{\sigma_{\parallel} - \sigma_{\perp}}{\sigma_{\parallel} + \sigma_{\perp}} , \quad (60)$$

is either positive or negative.

Exciting observations in the Higgs sector at photon colliders are predicted in  $\mathcal{CP}$ -violating extensions. Particularly in the decoupling regime the near degeneracy of the  $\mathcal{CP}$ -even and  $\mathcal{CP}$ -odd  $H, A$  states gives rise potentially to large mixing effects, rotating the current eigenstates  $H, A$  into the mass eigenstates  $H_2, H_3$ . In this configuration large asymmetries,

$$\mathcal{A} = \frac{\sigma_{++} - \sigma_{--}}{\sigma_{++} + \sigma_{--}} , \quad (61)$$

can be generated in single Higgs  $\gamma\gamma$  formation between right- and left-circularly polarized  $\gamma$  beams [95].

### 3.7 Non-minimal supersymmetric extensions

The minimal supersymmetric extension of the Standard Model may appear very restrictive for supersymmetric theories in general, in particular in the Higgs sector where the quartic couplings are identified with the gauge couplings. However, it turns out that the mass pattern of the MSSM is quite typical if the theory is assumed to be valid up to the GUT scale—the motivation for supersymmetry *sui generis*. This general pattern has been studied thoroughly within the next-to-minimal extension: the NMSSM, incorporating two Higgs isodoublets, is extended by introducing an additional isosinglet field  $N$ . This extension leads to a model [96–98] that is generally referred to as the NMSSM.

The additional Higgs singlet can solve the so-called  $\mu$ -problem (i.e.,  $\mu \sim \text{order } M_W$ ) by eliminating the  $\mu$  higgsino parameter from the potential and by replacing it by the vacuum expectation value of the  $N$  field, which can naturally be related to the usual vacuum expectation values of the Higgs isodoublet fields. In this scenario the superpotential involves the two trilinear couplings  $H_1 H_2 N$  and  $N^3$ . The consequences of this extended Higgs sector will be outlined in the context of grand unification, including universal soft breaking terms of the supersymmetry [97, 98].

The Higgs spectrum of the NMSSM includes, besides the minimal set of Higgs particles, one additional scalar and pseudoscalar Higgs particle:

$$\begin{aligned} \text{neutral } CP = + & \quad H_1, H_2, H_3 \\ \text{neutral } CP = - & \quad A_1, A_2 \\ \text{charged} & \quad H^{\pm} . \end{aligned}$$

The neutral Higgs particles are in general mixtures of isodoublets, which couple to  $W, Z$  bosons and fermions, and the isosinglet, decoupled from the non-Higgs sector. The trilinear self-interactions contribute to the masses of the Higgs particles; for the lightest Higgs boson of each species:

$$\begin{aligned} M^2(H_1) &\leq M_Z^2 \cos^2 2\beta + \lambda^2 v^2 \sin^2 2\beta \\ M^2(A_1) &\leq M^2(A) \\ M^2(H^\pm) &\leq M^2(W) + M^2(A) - \lambda^2 v^2 . \end{aligned} \quad (62)$$

In contrast to the minimal model, the mass of the charged Higgs particle could be smaller than the  $W$  mass. An example of the mass spectrum is shown in Fig. 30. Since the trilinear couplings increase with energy, upper bounds on the mass of the lightest neutral Higgs boson  $H_1$  can be derived, in analogy to the Standard Model, from the assumption that the theory be valid up to the GUT scale:  $m(H_1) \lesssim 140$  GeV. Thus despite the additional interactions, the distinct pattern of the minimal extension remains valid also in more complex supersymmetric scenarios. If  $H_1$  is (nearly) pure isosinglet, it decouples from the gauge boson and fermion system and its role is taken by the next Higgs particle with a large isodoublet component, implying the validity of the mass bound again.

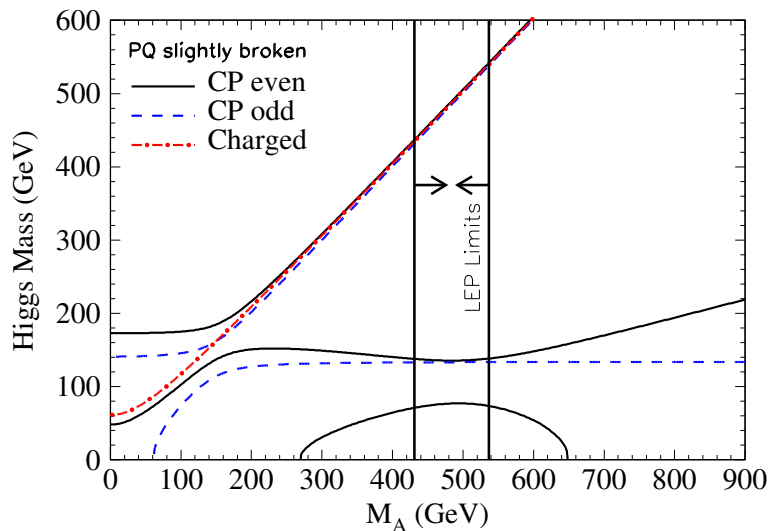


**Fig. 30:** The one-loop Higgs boson masses as a function of  $M_A$  for  $\lambda = 0.3$ ,  $\kappa = 0.1$ ,  $v_s = 3v$ ,  $\tan \beta = 3$  and  $A_\kappa = -100$  GeV. The arrows denote the region allowed by LEP searches with 95% confidence. Ref. [98].

For a primarily isosinglet Higgs particle  $H_1$  the coupling  $ZZH_1$  is small and the particle cannot be produced by Higgs-strahlung. However, in this case  $H_2$  is generally light and couples with sufficient strength to the  $Z$  boson; if not,  $H_3$  plays this role.

A large variety of other extensions beyond the minimal supersymmetric model have been analysed theoretically. For example, if the gauge boson sector is expanded by an additional  $U(1)'$  Abelian symmetry at high energies [99, 100], the additional pseudoscalar Higgs field is absorbed to generate the mass of the new  $Z'$  boson while the scalar part of the Higgs field can be observed as a new Higgs boson beyond the MSSM set. If generated by an extended symmetry like  $E_6$ , the Higgs sector is expanded by an ensemble of new states [101] with quite unconventional properties.

Quite generally, so long as the fields in supersymmetric theories remain weakly interacting up to the canonical Planck scale, the mass of the lightest Higgs bosons is bounded by about 200 GeV as the Yukawa couplings are restricted to be small in the same way as the quartic coupling in the standard Higgs potential. Moreover, the mass bound of 140 GeV for the lightest Higgs particle is realized in almost all

supersymmetric theories [102]; cf. Ref. [21] for expansions of this limit. Experiments at  $e^+e^-$  colliders are in a ‘no-lose’ situation [103] for detecting the Higgs particles in general supersymmetric theories, even for c.m. energies as low as  $\sqrt{s} \sim 500$  GeV.

## 4 Dynamical symmetry breaking

The Higgs mechanism is based on the theoretical concept of spontaneous symmetry breaking [1]. In the canonical formulation, adopted in the Standard Model, a four-component *fundamental* scalar field is introduced, which is endowed with a self-interaction such that the field acquires a non-zero value in the ground state. The specific direction in isospace, which is singled out by the ground-state solution, breaks the isospin invariance of the interaction spontaneously<sup>3</sup>. The interaction of the gauge fields with the scalar field in the ground state generates the masses of these fields. The longitudinal degrees of freedom of the gauge fields are built up by absorption of the Goldstone modes, which are associated with the spontaneous breaking of the electroweak symmetries in the scalar field sector. Fermions acquire masses through Yukawa interactions with the ground-state field. While three scalar components are absorbed by the gauge fields, one degree of freedom manifests itself as a physical particle, the Higgs boson. The exchange of this particle in scattering amplitudes, including longitudinal gauge fields and massive fermion fields, guarantees the unitarity of the theory up to asymptotic energies.

Alternatively, the interpretation of the Higgs boson as a (pseudo-)Goldstone boson associated with the spontaneous breaking of new strong interactions has been a very attractive idea for a long time.

### 4.1 Little Higgs models

The interest in this picture has been renewed within the Little Higgs scenarios [3] that have recently been developed to generate the electroweak symmetry breaking dynamically by new strong interactions. Little Higgs models are based on a complex system of symmetries and symmetry breaking mechanisms; for a recent review see Ref. [104]. Three points are central in realizing the idea:

- (i) The Higgs field is a Goldstone field associated with the breaking of a global symmetry  $G$ . The strong interactions are characterized by a scale  $\Lambda \sim 10$  to  $30$  TeV, while the dynamical Goldstone scale is estimated to be  $f \sim \Lambda/4\pi \sim 1$  to  $3$  TeV;
- (ii) In the same step, the gauge symmetry  $G_0 \subset G$  is broken down to the gauge group  $SU(2) \times U(1)$  of the Standard Model, generating masses for heavy vector bosons and fermions of the intermediate size  $M \sim gf \sim 1$  TeV;
- (iii) The Higgs boson acquires a mass finally by collective radiative symmetry breaking, i.e., to second order, at the standard electroweak scale  $v \sim g^2 f/4\pi \sim 100$  to  $300$  GeV.

Thus three characteristic scales are encountered in these models: the strong interaction scale  $\Lambda$ , the new mass scale  $M$  and the electroweak breaking scale  $v$ , ordered in the hierarchical chain  $\Lambda \gg M \gg v$ . The light Higgs boson mass is protected at small value by requiring the collective breaking of two symmetries. In contrast to the boson–fermion symmetry that cancels quadratic divergences in supersymmetry, the cancellation in Little Higgs models operates in the boson and fermion sectors individually, the cancellation ensured by the symmetries among the couplings of the SM fields and the new fields,  $\mathcal{O}(M)$ , to the Higgs field.

---

<sup>3</sup>We retain this language commonly used also in the context of gauge theories, although the gauge symmetry is not broken, in effect, by the Higgs mechanism.

#### 4.1.1 Example: Littlest Higgs model

An interesting example in which these concepts are realized, is provided by the Littlest Higgs model [105, 106]. The model is formulated as a non-linear sigma model with a global  $SU(5)$  symmetry group. This group is broken down to  $SO(5)$  by the non-zero vacuum expectation value

$$\Sigma_0 = \text{crossdiag} [\mathbb{1}, 1, \mathbb{1}] \quad (63)$$

of the  $\Sigma$  field. Assuming the subgroup  $[SU(2) \times U(1)]^2$  to be gauged, the global symmetry breaking leads also to the breaking of this gauge group down to  $[SU(2) \times U(1)]$ . The global symmetry breaking generates  $24 - 10 = 14$  Goldstone bosons, four of which are absorbed by the gauge bosons associated with the broken gauge group. The remaining 10 Goldstone bosons, incorporated in the  $\Sigma$  field

$$\Sigma = \exp[2i\Pi/f] : \quad \Pi = \left\| \begin{array}{ccc} 0 & h^\dagger/\sqrt{2} & \varphi^\dagger \\ h/\sqrt{2} & 0 & h^*/\sqrt{2} \\ \varphi & h^T/\sqrt{2} & 0 \end{array} \right\| \quad (64)$$

are identified as an iso-doublet  $h$  that becomes the light Higgs field of the Standard Model, and a Higgs triplet  $\varphi$  that acquires a mass of order  $M$ .

The main construction principles of the model should be illustrated by analysing the gauge and the Higgs sector qualitatively. The top sector, extended by a new heavy  $[T_L, T_R]$  doublet, can be treated in a similar way after introducing the appropriate top-Higgs interactions.

#### 4.1.2 Vector boson sector:

Inserting the  $[SU(2) \times U(1)]^2$  gauge fields into the sigma Lagrangian,

$$\mathcal{L} = \frac{1}{2} \frac{f^2}{4} \text{Tr} |\mathcal{D}_\mu \Sigma|^2 \quad (65)$$

with

$$\mathcal{D}_\mu \Sigma = \partial_\mu \Sigma - i \sum_{j=1}^2 [g_j (W_j \Sigma + \Sigma W_j^T) + \{U(1)\}], \quad (66)$$

the four vector bosons of the broken  $[SU(2) \times U(1)]$  gauge symmetry acquire masses

$$M[W_H, Z_H, A_H] \sim gf \quad (67)$$

where  $W_H$  etc. denote the heavy electroweak gauge fields.

Remarkably, the  $W_H$  gauge bosons couple with the opposite sign to the square of the light Higgs boson compared with the standard  $W$  bosons:

$$\begin{aligned} \mathcal{L} &= +\frac{g^2}{4} W^2 \text{Tr} h^\dagger h \\ &\quad -\frac{g^2}{4} W_H^2 \text{Tr} h^\dagger h + \dots \end{aligned} \quad (68)$$

The quadratic divergences of the two closed  $W$  and  $W_H$ -loop diagrams attached to the light Higgs field, therefore cancel each other and, similarly to supersymmetric degrees of freedom, the new vector bosons should have masses not exceeding 1 to 3 TeV to avoid excessive fine tuning.

The Standard Model gauge bosons still remain massless at this point; they acquire non-zero masses after the standard electroweak breaking mechanism is in operation.

### 4.1.3 Higgs sector:

Up to this level of the evolution of the theory, the global symmetries prevent a non-zero Higgs potential. Only if radiative corrections are switched on, does the Coleman–Weinberg mechanism generate the Higgs potential that endows the Higgs bosons with masses and breaks the gauge symmetry of the Standard Model.

Casting the Higgs potential into the form

$$V = m_\varphi^2 \text{Tr}\varphi^\dagger\varphi - \mu^2 hh^\dagger + \lambda_4 (hh^\dagger)^2 \quad (69)$$

the first term provides a non-zero mass to the  $\varphi$  Higgs boson while the next two terms are responsible for the symmetry breaking in the gauge sector of the Standard Model.

– Cutting-off the quadratically divergent contributions to the Coleman–Weinberg potential at  $\Lambda$ , the masses squared of the (now) pseudo-Goldstone bosons  $\varphi$  are of the order

$$m_\varphi^2 \sim g^2 (\Lambda/4\pi)^2 \sim g^2 f^2. \quad (70)$$

Thus the heavy Higgs bosons acquire masses of the size of the heavy vector bosons.

– The quartic coupling of the light Higgs boson is of order  $g^2$ . The coefficient  $\mu^2$ , however, receives contributions only from one-loop logarithmically divergent and two-loop quadratically divergent parts in the Coleman–Weinberg potential:

$$\begin{aligned} \mu^2 = \mu_1^2 + \mu_2^2 : \quad \mu_1^2 &\sim (\Lambda/4\pi)^2 \log(\Lambda^2/f^2) / 16\pi^2 \sim f^2 \log(\Lambda^2/f^2) / 16\pi^2 \\ \mu_2^2 &\sim \Lambda^2 / (16\pi^2)^2 \sim f^2 / 16\pi^2. \end{aligned} \quad (71)$$

Both contributions are naturally of the order  $f/4\pi$ , i.e., they are an order of magnitude smaller than the intermediate scale  $M$  of the heavy Higgs and vector masses.

Thus, a light Higgs boson with mass of order 100 GeV can be generated in Little Higgs models as a pseudo-Goldstone boson associated with the spontaneous breaking of new strong interactions. The light mass is protected against large radiative corrections individually in the boson and the fermion sectors.

### 4.1.4 Phenomenology

Such scenarios give rise to many predictions that can be checked experimentally. Foremost, the spectrum of new heavy vector bosons and fermions should be observed with masses in the intermediate range of 1 to a few TeV at the LHC or TeV/multi-TeV  $e^+e^-$  linear colliders. Extensions beyond the minimal version may generate additional scalars with a strong impact also on the spectrum of the light Higgs sector.

However, the model can already be checked by analysing existing precision data from LEP and elsewhere. The impact of the new degrees of freedom on the Little Higgs models must be kept small enough not to spoil the success of the radiative corrections including just the light Higgs boson in the description of the data. This leads to a constraint of order 3 to 5 TeV on the parameter  $f$ , Fig. 31. Thus the theory is compatible with present precision data, but only marginally and the overlap is narrow.

Extensions of the system in which a new parity [108] is introduced,  $T$ -parity, reduce the radiative corrections to closed loops of the new degrees of freedom so that lighter new particles are not excluded. However, potential anomalies [109] which break  $T$ -invariance must be avoided in designing such scenarios.

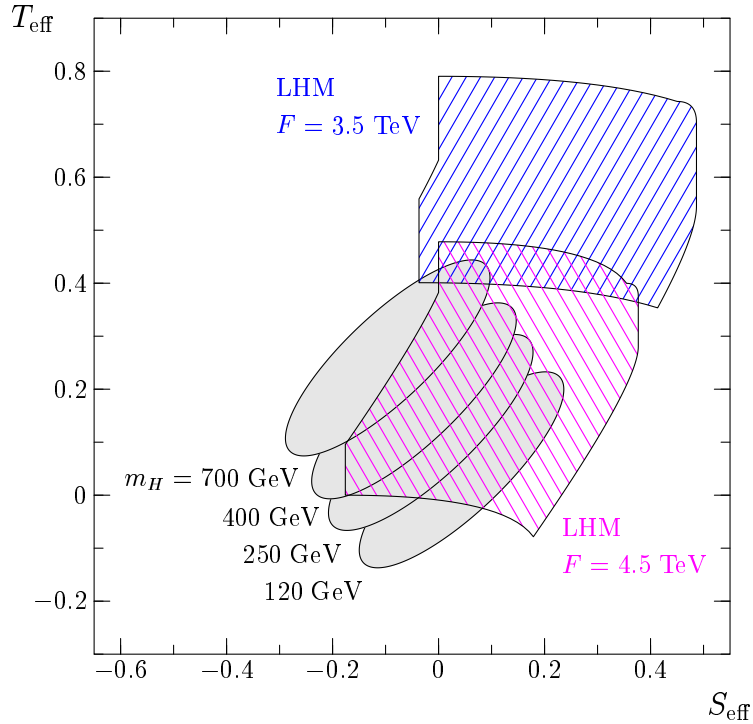


**Fig. 31:** Predictions of the  $S, T$  precision parameters for the Littlest Higgs model with standard  $U(1)$  charge assignments. The shaded ellipses are the 68% exclusion contours which follow from the electroweak precision data, assuming four different Higgs masses. The hatched areas are the allowed parameter ranges of the Littlest Higgs model for two different values of the scale  $F$ . The limits from contact interactions have been taken into account. Ref. [107].

## 4.2 Strongly interacting $W$ bosons

In alternative scenarios [2] a system of novel fermions is introduced, which interact strongly at a scale of order 1 TeV. In the ground state of such a system a scalar condensate of fermion–antifermion pairs may form. Such a process is generally expected to be realized in any non-Abelian gauge theory of the novel strong interactions (as in QCD). Since the scalar condensate breaks the chiral symmetry of the fermion system, Goldstone fields will form, and they are absorbed by the electroweak gauge fields to build up the longitudinal components and the masses of the gauge fields. Novel gauge interactions must be introduced, that couple the leptons and quarks of the Standard Model to the new fermions in order to generate lepton and quark masses by interactions with the ground-state fermion–antifermion condensate. In the low-energy sector of the electroweak theory, the fundamental Higgs-field approach and the dynamical alternative are effectively equivalent. However, the two theories are quite different at high energies. While the unitarity of the electroweak gauge theory is guaranteed by the exchange of the scalar Higgs particle in scattering processes, unitarity is restored in the dynamical theory at high energies by the non-perturbative strong interactions between the particles. Since the longitudinal gauge field components are equivalent to the Goldstone fields associated with the microscopic theory, their strong interactions at high energies are transferred to the electroweak gauge bosons. By unitarity, the  $S$ -wave scattering amplitude of longitudinally polarized  $W, Z$  bosons in the isoscalar channel  $(2W^+W^- + ZZ)/\sqrt{3}$ ,  $a_0^0 = \sqrt{2}G_F s/16\pi$ , is bounded by  $1/2$ , so that the characteristic scale of the new strong interactions must be close to 1.2 TeV. Thus near the critical energy of 1 TeV the  $W, Z$  bosons interact strongly with each other. Technicolour-type theories provide an elaborate form of such scenarios.

### 4.2.1 Theoretical basis

Physical scenarios of dynamical symmetry breaking may be based on new strong interaction theories, which extend the spectrum of matter particles and of the interactions beyond the degrees of freedom realized in the Standard Model. If the new strong interactions are invariant under transformations of a chiral  $SU(2) \times SU(2)$  group, the chiral invariance is generally broken spontaneously down to the diagonal custodial isospin group  $SU(2)$ . This process is associated with the formation of a chiral condensate in the ground state and the existence of three massless Goldstone bosons.



**Fig. 32:** Generating gauge-boson masses (V) through the interaction with the Goldstone bosons (G)

The Goldstone bosons can be absorbed by the gauge fields, generating longitudinal states and non-zero masses of the gauge bosons, as shown in Fig. 32. Summing up the geometric series of vector-boson–Goldstone-boson transitions in the propagator leads to a shift of the mass pole:

$$\begin{aligned} \frac{1}{q^2} &\rightarrow \frac{1}{q^2} + \frac{1}{q^2} q_\mu \frac{g^2 F^2 / 2}{q^2} q_\mu \frac{1}{q^2} + \frac{1}{q^2} \left[ \frac{g^2 F^2}{2} \frac{1}{q^2} \right]^2 + \dots \\ &\rightarrow \frac{1}{q^2 - M^2} . \end{aligned} \quad (72)$$

The coupling between gauge fields and Goldstone bosons has been defined as  $igF/\sqrt{2}q_\mu$ . The mass generated for the gauge field is related to this coupling by

$$M^2 = \frac{1}{2} g^2 F^2 . \quad (73)$$

The numerical value of the coupling  $F$  must coincide with  $v/\sqrt{2} = 174$  GeV.

The remaining custodial  $SU(2)$  symmetry guarantees that the relative strength (squared) of the neutral and charged current couplings  $\rho = 1$ . Denoting the  $W/B$  mass matrix elements by

$$\begin{aligned} \langle W^i | \mathcal{M}^2 | W^j \rangle &= \frac{1}{2} g^2 F^2 \delta_{ij} & \langle W^3 | \mathcal{M}^2 | B \rangle &= \langle B | \mathcal{M}^2 | W^3 \rangle \\ \langle B | \mathcal{M}^2 | B \rangle &= \frac{1}{2} g'^2 F^2 & &= \frac{1}{2} g g' F^2 \end{aligned} \quad (74)$$

the universality of the coupling  $F$  leads to the ratio  $M_W^2/M_Z^2 = g^2/(g^2 + g'^2) = \cos^2 \theta_W$  of the mass eigenvalues, equivalent to  $\rho = 1$ .

Since the wave functions of longitudinally polarized vector bosons grow with the energy, the longitudinal field components are the dominant degrees of freedom at high energies. These states can, however, for asymptotic energies be identified with the absorbed Goldstone bosons. This equivalence [110] is apparent in the 't Hooft–Feynman gauge where, for asymptotic energies,

$$\epsilon_\mu^L W_\mu \rightarrow k_\mu W_\mu \sim M^2 \Phi . \quad (75)$$

The dynamics of gauge bosons can therefore be identified at high energies with the dynamics of scalar Goldstone fields. An elegant representation of the Goldstone fields  $\vec{G}$  in this context is provided by the exponentiated form

$$U = \exp[-i\vec{G}\vec{\tau}/v] , \quad (76)$$

which corresponds to an  $SU(2)$  matrix field.

The Lagrangian of a system of strongly interacting bosons consists in such a scenario of the Yang–Mills part  $\mathcal{L}_{YM}$  and the interactions  $\mathcal{L}_G$  of the Goldstone fields,

$$\mathcal{L} = \mathcal{L}_{YM} + \mathcal{L}_G . \quad (77)$$

The Yang–Mills part is written in the usual form  $\mathcal{L}_{YM} = -\frac{1}{4}\text{Tr}[W_{\mu\nu}W_{\mu\nu} + B_{\mu\nu}B_{\mu\nu}]$ . The interaction of the Goldstone fields can be systematically expanded in chiral theories in the derivatives of the fields, corresponding to expansions in powers of the energy for scattering amplitudes [111]:

$$\mathcal{L}_G = \mathcal{L}_0 + \sum_{dim=4} \mathcal{L}_i + \dots . \quad (78)$$

Denoting the SM covariant derivative of the Goldstone fields by

$$D_\mu U = \partial_\mu U - igW_\mu U + ig'B_\mu U \quad (79)$$

the leading term  $\mathcal{L}_0$ , which is of dimension = 2, is given by

$$\mathcal{L}_0 = \frac{v^2}{4}\text{Tr}[D_\mu U^+ D_\mu U] . \quad (80)$$

This term generates the masses of the  $W, Z$  gauge bosons:  $M_W^2 = \frac{1}{4}g^2v^2$  and  $M_Z^2 = \frac{1}{4}(g^2 + g'^2)v^2$ . The only parameter in this part of the interaction is  $v$ , which, however, is fixed uniquely by the experimental value of the  $W$  mass; thus the amplitudes predicted by the leading term in the chiral expansion can effectively be considered as parameter-free.

The next-to-leading component in the expansion with dimension = 4 consists of ten individual terms. If the custodial  $SU(2)$  symmetry is imposed, only two terms are left, which do not affect propagators and 3-boson vertices but only 4-boson vertices. Introducing the vector field  $V_\mu$  by

$$V_\mu = U^+ D_\mu U \quad (81)$$

these two terms are given by the interaction densities

$$\mathcal{L}_4 = \alpha_4 [\text{Tr}V_\mu V_\nu]^2 \quad \text{and} \quad \mathcal{L}_5 = \alpha_5 [\text{Tr}V_\mu V_\mu]^2 . \quad (82)$$

The two coefficients  $\alpha_4, \alpha_5$  are parameters which characterize the underlying microscopic theory. In phenomenological approaches they must be adjusted experimentally from  $WW$  scattering data.

Higher orders in the chiral expansion give rise to an energy expansion of the scattering amplitudes of the form  $\mathcal{A} = \sum c_n (s/v^2)^n$ . This series will diverge at energies for which the resonances of the new strong interaction theory can be formed in  $WW$  collisions:  $0^+$  ‘Higgs-like’,  $1^-$  ‘ $\rho$ -like’ resonances, etc. The masses of these resonance states are expected in the range  $M_R \sim 4\pi v$  where chiral loop expansions diverge, i.e., between about 1 and 3 TeV.

#### 4.2.2 An example: technicolour-type theories

A simple example for such scenarios is provided by technicolour-type theories, see e.g., Ref. [112]. They are built on a pattern similar to QCD but characterized by a scale  $\Lambda_{TC}$  in the TeV range so that the interaction becomes strong already at short distances of order  $10^{-17}$  cm.

The basic degrees of freedom in the simplest version are a chiral set  $[(U, D)_L; U_R, D_R]$  of massless fermions that interact with technicolour gauge fields. The chiral  $SU(2)_L \times SU(2)_R$  symmetry of this theory is broken down to the diagonal  $SU(2)_{L+R}$  vector symmetry by the formation of  $\langle \bar{U}U \rangle = \langle \bar{D}D \rangle = \mathcal{O}(\Lambda_{TC}^3)$  vacuum condensates. The breaking of the chiral symmetry generates three massless Goldstone

bosons  $\sim \bar{Q}i\gamma_5 \vec{\tau} Q$ , that can be absorbed by the gauge fields of the Standard Model to build the massive states with  $M_W \sim 100$  GeV. From the chain

$$M_W = gF/\sqrt{2} \quad \text{and} \quad F \sim \Lambda_{TC}/4\pi \quad (83)$$

the parameter  $F$  is estimated to be below 1 TeV while  $\Lambda_{TC}$  should be in the TeV range.

While the electroweak gauge sector can be formulated consistently in this picture, generating fermion masses leads to severe difficulties. Since gauge interactions couple only left–left and right–right field components, a helicity-flip left–right mass operator  $\bar{f}_L f_R$  is not generated for the fermions of the Standard Model. To solve this problem, new gauge interactions between the SM and TC fermions must be introduced (Extended Technicolour) so that the helicity can flip through the ETC condensate in the vacuum. The SM masses predicted this way are of order  $m_f \sim g_E^2 \Lambda_{ETC}^3 / M_E^2$  with  $g_E$  being the coupling in the extended technicolour gauge theory and  $M_E$  the mass of the ETC gauge fields. However, estimates of  $M_E$  lead to a clash if one tries to reconcile the size of the scale needed for generating the top mass, order TeV, with the suppression of flavour-changing processes, like  $K\bar{K}$  oscillations, which require a size of order PeV.

Thus, the simplest realization of the technicolour theories suffers from internal conflicts in the fermion sector. More involved theoretical models are needed to reconcile these conflicting estimates [112]. Nevertheless, the idea of generating electroweak symmetry breaking dynamically, is a theoretically attractive and interesting scenario.

### 4.3 $WW$ scattering at high-energy colliders

Independently of specific realizations of dynamical symmetry breaking, theoretical tools have been developed which can serve to investigate these scenarios quite generally. The (quasi-) elastic 2–2  $WW$  scattering amplitudes can be expressed at high energies by a master amplitude  $A(s, t, u)$ , which depends on the three Mandelstam variables of the scattering processes:

$$\begin{aligned} A(W^+W^- \rightarrow ZZ) &= A(s, t, u) \\ A(W^+W^- \rightarrow W^+W^-) &= A(s, t, u) + A(t, s, u) \\ A(ZZ \rightarrow ZZ) &= A(s, t, u) + A(t, s, u) + A(u, s, t) \\ A(W^-W^- \rightarrow W^-W^-) &= A(t, s, u) + A(u, s, t) . \end{aligned} \quad (84)$$

To lowest order in the chiral expansion  $\mathcal{L} \rightarrow \mathcal{L}_{YM} + \mathcal{L}_0$  the master amplitude is given, in a parameter-free form, by the energy squared  $s$ :

$$A(s, t, u) \rightarrow \frac{s}{v^2} . \quad (85)$$

This representation is valid for energies  $s \gg M_W^2$  but below the new resonance region, i.e., in practice at energies  $\sqrt{s} = \mathcal{O}(1 \text{ TeV})$ . Denoting the scattering length for the channel carrying isospin  $I$  and angular momentum  $J$  by  $a_{IJ}$ , the only non-zero scattering channels predicted by the leading term of the chiral expansion correspond to

$$a_{00} = +\frac{s}{16\pi v^2} \quad (86)$$

$$a_{11} = +\frac{s}{96\pi v^2}$$

$$a_{20} = -\frac{s}{32\pi v^2} . \quad (87)$$

While the exotic  $I = 2$  channel is repulsive, the  $I = J = 0$  and  $I = J = 1$  channels are attractive, indicating the formation of non-fundamental Higgs-type and  $\rho$ -type resonances.

Taking into account the next-to-leading terms in the chiral expansion, the master amplitude turns out to be [26]

$$A(s, t, u) = \frac{s}{v^2} + \alpha_4 \frac{4(t^2 + u^2)}{v^4} + \alpha_5 \frac{8s^2}{v^4} + \dots, \quad (88)$$

including the two parameters  $\alpha_4$  and  $\alpha_5$ .

Increasing the energy, the amplitudes will approach the resonance area. There, the chiral character of the theory no longer provides a guiding principle for constructing the scattering amplitudes. Instead, *ad-hoc* hypotheses must be introduced to define the nature of the resonances; see, e.g., Ref. [27].

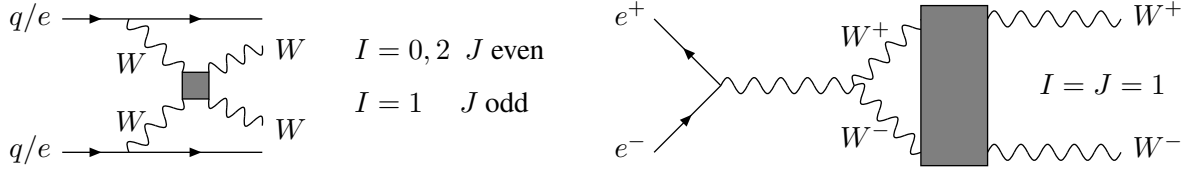


**Fig. 33:**  $WW$  scattering and rescattering at high energies at the LHC and TeV  $e^+e^-$  linear colliders

$WW$  scattering can be studied at the LHC and at TeV  $e^+e^-$  linear colliders. At high energies, equivalent  $W$  beams accompany the quark and electron/positron beams (Fig. 33) in the fragmentation processes  $pp \rightarrow qq \rightarrow qqWW$  etc. and  $ee \rightarrow \nu\nu WW$  etc.; the spectra of the longitudinally polarized  $W$  bosons have been given in Eq. (26). In the hadronic LHC environment the final-state  $WW$  etc. bosons can only be observed in leptonic and mixed hadronic/leptonic decays. The clean environment of  $e^+e^-$  colliders will allow the reconstruction of resonances from copious  $W$  decays to jet pairs. The results of three experimental simulations are displayed in Fig. 34. In Fig. 34(a) the sensitivity to the parameters  $\alpha_4, \alpha_5$  of the chiral expansion is shown for  $WW$  scattering in  $e^+e^-$  colliders [26]. The results of this analysis can be reinterpreted as sensitivity to the parameter-free prediction of the chiral expansion, corresponding to an error of about 10% in the first term of the master amplitude  $s/v^2$ . These experiments test the basic concept of dynamical symmetry breaking through spontaneous symmetry breaking. The production of a vector-boson resonance of mass  $M_V = 1$  TeV is exemplified in Fig. 34(b) [27].

The LHC allows the observation of  $WW$  resonances in these channels up to a mass range of about 1.5 TeV [13].

A second powerful method measures the elastic  $W^+W^- \rightarrow W^+W^-$  scattering in the  $I = 1, J = 1$  channel. The rescattering of  $W^+W^-$  bosons produced in  $e^+e^-$  annihilation, cf. Fig. 33, depends at high energies on the  $WW$  scattering phase  $\delta_{11}$  [113]. The production amplitude  $F = F_{LO} \times R$  is the product of the lowest-order perturbative diagram with the Mushkelishvili–Omnès rescattering amplitude  $\mathcal{R}_{11}$ ,

$$\mathcal{R}_{11} = \exp \frac{s}{\pi} \int \frac{ds'}{s'} \frac{\delta_{11}(s')}{s' - s - i\epsilon}, \quad (89)$$

which is determined by the  $I = J = 1$   $WW$  phase shift  $\delta_{11}$ . The power of this method derives from the fact that the entire  $e^+e^-$  collider energy is transferred to the  $WW$  system (while a major fraction of the energy is lost in the fragmentation of  $e \rightarrow \nu W$  if the  $WW$  scattering is studied in the process  $ee \rightarrow \nu\nu WW$ ). Detailed simulations [113] have shown that this process is sensitive to vector-boson masses up to about  $M_V \lesssim 6$  TeV in technicolour-type theories.

The experimental analysis of the  $\alpha$  parameters at the  $e^+e^-$  linear collider in the first phase with energy up to  $\sim 1$  TeV can be reinterpreted in the following way. Associating the parameters  $\alpha$  with new strong interaction scales,  $\Lambda_* \sim v/\sqrt{\alpha}$ , upper bounds on  $\Lambda_*$  of  $\sim 3$  TeV can be probed in  $WW$  scattering. Thus this instrument allows one to cover the entire threshold region  $\lesssim 4\pi v \sim 3$  TeV of the new strong interactions. In the  $W^+W^-$  production channel of  $e^+e^-$  collisions a range even up to order 10 TeV can

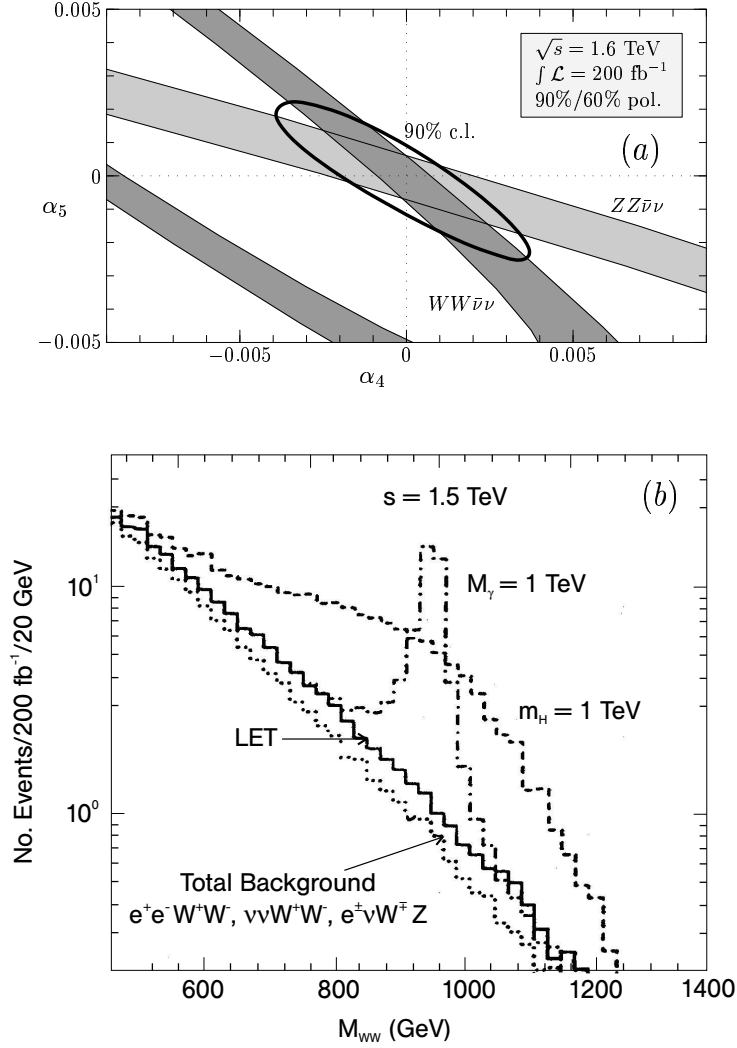


**Fig. 34:** Upper part: Sensitivity to the expansion parameters in chiral electroweak models of  $WW \rightarrow WW$  and  $WW \rightarrow ZZ$  scattering at the strong-interaction threshold; Ref. [26]. Lower part: The distribution of the  $WW$  invariant energy in  $e^+e^- \rightarrow \bar{\nu}\nu WW$  for scalar and vector resonance models [ $M_H, M_V = 1$  TeV]; Ref. [27].

be probed indirectly. If a new scale  $\Lambda_*$  would be discovered below  $\sim 3$  TeV, novel  $WW$  resonances could be searched for at the LHC while CLIC could investigate new resonance states with masses up to 3 TeV, and virtual states even far beyond.

## 5 Summary

The mechanism of electroweak symmetry breaking can be established in the present or the next generation of hadron and lepton colliders:

- Whether there exists a light fundamental Higgs boson.
- The profile of the Higgs particle can be reconstructed, which reveals the physical nature of the underlying mechanism of electroweak symmetry breaking.
- Analyses of strong  $WW$  scattering can be performed if the symmetry breaking is generated dynamically by novel strong interactions.

Moreover, depending on the experimental answer to these questions, the electroweak sector will provide the platform for extrapolations into physical areas beyond the Standard Model: either to the low-energy supersymmetry sector; or to a new strong interaction theory at a characteristic scale of order 1 TeV and beyond; or, alternatively, to extra space dimensions.

### **Acknowledgements**

P.M. Zerwas is very thankful to the organizers for the invitation to the 4th CERN–CLAF School of High-Energy Physics, Viña del Mar, Chile, 2007. The writing of the report was supported in part by the grant PAPIIT-IN115207.

## Appendices

### A The O(3) $\sigma$ model

A transparent but, at the same time, sufficiently complex model to study all the aspects of electroweak symmetry breaking is the O(3)  $\sigma$  model. By starting from the standard version, in a number of variants it allows one to develop the idea of spontaneous symmetry breaking and the Goldstone theorem while gauging the theory leads to the Higgs phenomenon. This evolution will be described step by step in the next three subsections.

The O(3)  $\sigma$  model includes a triplet of field components:

$$\sigma = (\sigma_1, \sigma_2, \sigma_3) . \quad (\text{A.1})$$

If the self-interaction potential of the field depends only on the overall field-strength, the theory, described by the Lagrangian

$$\mathcal{L} = \frac{1}{2}(\partial\sigma)^2 - V(\sigma^2) \quad (\text{A.2})$$

is O(3) rotationally invariant. These iso-rotations are generated by the transformation

$$\sigma \rightarrow e^{i\alpha t} \sigma \quad \text{with} \quad (t^i)_{jk} = i\epsilon_{ijk} \quad (\text{A.3})$$

with rotation parameters  $\alpha = (\alpha_1, \alpha_2, \alpha_3)$ . Choosing a quartic interaction for the potential, the theory is renormalizable and thus well defined.

#### A.1 Normative theory:

If the quartic potential  $V$  is chosen to be, cf. Fig. A.1,

$$V(\sigma^2) = \lambda^2(\sigma^2 + \mu^2)^2 \quad (\text{A.4})$$

the spectrum of particles and the interactions can easily be derived from the form

$$V(\sigma^2) = 2\lambda^2\mu^2\sigma^2 + \lambda^2\sigma^4 + \text{const.} . \quad (\text{A.5})$$

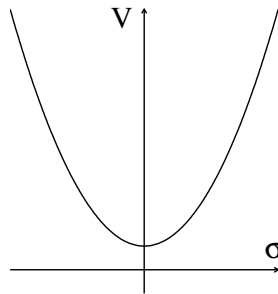


**Fig. A.1:**

The bilinear field-term describes three degenerate masses

$$m(\sigma_1) = m(\sigma_2) = m(\sigma_3) = 2\lambda\mu \quad (\text{A.6})$$

corresponding to three physical particle degrees of freedom. The fields interact through the second quartic term. The ground state of the system is reached for zero field-strength:

$$\sigma^0 = (0, 0, 0) . \quad (\text{A.7})$$

This theory describes a standard particle system in which the ground state preserves the rotational invariance of the Lagrangian. Thus the Lagrangian and the solution of the field equation obey the same degree of symmetry.

## A.2 Spontaneous symmetry breaking and Goldstone theorem

However, if the sign in the mass parameter in the potential flips to negative values,

$$V(\sigma^2) = \lambda^2(\sigma^2 - \mu^2)^2 \quad (\text{A.8})$$

the ground state is a state of non-zero field strength, cf. Fig. A.2. Fixing the axis of the ground state such that

$$\sigma^0 = (0, 0, v) \quad \text{with} \quad v = \mu \quad (\text{A.9})$$

the original O(3) rotational invariance of the Lagrangian is not obeyed any more by the ground-state solution which singles out a specific direction in iso-space. However, no principle determines the arbitrary direction of the ground-state vector in iso-space. Such a phenomenon in which solutions of the field equations do not respect the symmetry of the Lagrangian, is generally termed ‘spontaneous symmetry breaking’. Expanding the  $\sigma$  field about the ground state,

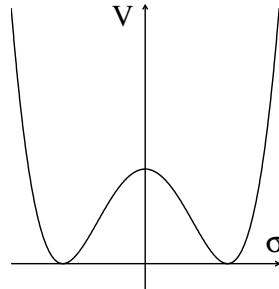


Fig. A.2:

$$\sigma = (\sigma'_1, \sigma'_2, v + \sigma'_3) , \quad (\text{A.10})$$

an effective theory emerges for the new dynamical degrees of freedom  $\sigma'_1, \sigma'_2$  and  $\sigma'_3$ . Evaluating the potential for the new fields,

$$V = 4v^2\lambda^2\sigma'^2_3 + 4v\lambda^2\sigma'_3(\sigma'^2_1 + \sigma'^2_2 + \sigma'^2_3) + \lambda^2(\sigma'^2_1 + \sigma'^2_2 + \sigma'^2_3)^2 , \quad (\text{A.11})$$

two massless particles plus one massive particle correspond to the bilinear field terms:

$$\begin{aligned} m(\sigma'_1) &= m(\sigma'_2) = 0 \\ m(\sigma'_3) &= 2\sqrt{2}\lambda v \neq 0 . \end{aligned} \quad (\text{A.12})$$

The two massless particles are called Goldstone bosons, Ref. [114].

In addition to the standard quartic terms, the Goldstone bosons and the massive particle interact with each other through trilinear terms in the effective potential.

The symmetry of the effective theory is reduced from the original O(3) rotational invariance to O(2) invariance restricted to rotations about the ground-state axis.

This  $\sigma$  model is only a simple example of the general Goldstone theorem:

*If  $N$  is the dimension of the symmetry group of the basic Lagrangian, but the symmetry of the ground-state solution is reduced to  $M$ , then the theory includes  $(N-M)$  massless scalar Goldstone bosons.*

For each destroyed symmetry degree of freedom, a massless particle appears in the spectrum. A most famous example of this theorem are the three nearly massless pions which emerge from spontaneously broken chiral isospin symmetry in QCD.

### A.3 The Higgs mechanism

The Higgs mechanism Ref. [1] provides the vector bosons in gauge theories with masses without destroying the renormalizability of the theory. Were masses to be introduced by hand, the gauge invariance which ensures the renormalizability would be destroyed by the *ad hoc* mass terms in the Lagrangian.

The global isospin symmetry of the O(3)  $\sigma$  model can be extended to a local symmetry by introducing an iso-triplet  $W$  of gauge fields coupled minimally to the  $\sigma$  field. Introducing the covariant derivative

$$\partial_\mu \sigma \rightarrow \partial_\mu \sigma +igtW_\mu \sigma \quad (\text{A.13})$$

into the Lagrangian,

$$\mathcal{L} = \frac{1}{2}[(\partial +igtW)\sigma]^2 - V(\sigma^2) + \mathcal{L}_{kin}(W) \quad (\text{A.14})$$

the theory is invariant under the local gauge transformation

$$\sigma \rightarrow e^{i\alpha t} \sigma \quad \text{with} \quad \alpha = \alpha(x) \quad (\text{A.15})$$

with the matter transformation complemented by the usual transformation of the non-Abelian gauge field. The gauged Lagrangian includes the gauge kinetic part, the  $\sigma$  kinetic part and the  $\sigma$ -gauge interaction, as well as the potential.

- If the  $\sigma$  potential is just the standard potential,  $V = \lambda^2(\sigma^2 + \mu^2)^2$ , the theory is a non-Abelian Yang–Mills gauge theory with a mass-degenerate triplet of  $\sigma$  particles interacting in the standard way with the massless  $W$  gauge triplet fields.
- However, if the potential is chosen of the Mexican type,  $V = \lambda^2(\sigma^2 - \mu^2)^2$ , which leads in the  $\sigma$  model to spontaneous symmetry breaking, the physical field/particle content of the theory changes dramatically (a phenomenon similar to the non-gauged theory):

Parametrizing the  $\sigma$  triplet-field by a rotation of the field about the ground-state axis,

$$\sigma = e^{i\Theta t/v}(\sigma^0 + \eta) \quad (\text{A.16})$$

with

$$\sigma^0 = (0, 0, v); \quad \eta = (0, 0, \eta); \quad \Theta = (\Theta_1, \Theta_2, 0), \quad (\text{A.17})$$

the  $\Theta$  components of  $\sigma$  perpendicular to the ground-state axis can be removed by the gauge transformation  $\sigma \rightarrow \exp[-i\Theta t/v]\sigma$  supplemented by the corresponding transformation of the gauge field. Keeping the original notation for the gauge-transformed fields, the new Lagrangian for the physical degrees of freedom is given by

$$\mathcal{L} = \frac{1}{2}[(\partial + igWt)(\sigma^0 + \eta)]^2 - V([\sigma^0 + \eta]^2) + \mathcal{L}_{kin}(W). \quad (\text{A.18})$$

After writing the resulting Lagrangian of the effective theory as

$$\mathcal{L} = \mathcal{L}_{kin}(W) + \frac{1}{4}g^2v^2(W_1^2 + W_2^2) + \frac{1}{2}(\partial\eta)^2 - V + \mathcal{L}_{int}(\eta, W), \quad (\text{A.19})$$

the physical particle/field content becomes manifest:

- a massless vector field  $W_3$  corresponding to the residual rotational invariance about the ground-state 3-axis;
- two massive  $W$  fields  $W_1$  and  $W_2$  perpendicular to the ground-state axis with masses determined by the ground-state  $\sigma$  field-strength  $v$  and the gauge coupling  $g$ . These two massive fields correspond to the symmetry degrees of freedom that were broken spontaneously in the non-gauged  $\sigma$  model;
- the Goldstone bosons have disappeared from the spectrum, absorbed to build up the longitudinal degrees of the massive gauge bosons;
- a real scalar Higgs boson  $\eta$ .

This example can easily be extended, in parallel to the Goldstone theorem, to formulate the general Higgs mechanism:

*If  $N$  is the dimension of the symmetry group of the original Lagrangian,  $M$  the dimension of the symmetry group leaving invariant the ground state of the  $n$  scalar fields, then the physical theory consists of  $M$  massless vector fields,  $(N-M)$  massive vector fields, and  $n-(N-M)$  scalar Higgs fields.*

## References

- [1] P. W. Higgs, Phys. Rev. Lett. **12** (1964) 132 and Phys. Rev. **145** (1966) 1156; F. Englert and R. Brout, Phys. Rev. Lett. **13** (1964) 321; G. S. Guralnik, C. R. Hagen and T. W. Kibble, Phys. Rev. Lett. **13** (1964) 585.
- [2] S. Weinberg, Phys. Rev. **D13** (1979) 974, *ibid.* **D19** (1979) 1277; L. Susskind, Phys. Rev. **D20** (1979) 2619.
- [3] N. Arkani-Hamed, A.G. Cohen and H. Georgi, Phys. Lett. **B513** (2001) 232; M. Schmaltz and D. Tucker-Smith, Report hep-ph/0502182.
- [4] C. Csaki, C. Grojean, H. Murayama, L. Pilo and J. Terning, Phys. Rev. **D69** (2004) 055006.
- [5] S.L. Glashow, Nucl. Phys. **20** (1961) 579; S. Weinberg, Phys. Rev. Lett. **19** (1967) 1264; A. Salam, in *Elementary Particle Theory*, ed. N. Svartholm (Almqvist and Wiksell, Stockholm, 1968).
- [6] N. Cabibbo, L. Maiani, G. Parisi and R. Petronzio, Nucl. Phys. **B158** (1979) 295; R.A. Flores and M. Sher, Phys. Rev. **D27** (1983) 1679; M. Lindner, Z. Phys. **C31** (1986) 295; M. Sher, Phys. Rep. **179** (1989) 273; J. Casas, J. Espinosa and M. Quiros, Phys. Lett. **B342** (1995) 171.
- [7] G. Altarelli and G. Isidori, Phys. Lett. **B337** (1994) 141; J. Espinosa and M. Quiros, Phys. Lett. **B353** (1995) 257.
- [8] A. Hasenfratz, K. Jansen, C. Lang, T. Neuhaus and H. Yoneyama, Phys. Lett. **B199** (1987) 531; J. Kuti, L. Liu and Y. Shen, Phys. Rev. Lett. **61** (1988) 678; M. Lüscher and P. Weisz, Nucl. Phys. **B318** (1989) 705.
- [9] M. Veltman, Acta Phys. Polon. **B8** (1977) 475.
- [10] LEP Electroweak Working Group, <http://lepewwg.web.cern.ch/LEPEWWG/>; M. W. Grunewald, arXiv:0709.3744 [hep-ex].
- [11] G. Abbiendi *et al.*, Phys. Lett. **B565** (2003) 61 [arXiv:hep-ex/0306033].
- [12] *Future Electroweak Physics at the Fermilab Tevatron*, FERMI LAB-PUB-96/082 [hep-ph/9602250]; M. Carena *et al.* [Higgs Working Group Collaboration], arXiv:hep-ph/0010338.
- [13] CMS Collaboration, Technical Design Report, Vol 2, CERN/LHCC 2006-021; ATLAS Collaboration, Technical Design Report, Vols. 1 and 2, CERN-LHCC-99-14 and CERN-LHCC-99-15.
- [14] V. Buscher and K. Jakobs, Int. J. Mod. Phys. **A20** (2005) 2523 [arXiv:hep-ph/0504099].
- [15] E. Accomando *et al.*, Phys. Rep. **299** (1998) 1; J.A. Aguilar-Saavedra *et al.*, TESLA TDR, hep-ph/0106315; A. Djouadi *et al.*, ILC RDR, arXiv:0709.1893 [hep-ph].
- [16] P. Fayet and S. Ferrara, Phys. Rep. **32** (1977) 249; H.P. Nilles, Phys. Rep. **110** (1984) 1; H. Haber and G. Kane, Phys. Rep. **117** (1985) 75; R. Barbieri, Riv. Nuovo Cimento **11** (1988) 1.
- [17] E. Witten, Phys. Lett. **B105** (1981) 267.
- [18] L.E. Ibañez and G.G. Ross, Phys. Lett. **B105** (1981) 439; S. Dimopoulos, S. Raby and F. Wilczek, Phys. Rev. **D24** (1981) 1681; J. Ellis, S. Kelley and D.V. Nanopoulos, Phys. Lett. **B249** (1990) 441; P. Langacker and M. Luo, Phys. Rev. **D44** (1991) 817; U. Amaldi, W. de Boer and H. Fürstenaun, Phys. Lett. **B260** (1991) 447; B. Allanach *et al.*, in *LHC/LC Report*, DESY 04-044 [hep-ph/0403133].
- [19] K. Inoue, A. Kakuto, H. Komatsu and S. Takeshita, Prog. Theor. Phys. **67** (1982) 1889; R. Flores and M. Sher, Ann. Phys. **148** (1983) 95; H.P. Nilles and M. Nusbaumer, Phys. Lett. **B145** (1984) 73; P. Majumdar and P. Roy, Phys. Rev. **D30** (1984) 2432.
- [20] J.F. Gunion and H.E. Haber, Nucl. Phys. **B272** (1986) 1 and **B278** (1986) 449.
- [21] M. Quiros and J. R. Espinosa, PASCOS 98, Boston 1998, arXiv:hep-ph/9809269.
- [22] S. Dawson, Nucl. Phys. **B249** (1985) 42; M. Chanowitz and M.K. Gaillard, Phys. Lett. **B142** (1984) 85; G. Kane, W. Repko and W. Rolnick, Phys. Lett. **B148** (1984) 367.

- [23] R.N. Cahn and S. Dawson, Phys. Lett. **B136** (1984) 196; K. Hikasa, Phys. Lett. **B164** (1985) 341; G. Altarelli, B. Mele and F. Pitolli, Nucl. Phys. **B287** (1987) 205; T. Han, G. Valencia and S. Willenbrock, Phys. Rev. Lett. **69** (1992) 3274.
- [24] A. Dobado, M.J. Herrero, J.R. Pelaez, E. Ruiz Morales and M.T. Urdiales, Phys. Lett. **B352** (1995) 400; A. Dobado and M.T. Urdiales, Z. Phys. **C71** (1996) 659.
- [25] J. Bagger, V. Barger, K. Cheung, J. Gunion, T. Han, G.A. Ladinsky, R. Rosenfeld and C.-P. Yuan, Phys. Rev. **D52** (1995) 3878.
- [26] E. Boos, H.-J. He, W. Kilian, A. Pukhov, C.-P. Yuan and P.M. Zerwas, Phys. Rev. **D57** (1998) 1553.
- [27] V. Barger, K. Cheung, T. Han and R.J.N. Phillips, Phys. Rev. **D52** (1995) 3815.
- [28] M. Gomez-Bock, M. Mondragon, M. Muhlleitner, R. Noriega-Papaqui, I. Pedraza, M. Spira and P. M. Zerwas, J. Phys. Conf. Ser. **18** (2005) 74 [arXiv:hep-ph/0509077].
- [29] M. Spira and P.M. Zerwas, Lectures, Schladming 1997, hep-ph/9803257; M. Spira, Fortschr. Phys. **46** (1998) 203; H. Spiesberger, M. Spira and P. M. Zerwas, in *Scattering*, P. Sabatier (Ed.) (Academic Press, London 2000), hep-ph/0011255.
- [30] C. Quigg, Rep. Prog. Phys. **70** (2007) 1019 [arXiv:0704.2232 [hep-ph]]; J.R. Ellis, G. Ridolfi and F. Zwirner, arXiv:hep-ph/0702114.
- [31] J.F. Gunion, H.E. Haber, G. Kane and S. Dawson, *The Higgs Hunter's Guide* (Addison-Wesley, 1990).
- [32] M. Carena and H. Haber, Prog. Part. Nucl. Phys. **50** (2003) 63; A. Djouadi, arXiv:hep-ph/0503172 and arXiv:hep-ph/0503173; D. Rainwater, arXiv:hep-ph/0702124.
- [33] B.W. Lee, C. Quigg and H.B. Thacker, Phys. Rev. Lett. **38** (1977) 883.
- [34] E. Braaten and J.P. Leveille, Phys. Rev. **D22** (1980) 715; N. Sakai, Phys. Rev. **D22** (1980) 2220; T. Inami and T. Kubota, Nucl. Phys. **B179** (1981) 171; S.G. Gorishny, A.L. Kataev and S.A. Larin, Sov. J. Nucl. Phys. **40** (1984) 329; M. Drees and K. Hikasa, Phys. Rev. **D41** (1990) 1547; Phys. Lett. **B240** (1990) 455 and (E) **B262** (1991) 497; K.G. Chetyrkin, Phys. Lett. **B390** (1997) 309.
- [35] B.A. Kniehl, Nucl. Phys. **B352** (1991) 1 and **B357** (1991) 357; D.Yu. Bardin, B.M. Vilenskiĭ and P.Kh. Khristova, Report JINR-P2-91-140.
- [36] T.G. Rizzo, Phys. Rev. **D22** (1980) 389; W.-Y. Keung and W.J. Marciano, Phys. Rev. **D30** (1984) 248.
- [37] A. Djouadi, M. Spira and P.M. Zerwas, Phys. Lett. **B264** (1991) 440.
- [38] J. Ellis, M.K. Gaillard and D.V. Nanopoulos, Nucl. Phys. **B106** (1976) 292.
- [39] A. Djouadi, J. Kalinowski and M. Spira, Comput. Phys. Commun. **108** (1998) 56.
- [40] M. Spira, A. Djouadi, D. Graudenz and P.M. Zerwas, Nucl. Phys. **B453** (1995) 17.
- [41] H. Georgi, S.L. Glashow, M. Machacek and D. Nanopoulos, Phys. Rev. Lett. **40** (1978) 692.
- [42] S. Dawson, Nucl. Phys. **B359** (1991) 283.
- [43] D. Graudenz, M. Spira and P.M. Zerwas, Phys. Rev. Lett. **70** (1993) 1372; M. Spira, Ph. D. Thesis, RWTH Aachen, 1992; S. Dawson and R.P. Kauffman, Phys. Rev. **D49** (1994) 2298; M. Spira, A. Djouadi, D. Graudenz and P.M. Zerwas, Phys. Lett. **B318** (1993) 347.
- [44] R.V. Harlander and W.B. Kilgore, Phys. Rev. Lett. **88** (2002) 201801; C. Anastasiou and K. Melnikov, Nucl. Phys. **B646** (2002) 220, and V. Ravindran, J. Smith and W.L. van Neerven, Nucl. Phys. **B665** (2003) 325.
- [45] S. Moch and A. Vogt, Phys. Lett. B **631** (2005) 48 [arXiv:hep-ph/0508265].
- [46] T. Figy, C. Oleari and D. Zeppenfeld, Phys. Rev. **D68** (2003) 073005; E.L. Berger and J. Campbell, Phys. Rev. **D70** (2004) 073011.

- [47] W. Beenakker, S. Dittmaier, M. Krämer, B. Plümper, M. Spira and P.M. Zerwas, Phys. Rev. Lett. **87** (2001) 201805, Nucl. Phys. **B653** (2003) 151; L. Reina and S. Dawson, Phys. Rev. Lett. **87** (2001) 201804; L. Reina, S. Dawson and D. Wackerroth, Phys. Rev. **D65** (2002) 053017; S. Dawson, L.H. Orr, L. Reina and D. Wackerroth, Phys. Rev. **D67** (2003) 071503, and S. Dawson, C. Jackson, L.H. Orr, L. Reina and D. Wackerroth, Phys. Rev. **D68** (2003) 034022.
- [48] B.L. Ioffe and V.A. Khoze, Sov. J. Part. Nucl. **9** (1978) 50; J.D. Bjorken, Proc. Summer Institute on Particle Physics, Report SLAC-198 (1976).
- [49] B.W. Lee, C. Quigg and H.B. Thacker, Phys. Rev. **D16** (1977) 1519.
- [50] R.N. Cahn and S. Dawson, Phys. Lett. **B136** (1984) 96; G.L. Kane, W.W. Repko and W.B. Rolnick, Phys. Lett. **B148** (1984) 367; G. Altarelli, B. Mele and F. Pitolli, Nucl. Phys. **B287** (1987) 205; W. Kilian, M. Krämer and P.M. Zerwas, Phys. Lett. **B373** (1996) 135.
- [51] CLIC Physics Working Group, *Physics at the CLIC Multi-TeV Linear Collider*, hep-ph/0412251.
- [52] J. Fleischer and F. Jegerlehner, Nucl. Phys. **B216** (1983) 469; B. Kniehl, Z. Phys. **C55** (1992) 605; A. Denner *et al.*, Z. Phys. **C56** (1992) 261.
- [53] G. Bélanger *et al.*, Phys. Lett. **B559** (2003) 252 and Nucl. Phys. Proc. Suppl. **116** (2003) 353; A. Denner *et al.*, Phys. Lett. **B560** (2003) 196 and Nucl. Phys. **B660** (2003) 289.
- [54] M. Duhrssen *et al.*, Phys. Rev. **D70** (2004) 113009.
- [55] S.Y. Choi, D.J. Miller, M.M. Mühlleitner and P.M. Zerwas, Phys. Lett. B **553** (2003) 61 [arXiv:hep-ph/0210077].
- [56] C.P. Buszello, I. Fleck, P. Marquard and J.J. van der Bij, Eur. Phys. J. **C32** (2004) 209 [arXiv:hep-ph/0212396].
- [57] V. Hankele, G. Klamke and D. Zeppenfeld, arXiv:hep-ph/0605117.
- [58] V. Barger, K. Cheung, A. Djouadi, B.A. Kniehl and P. Zerwas, Phys. Rev. **D49** (1994) 79.
- [59] D.J. Miller, S.Y. Choi, B. Eberle, M.M. Mühlleitner and P.M. Zerwas, Phys. Lett. **B505** (2001) 149.
- [60] M.T. Dova, P. Garcia-Abia and W. Lohmann, LC-PHSM-2001-054 [arXiv:hep-ph/0302113].
- [61] M. Duhrssen, S. Heinemeyer, H. Logan, D. Rainwater, G. Weiglein and D. Zeppenfeld, Phys. Rev. **D70** (2004) 113009 [arXiv:hep-ph/0406323].
- [62] **SM**: A. Djouadi, J. Kalinowski and P.M. Zerwas, Mod. Phys. Lett. **A7** (1992) 1765 and Z. Phys. **C54** (1992) 255; S. Dittmaier, M. Krämer, Y. Liao, M. Spira and P.M. Zerwas, Phys. Lett. **B441** (1998) 383; S. Dawson and L. Reina, Phys. Rev. **D57** (1998) 5851 and **D59** (1999) 054012; G. Bélanger, F. Boudjema, J. Fujimoto, T. Ishikawa, T. Kaneko, K. Kato, Y. Shimizu and Y. Yasui, Phys. Lett. **B571** (2003) 163; A. Denner, S. Dittmaier, M. Roth and M. Weber, Phys. Lett. **B575** (2003) 290 and Nucl. Phys. **B680** (2004) 85; Y. You, W.-G. Ma, H. Chen, R.-Y. Zhang, S. Yan-Bin and H.-S. Hou, Phys. Lett. **B571** (2003) 85; **MSSM**: S. Dittmaier, M. Krämer, Y. Liao, M. Spira and P.M. Zerwas, Phys. Lett. **B478** (2000) 247; S. Dawson and L. Reina, Phys. Rev. **D60** (1999) 015003; S.H. Zhu, hep-ph/0212273; P. Häfliger and M. Spira, Nucl. Phys. **B719** (2005) 35.
- [63] K. Hagiwara, H. Murayama and I. Watanabe, Nucl. Phys. **B367** (1991) 257.
- [64] *GLC project: Linear Collider for TeV physics*, KEK-REPORT-2003-7.
- [65] A. Djouadi, W. Kilian, M. Mühlleitner and P.M. Zerwas, Eur. Phys. J **C10** (1999) 27 and Eur. Phys. J **C10** (1999) 45; R. Lafaye, D.J. Miller, S. Moretti and M. Mühlleitner, arXiv:hep-ph/0002238; M. Mühlleitner, arXiv:hep-ph/0008127; G. Bélanger *et al.*, Phys. Lett. **B576** (2003) 152; U. Baur, T. Plehn and D. Rainwater, Phys. Rev. **D69** (2004) 053004; A. Krause, T. Plehn, M. Spira and P.M. Zerwas, Nucl. Phys. **B519** (1998) 85.
- [66] C. Castanier *et al.*, arXiv:hep-ex/0101028, and references in Ref. [15].
- [67] J. Wess and B. Zumino, Nucl. Phys. B **70** (1974) 39.
- [68] J. Polchinski and L. Susskind, Phys. Rev. **D26** (1982) 3661; S. Dimopoulos and H. Georgi, Nucl. Phys. **B193** (1981) 150; N. Sakai, Z. Phys. **C11** (1981) 153.

- [69] L.E. Ibañez and G.G. Ross, Phys. Lett. **B110** (1982) 215.
- [70] Y. Okada, M. Yamaguchi and T. Yanagida, Prog. Theor. Phys. **85** (1991) 1; H. Haber and R. Hempfling, Phys. Lett. **66** (1991) 1815; J. Ellis, G. Ridolfi and F. Zwirner, Phys. Lett. **257B** (1991) 83; M. Carena, J.R. Espinosa, M. Quiros and C.E.M. Wagner, Phys. Lett. **B335** (1995) 209.
- [71] S. Heinemeyer, W. Hollik and G. Weiglein, Phys. Rep. **425** (2006) 265, and update by the authors (*private communication*).
- [72] E. Boos, A. Djouadi, M. Mühlleitner and A. Vologdin, Phys. Rev. **D66** (2002) 055004.
- [73] M. Carena and H.E. Haber, Prog. Part. Nucl. Phys. **50** (2003) 63.
- [74] W.-M. Yao et al. [Particle Data Group], J. Phys. **G33** (2006) 1.
- [75] J.F. Gunion and H.E. Haber, Phys. Rev. **D67** (2003) 075019; S.Y. Choi, J. Kalinowski, Y. Liao and P.M. Zerwas, Eur. Phys. J. **C40** (2005) 555.
- [76] A. Djouadi, J. Kalinowski and P.M. Zerwas, Z. Phys. **C70** (1996) 435.
- [77] A. Djouadi, P. Janot, J. Kalinowski and P.M. Zerwas, Phys. Lett. **B376** (1996) 220.
- [78] A. Djouadi, J. Kalinowski, P. Ohmann and P.M. Zerwas, Z. Phys. **C74** (1997) 93.
- [79] A. Bartl, H. Eberl, K. Hidaka, T. Kon, W. Majerotto and Y. Yamada, Phys. Lett. **B389** (1996) 538.
- [80] Z. Kunszt and F. Zwirner, Nucl. Phys. **B385** (1992) 3.
- [81] G. Kane, G. Kribs, S. Martin and J. Wells, Phys. Rev. **D53** (1996) 213; B. Kileng, P. Osland and P. Pandita, *Proceedings 10th International Workshop on High Energy Physics and Quantum Field Theory, Zvenigorod, Russia, September 1995*, hep-ph/9601284.
- [82] S. Dawson, A. Djouadi and M. Spira, Phys. Rev. Lett. **77** (1996) 16.
- [83] M. Muhlleitner and M. Spira, hep-ph/0612254, Nucl. Phys. **B** *in press*.
- [84] S. Dittmaier, M. Kramer and M. Spira, Phys. Rev. D **70** (2004) 074010 [arXiv:hep-ph/0309204]; J. Campbell *et al.*, arXiv:hep-ph/0405302.
- [85] S. Gentile, ATL-PHYS-2004-009.
- [86] A. Djouadi, J. Kalinowski and P.M. Zerwas, Z. Phys. **C57** (1993) 569.
- [87] I.F. Ginzburg, G.L. Kotkin, V.G. Serbo and V.I. Telnov, Pisma ZhETF **34** (1981) 514, JETP Lett. **34** (1982) 491 and Nucl. Instrum. Methods **205** (1983) 47; I.F. Ginzburg, G.L. Kotkin, S.L. Panfil, V.G. Serbo and V.I. Telnov, Nucl. Instrum. Methods **A2** (1984) 5.
- [88] B. Badelek *et al.* (ECFA/DESY Photon Collider Working Group), *TESLA Technical Design Report, Part VI: Photon Collider*, Int. J. Mod. Phys. A **19** (2004) 5097 [arXiv:hep-ex/0108012].
- [89] M. M. Muhlleitner and P. M. Zerwas, Acta Phys. Polon. **B37** (2006) 1021 [arXiv:hep-ph/0511339].
- [90] M. Muhlleitner, M. Kramer, M. Spira and P.M. Zerwas, Phys. Lett. **B508** (2001) 311 [arXiv:hep-ph/0101083]; M. Muhlleitner, Acta Phys. Polon. **B37** (2006) 1127 [arXiv:hep-ph/0512232].
- [91] P. Niezurawski, A.F. Zarnecki and M. Krawczyk, arXiv:hep-ph/0507006; M. Spira, P. Niezurawski, M. Krawczyk and A.F. Zarnecki, arXiv:hep-ph/0612369.
- [92] A. Djouadi, H.E. Haber and P.M. Zerwas, Phys. Lett. **B375** (1996) 203; T. Plehn, M. Spira and P.M. Zerwas, Nucl. Phys. **B479** (1996) 46.
- [93] M. Krämer, J. Kühn, M.L. Stong and P.M. Zerwas, Z. Phys. **C64** (1994) 21.
- [94] P.S. Bhupal Dev, A. Djouadi, R.M. Godbole, M.M. Muhlleitner and S.D. Rindani, arXiv:0707.2878 [hep-ph].
- [95] S.Y. Choi, J. Kalinowski, Y. Liao and P.M. Zerwas, Eur. Phys. J. **C40** (2005) 555.
- [96] P. Fayet, Nucl. Phys. **B90** (1975) 104; H.-P. Nilles, M. Srednicki and D. Wyler, Phys. Lett. **B120** (1983) 346; J.-P. Derendinger and C.A. Savoy, Nucl. Phys. **B237** (1984) 307; J.F. Gunion and H.E. Haber, Nucl. Phys. **B272** (1986) 1; J. Ellis, J.F. Gunion, H.E. Haber, L. Roszkowski and F. Zwirner, Phys. Rev. **D39** (1989) 844.

- [97] U. Ellwanger, M. Rausch de Traubenberg and C.A. Savoy, *Z. Phys.* **C67** (1995) 665; S.F. King and P.L. White, *Phys. Rev.* **D52** (1995) 4183; H. Asatrian and K. Eguin, *Mod. Phys. Lett.* **A10** (1995) 2943.
- [98] D.J. Miller, R. Nevzorov and P.M. Zerwas, *Nucl. Phys.* **B681** (2004) 3; S.Y. Choi, D.J. Miller and P.M. Zerwas, *Nucl. Phys.* **B711** (2005) 83.
- [99] S.Y. Choi, H.E. Haber, J. Kalinowski and P.M. Zerwas, *Nucl. Phys.* **B778** (2007) 85 [arXiv:hep-ph/0612218].
- [100] V. Barger, P. Langacker and G. Shaughnessy, *AIP Conf. Proc.* **903** (2007) 32 [arXiv:hep-ph/0611112].
- [101] S.F. King, S. Moretti and R. Nevzorov, *Phys. Rev.* **D73** (2006) 035009 [arXiv:hep-ph/0510419].
- [102] J.R. Espinosa and M. Quiros, *Phys. Lett.* **B279** (1992) 92; G.L. Kane, C. Kolda and J.D. Wells, *Phys. Rev. Lett.* **70** (1993) 2686.
- [103] J. Kamoshita, Y. Okada and M. Tanaka, *Phys. Lett.* **B328** (1994) 67.
- [104] T. Han, *Proceedings of SUSY04*, KEK, Tsukuba, 2004.
- [105] N. Arkani-Hamed, A.G. Cohen, E. Katz and A.E. Nelson, *JHEP* **0207** (2002) 034.
- [106] T. Han, H.E. Logan, B. McElrath and L.T. Wang, *Phys. Rev.* **D67** (2003) 095004.
- [107] W. Kilian and J. Reuter, *Phys. Rev.* **D70** (2004) 015004.
- [108] H.C. Cheng and I. Low, *JHEP* **0408** (2004) 061 [arXiv:hep-ph/0405243] and *JHEP* **0309** (2003) 051 [arXiv:hep-ph/0308199].
- [109] C.T. Hill and R.J. Hill, arXiv:0705.0697 [hep-ph].
- [110] J.M. Cornwall, D.N. Levin and G. Tiktopoulos, *Phys. Rev.* **D10** (1974) 1145; B. Lee, C. Quigg and H. Thacker, *Phys. Rev.* **D16** (1977) 1519; M. Chanowitz and M.K. Gaillard, *Nucl. Phys.* **B261** (1985) 379; G.J. Gounaris, R. Kogerler and H. Neufeld, *Phys. Rev.* **D34** (1986) 3257; Y.P. Yao and C.P. Yuan, *Phys. Rev.* **D38** (1988) 2237; H.-J. He, Y.-P. Kuang, and X.-Y. Li, *Phys. Rev. Lett.* **69** (1992) 2619.
- [111] T. Appelquist and C. Bernard, *Phys. Rev.* **D22** (1980) 200; A. Longhitano, *Phys. Rev.* **D22** (1980) 1166, *Nucl. Phys.* **B188** (1981) 118; T. Appelquist and G.-H. Wu, *Phys. Rev.* **D48** (1993) 3235.
- [112] K. Lane, *Two Lectures on Technicolor*, Fermilab-Pub-02/040-T, hep-ph/0202255.
- [113] T.L. Barklow, Snowmass Report 2001, hep-ph/0112286.
- [114] Y. Nambu, *Phys. Rev. Lett.* **4** (1960) 380; Y. Nambu and G. Jona-Lasinio, *Phys. Rev.* **122** (1961) 345 and **124** (1961) 246; J. Goldstone, *Nuovo Cimento* **19** (1961) 154; J. Goldstone, A. Salam and S. Weinberg, *Phys. Rev.* **127** (1962) 965.